Transition to turbulence in pipe flow of Newtonian and Non Newtonian fluids

Dissertation
zur Erlangung des Grades
des Doktors der Naturwissenschaften
der Naturwissenschaftlich-Technischen Fakultät II
- Physik und Mechatronik -
der Universität des Saarlandes

von Devranjan Samanta

Saarbrücken

November 27,2012

Tag des Kolloquiums: 16.01.2013

Dekan: Prof. Dr. Christian Wagner

Mitglieder des Prüfungsausschusses:
Vorsitzender: Prof. Dr. Helmut Seidel
Gutachter: Prof. Dr. Christian Wagner
Dr. Bjoern Hof
Akademischer Mitarbeiter: Dr. Andreas Tschoepe

Abstract

English: Experimental investigations were carried out in pipe flow of Newtonian and Non Newtonian fluids. The investigations of Newtonian flow were focused on the origin of laminar turbulent intermittency in the flow. It was found that upon reduction of the Reynolds number starting from fully turbulent flows laminar regions appear randomly. Unlike reported for other shear flows there was no wavelength induced instability in pipe flow. The development of intermittent patterns and in particular the minimum spacing between turbulent puffs is shown as a consequence of an interaction between neighboring puffs which has been identified. The puff interaction distance is found to decrease with increase in Re and it is in quantitative agreement with minimum spacing of plane Couette and Taylor Couette flow.

In the second part of this thesis the transition to dilute polymer solutions has been investigated. Compared to the Newtonian case transition is delayed. At higher concentrations however Newtonian like transition disappears. Instead disordered motion sets in globally and onset of transition is independent of additional perturbation to the flow. This new type of instability , a combined effect of elastic and inertial effects, termed as elasto inertial instability sets in and ultimately results in the asymptotic state of maximum drag reduction (MDR). Most strikingly disordered motion is observed at much lower Re than Newtonian turbulence.

German: Diese Arbeit beschäftigt sich mit der experimentellen Untersuchung des Turbulenzübergangs Newtonscher und nicht Newtonscher Fluessigkeiten in der Rohrströmung. Die Untersuchung Newtonscher Fluide konzentrierte sich auf den Ursprung laminar turbulent Intermittenter Strömungen. Es konnte gezeigt werden, dass als folge einer Reynoldszahlreduzierung, ausgfehend von einer voll turbulenten Strömung, laminare Regionen zufällig erscheinen. Dies steht im Gegensatz zu intermittenten Strömungmustern in anderen Scherströmungen für die eine feste Wellenlänge für solche Muster vorhergesagt wurde. Wir zeigen dass in der Rohrströmung intermittente Muster keine feste Wellenlänge haben stattdessen kann man einen minimalabstand definieren der eine Folge der puff-Interaktion ist.

Im zweiten Teil der Arbeit wurden Polymerlösungen untersucht und hier wurde fr niedrige Konzentrationen eine Verzögerung des Turbulenzübergangs beobachtet. Für höhere Konzentrationen trat überraschenderweise ein qualitativ anderer Übergang auf. Im Gegensatz zu Newtonschen Strömungen trat hier Turbulenz global und ohne zusätzliche äussere Störungen auf. Diese Intabilität tritt als Folge von Trägheits und elastischen Kräften auf. Die Vermessung der Reibungsbeiwerte zeigt dass die für Polymerlösungen wohlbekannte maximale Reibungsreduzierung eine Eigenschaft dieses neuen Turbulenzsutandes ist. Zudem kann diese Art der Trubulenz.

Declaration

I declare that this thesis is the result of my own research except as cited in the references. No portion of this thesis has been submitted in support of an application for another degree or qualification.

Acknowledgements

I am thankful to Dr. Bjoern Hof for providing the opportunity to pursue PhD under his guidance. I am thankful to Prof. Christian Wagner for his endeavor in arranging my admission in Saarbruecken university and his guidance. Thanks to Professor Alexander Morozov for many enlightening discussions during many conferences.

Mr. Jens Pick Nowack and Mr. Torsten Herenkamp will be always remembered for their service in giving me an excellent experimental setup for accurate measurements.

Thanks to Dr. Alberto de Lozar, Dr Marcus Holzner and Dr. Marc Avila for their guidance in different experimental techniques and data interpretations. Thanks to Christof Schaefer for doing the rheology measurements. Thanks to Dr. Mukund Vasudevan and Dr. Shreyash Jalikop for the afternoon coffee sessions and discussions on widely varying issues. Thanks to Jan for holding so many social events. I will cherish fond memories with all other labmates like Baofang, Kerstin, Liang, Nicholas, Paul, Sascha and Tobias.

Home sickness was never a issue due to great company of Anupam, Sakya and Sutanu. Frequent conversations with old friends like Anubhab, Baidurja , Bishakh, Chiranjib and Ishita have been also very entertaining. Thanks to Monomita for making last phase of my PhD more joyful.

Last but not the least, thanks to my family members for their constant encouragement and support throughout this eventful journey.

Contents

Chapter 1

Aim and scope of the thesis

1.1 General Introduction

Fluid mechanics has been an important branch of study at least since Archimedes' 'Eureka moment' when discovering the law of floatation. The legacy of fluid mechanics research had been carried by Bernoulli, Euler to Prandtl and Taylor in last century. Fluid dynamics is all pervasive to tiniest scales in micro fluidics apparatus or flow of blood vesicles to large scale oceanic circulations or planet formation. Fluid mechanics is useful in understanding many natural phenomena like cloud patterns, waves in atmospheric circulations, formation of sand dunes , earth's mantle convection and solar granulation (Tritton, 1988).

Understanding of fluid dynamics is vital for technological applications like hydraulic machineries e.g. pump or turbine and aerospace applications like airplanes and hypersonic rockets. Flow visualization images depicting various fluid dynamics phenomena presented in Van Dyke's Gallery of fluid motion book (figure 1.1) are beautiful enough to capture the attention of non specialists. Today the knowledge of fluid dynamics has been so vast that the whole domain of fluid dynamics is segregated into different sub branches like biofluid dynamics, micro fluidics, compressible flow and gas dynamics, environmental fluid dynamics, free surface flows, geophysical fluid dynamics (Stone, 2010) only to name a few. Although conservation of mass, momentum and energy equations prevail everywhere, it requires expertise to delve deep into each arena of fluid dynamics.

Figure 1.1: Kármán Vortex street behind a circular cylinder at Re=140 (VanDyke, 1982)

1.2 Transition to turbulence in pipe flow

Fluid motion comprises of two states. At low velocities, it is mathematically describable by well defined set of equations and accurate predictability. This well behaved state is laminar flow. Phenomena like motion of zooplanktons, applications in micro fluidic chips require a good understanding of this regime. However the more interesting and challenging state is the turbulent state involving flow of much higher velocities. In turbulent state the velocity field is fluctuating with time and is highly disordered in space resulting multitude of spatial and temporal scales. So far there are no analytical solutions to predict the turbulent motion accurately. It is unpredictable in a sense that small change in the initial systems can induce large changes in the fluid motion, reminiscent of chaotic systems. The celebrated physicist Richard Feynman once remarked turbulence as "the most important unsolved problem of classical physics". Between laminar and turbulent states, there exists a mixed state where laminar and turbulent states coexist. This state is known as laminar turbulent intermittency or as transitional flow. In some flows like Rayleigh Bénard systems, channel flow transition sets in at a well defined non dimensionless number. However, in cases like pipe flow, plane Couette or counter rotating Taylor Couette flow where there are no well defined points for transition, sudden increase in pressure fluctuations or torque occur, resulting in a drastic increase of the friction coefficient compared to laminar flow. The present thesis focuses on the transition regime in pipe flow. In chapter 2 there is a brief discussion on various issues of transition in Newtonian pipe flow. In chapter 5 experimental investigations on laminar turbulent spacing in the transition regime of pipe flow is presented.

1.3 Non Newtonian fluids

Fluids surrounding us are of two types. The first category of fluids like air, water is known as Newtonian fluids whose viscosity is independent of shear rate. However there exists another class of fluids known as Non Newtonian fluids whose viscosity depends on shear rate and shear history. Fluids like blood, syrup, paint or molasses are known as shear thinning liquids whose viscosity decreases with increasing shear whereas in cases of shear thickening fluids like suspensions of corn starch or quick sand viscosity increases with shear. A great deal of studies on characterization of Non Newtonian fluid properties and subsequent formulation of constitutive models has generated the branch of fluid Rheology. In addition to complexity of the non linear inertial terms (v.∇v) in Navier Stokes equation 1.1, the constitutive equation of polymeric stress involves non linear terms (equation 1.2):

$$\rho(\frac{\partial v}{\partial t} + v.\nabla v) = -\nabla p + \nabla \tau_s \tag{1.1}$$

$$\tau_p + \lambda(\frac{\partial \tau_p}{\partial t} + v.\nabla \tau_p - \nabla v^t.\tau_p - \tau_p.\nabla v) = \eta_p(\nabla v + \nabla v^t) \tag{1.2}$$

In equation 1.1 p, v, ρ and τ_s are pressure, velocity, density and Newtonian solvent shear stress respectively. In equation 1.2 λ is the relaxation time of polymer i.e. the time taken by a fully stretched polymer chain to regain its equilibrium configuration in absence of shear. The first two terms ($\tau_p + \lambda \frac{\partial \tau_p}{\partial t}$)

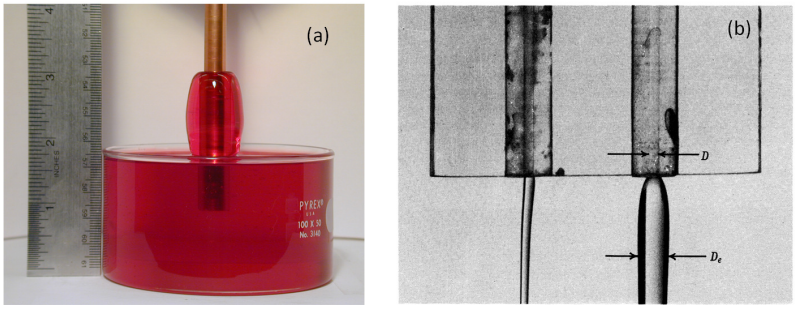

Figure 1.2: (a) Polymer solution rises along the rod when the rod is rotated. This phenomenon is known as Weissenberg effect (http://web.mit.edu/nnf/research/phenomena) (b) When a Newtonian fluid (N) is extruded through a dye there is no increase of diameter on coming out. Polymeric fluid (P) exhibits increase of diameter on being extruded out Bird *et al.* (1987)

is the change in τ_p on the time scale of λ. The terms $(\frac{\partial \tau_p}{\partial t}+\mathrm{v}.\nabla\ \tau_p)$ is the substantial derivative of polymeric stress. The remaining third $\nabla v^t.\tau_p$ and fourth term $\tau_p.\nabla v$ within the bracket are required to maintain frame invariance of the time dependent polymeric stress .

Many interesting phenomena due to non Newtonian properties like rod climbing (figure 1.2 a), die swell (figure 1.2 b), siphoning effect etc has been well documented in (Bird *et al.*, 1987). The rod climbing phenomenon (figure 1.2 a) popularly known as Weissenberg effect means that the non Newtonian fluid rises along the rod when the fluid is continuously rotated whereas there is dip near the rod when the Newtonian fluids like water is rotated. This happens due to non zero normal stress effects i.e. the magnitude of the stress along flow direction τ_{xx} is not equal to the stress along the direction of the flow gradient τ_{yy}. When a polymer melt is extruded through a die, diameter of the extruded liquid is much larger than the diameter of the circular die. This phenomenon known as die swelling effect(figure 1.2 b) also happens due to nonzero normal stress.

Among non Newtonian fluids, dilute polymer solutions are extensively studied by fluid dynamicists due to its drag reduction capacity which has important industrial applications like gas and oil transport through pipes over long distances. On minute addition of polymers to a Newtonian solvent, the friction factor or drag (Toms, 1948) as well as heat transfer (Hoyt, 1990) are reduced. This drag reduction capacity by polymers has generated a vast deal of literature focusing on the interactions of polymers with turbulent structures. Earlier findings on DR and transition in non Newtonian pipe flow are discussed in chapter 3. In the present thesis, drag reduction measurements and transitions in pipe flow of dilute polymer solutions are presented in chapter 6.

Chapter 2

Transition in pipe flow of Newtonian fluids

2.1 Introduction

Transition to turbulence in pipe flow is of great practical importance and despite many investigations since the pioneering work of Osborne Reynolds (1883), many aspects of the process are only poorly understood. In his original experiments Reynolds observed that at low flow rates a filament of dyed fluid would be transported to the end of the tube without mixing. At higher flow velocities on the other hand the dyed fluid mixed rapidly and the whole pipe section was colored. However at intermediate velocities, usually referred to as the transitional regime, laminar and turbulent states were observed to coexist (figure 2.1). Reynolds (1883) described this regime as follows "*Another phenomenon very marked in smaller tubes was the intermittent character of the disturbance. The disturbance would suddenly come on through a certain length of the tube and pass away and then come on again, giving the appearance of flashes, and these flashes would often commence successively at one point in the pipe. The appearance when the flashes succeeded each other rapidly was as shown.*" These 'flashes' of turbulence are now commonly referred to as turbulent puffs or slugs and will be discussed in more detail in section 2.3.

Reynolds' main observation was that for pipes of different diameter and fluids of different viscosity these turbulent structures could first be observed if the dimensionless parameter UD/ν (where U is the mean flow velocity; D is the pipe diameter and ν as kinematic viscosity) was larger than 2000. This non dimensional parameter was later named in his honour as Reynolds number (Re).

Figure 2.1: Intermittent character of transition stages as described by Reynolds (1883)

However in this paper (Reynolds, 1883) there was a caveat -"*the critical velocity was very sensitive to disturbance in the water before entering the tubes.*" He noticed that in a carefully constructed pipe setup this transition was delayed to Re 13000. Reynolds however also proposed that there should be a true critical point where turbulence once created by a sufficient disturbance, becomes sustained indefinitely. In later studies a variety of values of Re were reported for this critical point ranging from 1700 and 2300 (Kerswell, 2005). On the other hand, in absence of additional perturbation in the flow and by minimizing entry disturbances, transition to turbulence occurs at much higher Re and this value is not unique but depends on the ambient noise of the specific setup. In the subsequent sections the latter Re is called natural transition point. Experiments (Pfenniger, 1961) showed that the natural transition Re can be increased upto Re 10^5. In numerical simulations (Meseguer & Trefethen, 2003) the laminar profile was found to be stable upto Re=10^7 and it is generally believed that Hagen-Poiseuille flow is most likely linearly stable for all Re. Hence perturbations of finite amplitude are responsible for the transition to turbulence and this aspect will be discussed in more detail in section 2.2. Another question of interest is how minimum disturbance amplitude that triggers turbulence scales with Re. Recent experiments (Hof *et al.*, 2003) showed that for an injection perturbation this amplitude scales inversely proportional to Re from 2000 to 20000. So transition in pipe flow depends on initial conditions like type and amplitude of the disturbance as well as Re. This observation clearly signifies the complexity of the transition scenario.

The onset of turbulence in pipe flow is marked by a sudden increase in velocity and pressure fluctuations and hence friction factor. Increase of drag or friction factor can lead to less efficient fluid transport which has vast implications in industrial applications involving oil and gas transport through pipelines. The accompanying sudden enhancement of pressure fluctuations can increase structural vibrations causing damage of equipments (Park & Lauchle, 2009). This erratic behavior in transition regime is believed to be one of the reasons behind the growth and ultimately the rupture of aneurysms (Khanafer *et al.*, 2007; Tan *et al.*, 2009). Hence a better understanding of the transition process is not only of academic interest but also for many practical applications such as an efficient turbulence control (el Hak & Tsai, 2005).

2.2 Finite amplitude instability and transient growth

In many early studies of the transition to turbulence linear stability analysis was applied in order to predict hydrodynamic instability and the transition to turbulence (e.g. Rayleigh (1880*a*); Orr (1907a,b); Sommerfeld (1908); Taylor (1923); Heisenberg (1924)). Linear stability analysis was successful in predicting roll formation in circular Couette flow (Taylor, 1923) and onset of hexagon or roll patterns in Rayleigh-Bénard convection (Rayleigh, 1917). In case of pipe flow and plane Couette flow, linear stability analysis yielded no positive eigen values and hence growth of infinitesimal perturbations was ruled out. Therefore the laminar profile of pipe flow is believed to be linearly stable at all Re(Salwen *et al.*, 1980; Drazin, 2002). Other plane shear flows like plane Poiseuille and boundary layer flows are linearly unstable. However turbulence is usually observed below the linear instability threshold. The transition scenario in these

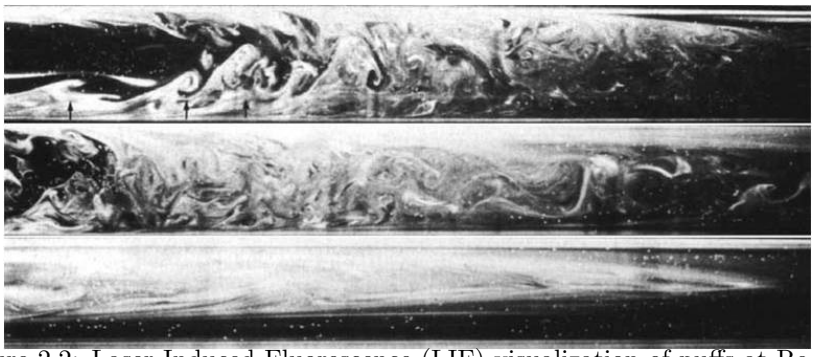

Figure 2.2: Laser Induced Fluorescence (LIF) visualization of puffs at Re 2250 (Bandyopadhyay, 1986). The flow is from left to right.

flows shares many features similar to the pipe flow such as localized turbulent structures (i.e. intermittency). Unlike Rayleigh Bénard convection or Taylor Couette flow, in pipe flow the linear operator is non normal. Non orthogonality of the linearized operator (Grossmann, 2000; Boberg & Z.Brosa, 1988; Brosa & Grossmann, 1999a; Trefethen *et al.*, 1993) can amplify perturbations temporarily by extracting energy from the laminar profile before its decay in the long run. This phenomenon therefore is called transient growth and is believed to be one of the key mechanisms responsible for transition in plane shear flow (Trefethen *et al.*, 1993; Henningson & Reddy, 1994). In pipe flow the fastest growing modes are streamwise rolls and they can create streaks several orders of magnitude larger. Although for the linear system all disturbances eventually decay, the reasoning is that once the disturbances have grown significantly the linear assumption breaks down. It is assumed that non linear instabilities will then give rise to turbulence. Numerical simulations (Meseguer & Trefethen, 2003) showed that at high Reynolds number of 10^7 perturbations can be amplified by several orders of magnitude.

2.3 Puffs and slugs

Localized turbulent structures (figure 2.2) observed in transitional pipe flow are usually referred to as puffs at lower Re (Re$\leq$2400) and slugs for larger Re$\geq$2600. The main difference between these two structures is that puffs maintain more or less constant size whereas slugs grow. Early works of Lindgren (1957, 1969),Wygnanski & Champagne (1973); Wygnanski *et al.* (1975) and Bandyopadhyay (1986) have revealed various features of these localized turbulent structures. In general, puffs are 20-30 D long. Puffs have a distinct laminar turbulent interface at the trailing edge and a not so clear interface at the leading edge (figure 2.3a). From figure 2.3a it is evident that at trailing edge of the puffs the parabolic profile is recovered immediately while at the downstream leading edge of the puff the parabolic profile is recovered slowly. The turbulent activity is strongest in the central region (figure 2.2) and comparatively less intense near the walls (Wygnanski & Champagne, 1973). Also turbulent intensity increases gradually towards the trailing edge where centerline velocity is the lowest. Puffs travel at approximately the mean velocity. The leading edge and trailing edge of puffs move with same speed.

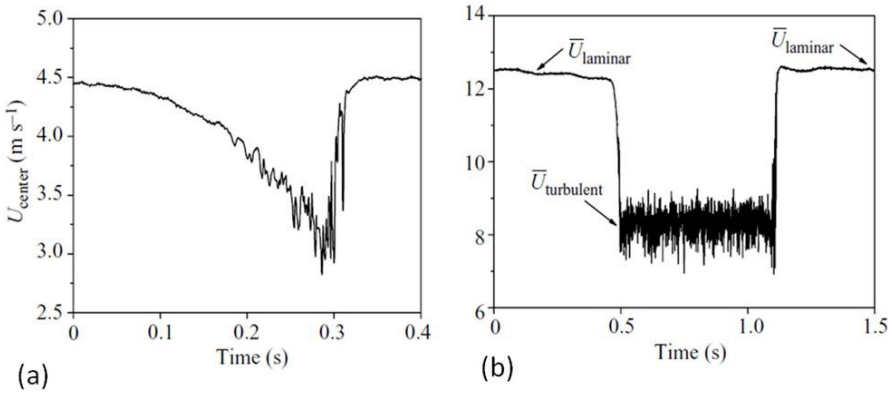

Figure 2.3: (a) Puff and (b) Slug center line velocity signal initiated by iris diaphragm triggering device (Nishi *et al.*, 2008)

In case of slugs, the leading edge is faster than the trailing edge and consequently their size increases as they travel downstream. Turbulent slugs have a distinct trailing and leading edge laminar turbulent interface (figure 2.3b) and the turbulence activity in the core region is uniform. Ensembled averages of the velocity profiles at the leading and trailing edge shows that they are axisymmetric and are blunt around pipe axis (Wygnanski & Champagne, 1973).

2.3.1 Lifetime measurements in Newtonian pipe flow

One salient feature of turbulent puffs is that they only have a finite lifetime. Brosa (1989) in his numerical simulations observed that turbulent states in shear flow occasionally decayed to laminar states. He conjectured that turbulence in shear flows is of transient nature. Such transient behavior is signature of systems which are dynamically a chaotic saddle and not a chaotic attractor (Kadanoff & Tang, 1984; Kantz & Grassberger, 1985; Tel, 1991). With the advancement of computational facilities and experimental techniques, systematic studies were carried out to quantify the transient nature of the puffs (Faisst & Eckhardt, 2004; Hof *et al.*, 2006; de Lozar & Hof, 2009; Kuik *et al.*, 2010; Avila *et al.*, 2010; Willis & Kerswell, 2009; Peixinho & Mullin, 2006). These investigations showed that the probability of a puff decay is independent of the time elapsed since its inception. Therefore the distribution of lifetimes is an exponential distribution, which is a memoryless process. A well known example of exponential process in nature is radioactive decay where the probability of a radioactive substance to decay by a certain amount is independent of previous history. Same exponential dependence applies to the decay of puffs for pipe flow and the probability for a puff to survive after time t at a fixed Reynolds number (Re) is then given by equation 2.1:

$$P(t - t_o, Re) = exp[-(t - t_o)/\tau(Re)] \tag{2.1}$$

where the total observation time since the introduction of perturbation in the flow t and t_o is the time required for the disturbance to transform into a puff. The characteristic lifetime of the puff i.e. the time for which a puff typically travels before it decays is τ (τ^{-1} can be interpreted as the escape or decay rate).

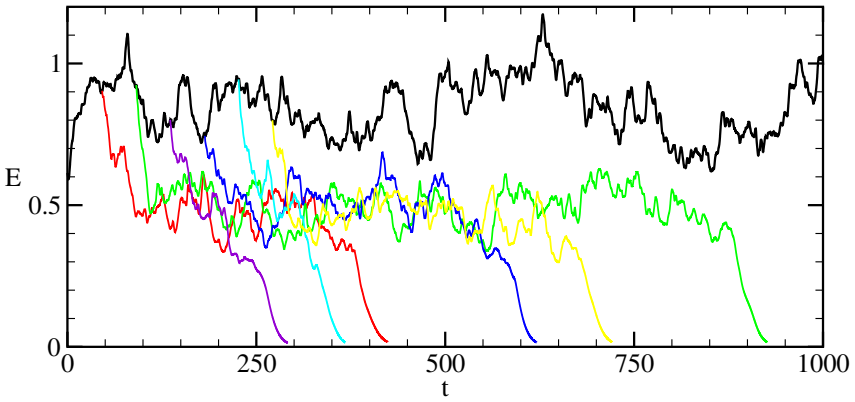

Figure 2.4: Time series of kinetic energy of a turbulent puff. Different colors represent different initial conditions.

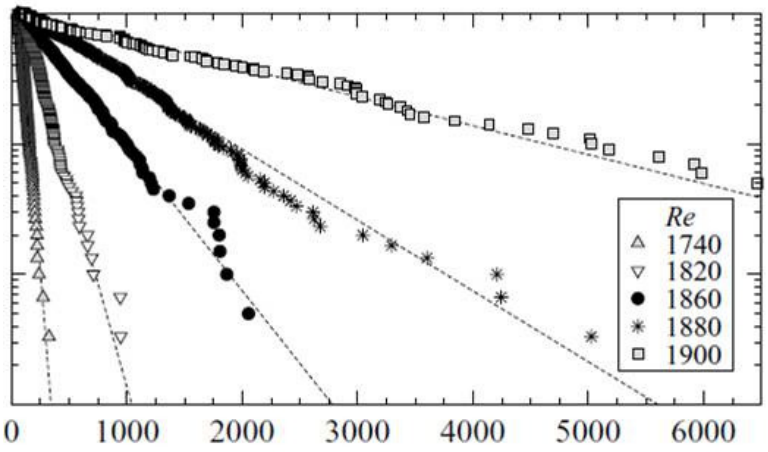

Figure 2.5: Puff survival probabilities at different Reynolds number (Avila *et al.*, 2010).

In the case of radioactive decay, it is common to state the half lifetime which is equal to the characteristic time τ times $ln2$. The exponential decay of localized turbulence has also been observed in other shear flows e.g. Couette flow (Bottin & Chate, 1998; Bottin *et al.*, 1998), Taylor Couette flow (Borrero-Echeverry *et al.*, 2010) and in superfluid turbulence (Schoepe, 2004). Typically there is a short initial period after the flow has been disturbed which is non exponential and depends on initial conditions. However the tail of the distribution soon loses its dependence on initial conditions and become exponential (Hof *et al.*, 2006).

The exponential scaling is a characteristic feature of a chaotic saddle (Eckhardt *et al.*, 2007). Various studies on lifetimes of puffs in pipe flow (Faisst & Eckhardt, 2004; Peixinho & Mullin, 2006; Willis & Kerswell, 2007) predicted that decay rates go to zero linearly with Re so that at a distinct Re puffs will lose their transient nature and become sustained. In terms of dynamical systems, then the chaotic saddle is transformed into a chaotic attractor. However in another study with much longer observation times (Hof *et al.*, 2006) no critical point could be determined and decay rates were observed to only approach zero

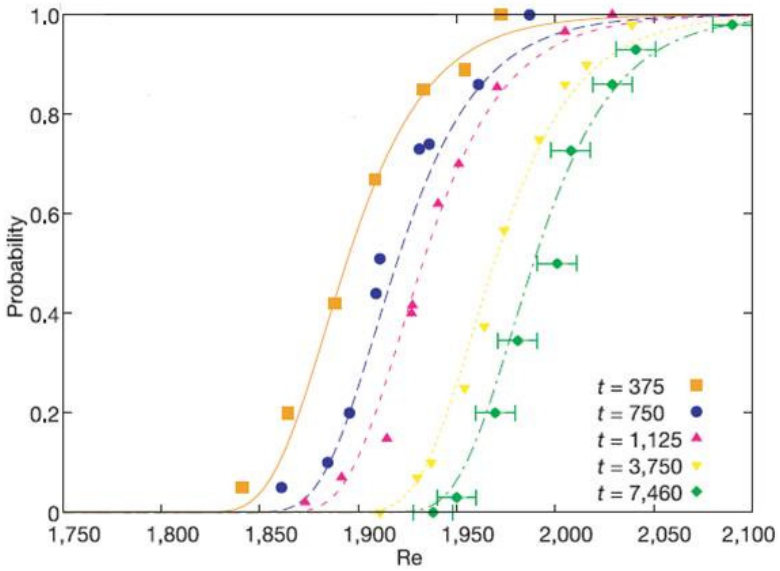

Figure 2.6: Experimental observations on probability for a puff survival (Hof *et al.*, 2006)

asymptotically for Re$\rightarrow \infty$. To resolve these conflicting observations further experimental investigations were carried out with more number of runs to enhance the sample population size and hence reduction of statistical uncertainty. Also the long term drifts in Re settings were reduced considerably by an improved temperature control and the puff detection was automated to avoid human intervention (Hof *et al.*, 2008; Kuik *et al.*, 2010), and these studies confirmed the nondivergence of lifetimes. Furthermore numerical simulations were carried out in large domains with much increased sample sizes (Avila *et al.*, 2010) and excellent agreement with the experimental data (Hof *et al.*, 2008) was found. It has been shown that the lifetime of individual puffs remains finite, which implies that turbulent state remains a chaotic repellor (de Lozar & Hof, 2009). The characteristic lifetime τ increases faster than exponentially with the Re.

Numerical simulations (Avila *et al.*, 2010) showed that puffs decay randomly at various times without any prior indication (fig. 2.4). Probability for a puff survival at a given Re falls on straight line in a loglog plot (fig. 2.5) highlighting its exponential nature. In experimental investigations (fig. 2.6) lifetime measurements were done at fixed pipe length (Hof *et al.*, 2006) for various Re and 'S' shaped probability curves for different lengths are obtained. In one of the studies (de Lozar & Hof, 2009) four different perturbation schemes like jet injection, simultaneous injection and extraction, placing a obstacle in the flow and reduction of Re are used to trigger puffs in the flow. Puff decay rate was observed to be invariant of perturbation schemes in the flow (figure 2.7), which is a feature of a chaotic saddle where the trajectories quickly erase memory of initial conditions.

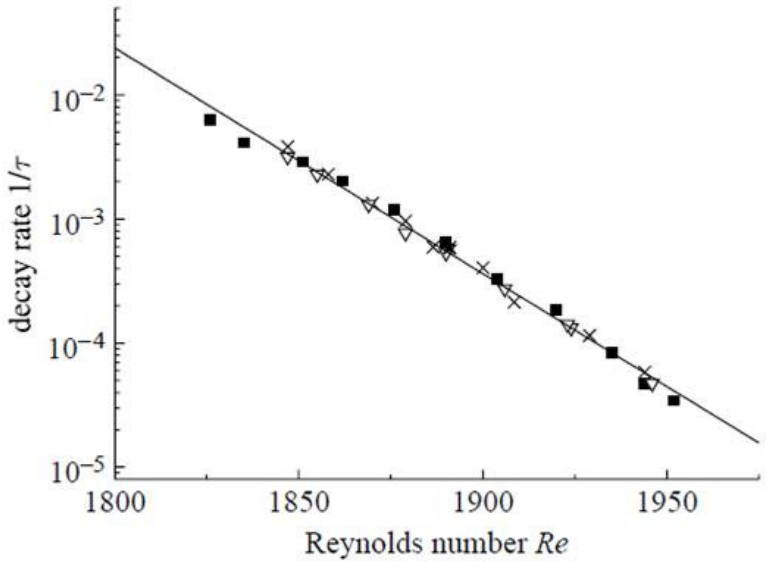

Figure 2.7: The decay rate τ^{-1} vs. Re (de Lozar & Hof, 2009). Different perturbation schemes [Square: injection; cross: injection/extraction; down triangle: decreasing Re; star: obstacle] are used to show invariance of puff decay process on initial conditions

2.3.2 Puff splitting

Puff splitting has been previously reported for Re $\geq$2300 (Wygnanski & Champagne, 1973; Nishi *et al.*, 2008). Avila *et al.* (2011) however showed that puffs already split at much lower Re, only with a much lower probability. Figure 2.8 vividly describes the temporal evolution of a puff splitting process. For sustenance of a turbulent puff, the velocity profile beyond the trailing edge of a puff must be laminar (Hof *et al.*, 2010). However just downstream of a turbulent puff the laminar profile is not yet fully recovered (Hof *et al.*, 2010). Hence turbulence can't be sustained just downstream of a turbulent puff. From figure 2.8 (bottommost) it is observed that new patches of vorticity are generated from the leading edge. Just downstream the parent puff, the patches of vorticity can not sustain themselves in absence of laminar profile (second and third picture from bottom in fig. 2.8) . When these offspring vortices manage to travel sufficient downstream distance where laminar profile is present, new puffs are formed (top picture in fig. 2.8) .

At lower Re $\approx$ 2000 there is a competition between puff decay and splitting process deciding its final outcome of persistently turbulent or laminar state. Therefore, in order to determine the critical Re beyond which turbulence becomes sustained, probability of both puff decay and puff splitting need to be measured. In figure 2.9, lifetime of a puff before decaying and lifetime of a puff before splitting is plotted with Re. At Re $\approx$ 2040 the lifetime for a puff survival is same as lifetime for a puff to split. To the right of the intersection point Re 2040, puff splitting dominates over puff decay resulting net increase in turbulent fraction. Hence the flow regime near Re 2040 can be interpreted as the zone where turbulence becomes sustained from transient state. Below this critical point the flow will eventually turn into fully laminar phase whereas above it

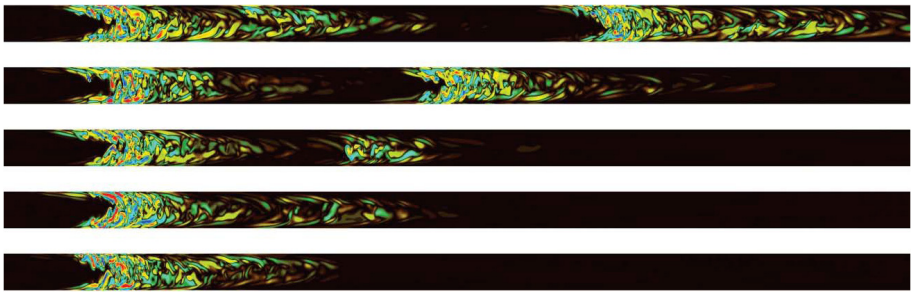

Figure 2.8: Visualisation of a puff splitting process at Re 2300. Temporal evolution is from bottom to top.(Avila *et al.*, 2011)

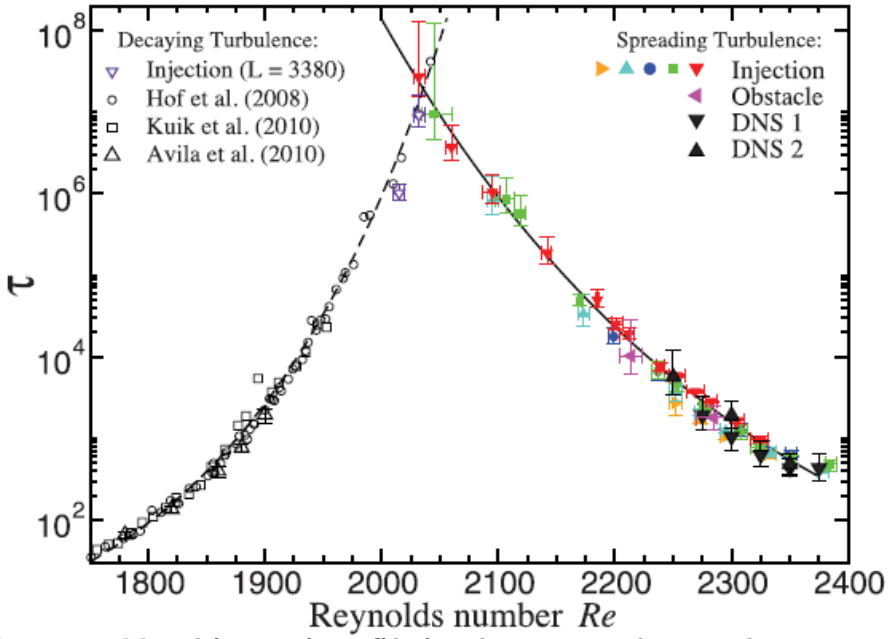

Figure 2.9: Mean lifetime of a puff before decaying or splitting. The two curves intersect at Re 2040 determining the onset of sustained turbulence from decaying state.(Avila *et al.*, 2011)

turbulent fraction will increase with the Re. Therefore Re ≈2040 is the critical transition point to the sustained turbulence.

This phase transition from laminar state to sustained turbulence is analogous to the phase transition observed in coupled map lattices (Kaneko, 1985). Also this study (Avila *et al.*, 2011) unlike previous studies (Moxey & Barkley, 2010; Nishi *et al.*, 2008; Wygnanski & Champagne, 1973) proved that spatial proliferation of chaotic domains does not set in abruptly at a critical Re, rather turbulence has the inherent propensity to grow in the form of splitting even at low Re. At Re>2400 puff dynamics becomes more complex. Besides splitting, growth and merging of individual turbulent segments increase percentage of turbulent fraction downstream. This recent study (Avila *et al.*, 2011) is in contrast with the classical Landau-Ruelle-Takens (Landau & Lifshitz, 1959; Ruelle & Takens, 1971) view of turbulence generation due to successive temporal complexity. Rather spatial growth of turbulent domains is the key factor in sustained turbulence in pipe flow. Therefore splitting and growth of turbulent puffs gradually lead to increase of turbulence fraction in pipe flow. This spatio temporal intermittency in the pipe flow can be linked to directed percolation process (Pomeau, 1986) where the disordered state (turbulence) would invade the laminar one through contamination. In this case laminar state would be 'absorbing' or 'passive' state while the turbulent state would be 'active' or 'contaminant' phase.

Numerical simulations (Moxey & Barkley, 2010) were also carried out to study puff splitting in more detail. Comparison of spatio-temporal intermittency at Re 2250 and Re 2350 showed that turbulent fraction at Re 2250 remains same along the distance whereas the turbulent fraction at Re 2350 increases downstream distance due to higher probability of puff splitting. Since the turbulence at Re 2250 remains independent of domain size, it's called intensive turbulence whereas turbulence at Re 2350 is termed as extensive due to its dependence on domain size.

2.4 Coherent structures and traveling waves

Chaotic turbulent dynamics in the transition stage is the cumulative effect of many simpler unstable periodic solutions. These unstable solutions are believed to evolve the turbulent dynamics and provide the building blocks of the turbulent state. These solutions are analogous to chaotic attractors in dynamical systems. It can be generally shown that chaotic attractors are dense in periodic orbits (Shea-Brown *et al.*, 2006). Periodic orbit theory suggests that out of these infinitely many orbits a finite number will dominate the dynamics(Cvitanovic, 1988; Auerbach *et al.*, 1987; Kawahara *et al.*, 2012). Following this analogy also turbulence should be dominated by a finite number of unstable solutions and this has inspired a quest for simple building blocks for shear flows yielded regular solutions in PC flow (Nagata, 1990; Clever & Busse, 1992, 1997; Waleffe, 2003), plane Poiseuille flow (Ehrenstein & Koch, 1991) in the form of traveling waves.

For pipe flow the first unstable invariant solutions have been identified by Faisst & Eckhardt (2003) and Wedin & Kerswell (2004) as coherent states in pipe flow comprising of different vortex pairs that generate 'n' (where n=1,2,3..) high speed streaks close to wall and 'n' low speed streaks to center (figure 2.10).

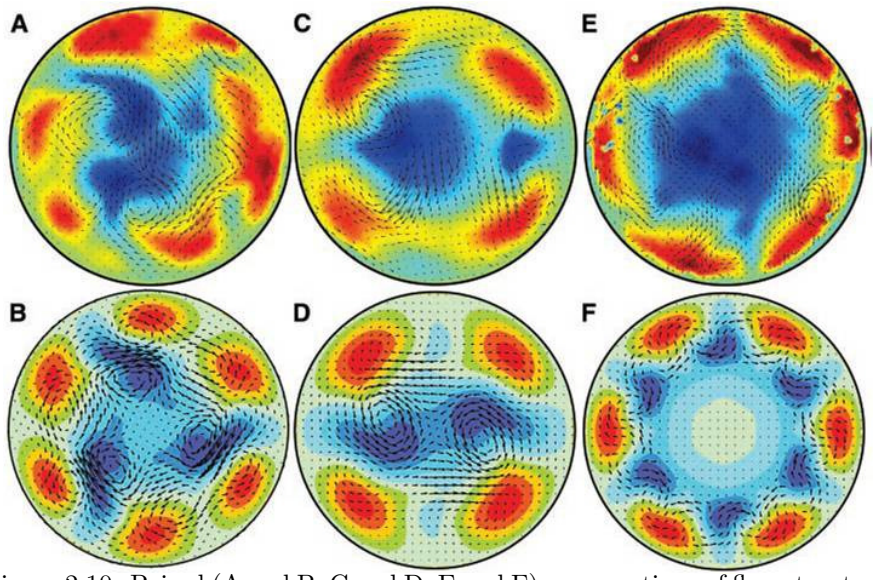

Figure 2.10: Paired (A and B, C and D, E and F) cross sections of flow structures detected experimentally (top row) and numerically determined traveling waves (bottom row)

These high speed streaks stay near to walls. The low speed streaks change shape and wriggle in an azimuthal direction. These different pairs of vortices generate symmetric coherent traveling states. These states have shift and reflect symmetry. The lowest Re at which they appear vary with n. For n=3 the traveling waves appear at Re as low as 1250. For n=2 and n=4 traveling waves are observed at Re 1350 and Re 1600 respectively in numerical simulations. The steep velocity gradients produced adjacent to the wall create higher pressure drop. So the friction factor of the traveling waves is higher than the laminar profile (Faisst & Eckhardt, 2003). Experimentally it was difficult to track individual solutions as they were unstable due to ambient noise in the pipe setup. By PIV, traveling waves of n=2, 3 and 6 of vortex pairs were detected in pipe flow at Re 2500, 2000 and 5300 respectively (Hof *et al.*, 2004) although they were not as periodic as those obtained from numerical simulations.

Energetically these unstable states are sustained by a sustaining mechanism originally suggested for turbulence in wall bounded flows (Hamilton *et al.*, 1995): here stream wise vortices draw faster fluid form center to the walls and slower fluid from wall to the center simultaneously. This creates anomalies in stream wise velocities generating inflexionally unstable streaks. Non linear self interaction of these unstable modes regenerates stream wise vortices completing the feedback loop and sustaining the flow states against viscous dissipation. The traveling waves are a signature of this self sustaining process.

2.5 Edge of chaos

To trigger turbulence in the transition stage perturbation has to be of sufficient amplitude, otherwise the perturbed state will decay very quickly. The so called edge state marks the boundary separating the perturbations strong enough to create turbulence from those which are unable to. By monitoring the lifetimes of

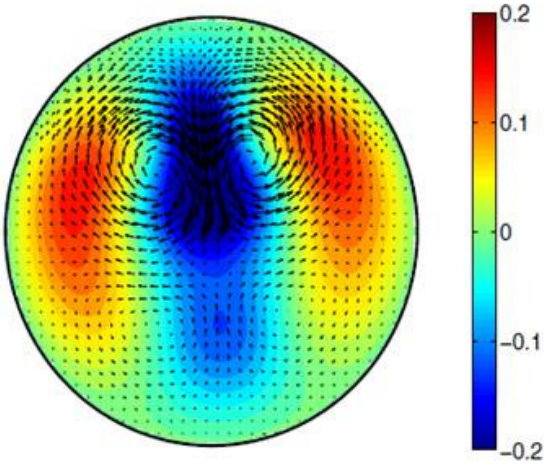

Figure 2.11: Edge state at Re 2875. Contour plot of streamwise velocity. Red regions are faster than the mean parabolic profile and blue is slower. Vectors indicate in-plane velocity (Schneider *et al.*, 2007)

the perturbations at a given Re the edge is constructed. The edge is not monotonically smooth and has sudden kinks. The unique time invariant dynamical state energetically different from both laminar and turbulent states existing in the edge of chaos is called edge state. Edge states in the flow field have two high speed streaks and a corresponding pair of counter rotating vortices adjacent to wall (figure 2.11). Isosurfaces of the axial vorticity showed that the dynamics doesn't settle down to periodic or quasiperiodic traveling waves.

Chapter 3

Introduction to Non Newtonian pipe flow

Out of a broad class of non Newtonian fluids, this chapter focuses on dilute polymer solutions in pipe flow. Due to the drag reduction capacity of polymers in wall bounded flows, this subject has received considerable attention. In this chapter we discuss the relevant literature of polymer drag reduction and earlier studies on transition in pipe flow of polymer solutions.

3.1 Drag reduction (DR)

Since Toms (1948) discovered that addition of high molecular weight flexible chain polymers like PEO (polyethylene oxide) or PAAM (polyacrylamide) to a Newtonian solvent can drastically reduce the drag by upto eighty percent, a vast amount of literature on polymer drag reduction (DR) has been generated. DR due to polymers is also known as 'Toms effect'. It is worth mentioning that Mysels (Mysels, 1949) noticed the DR effect at the same time but published later due to the ongoing second world war. The earliest evidence of DR was observed in works on paper pulp transport, although the investigators overlooked its significance (Forrest, 1931; Brautlecht & Sethi, 1933; Brecht & Heller, 1939). DR in bounded flows can also be achieved through addition of solid particle suspensions (Vanoni, 1946), biological additives (Hoyt & Soli, 1965), surfactants (Savins, 1967*b*), bubbles (den Berg *et al.*, 2007)in the flow and sensor actuation or surface modification among many strategies (Choi & Karniadakis, 2003; el Hak, 1980). From a fundamental viewpoint, detailed understanding of polymers interaction with turbulent structures can provide more insight into self-sustaining cycles of wall turbulence and eventually more efficient DR methods.

DR during fluid transport is one of the active areas of interest due to its huge implication on expenditure of transport of oil and gas through pipelines. Examples of applications and potential areas of interest include the annulus between the drill and the wall while drilling for oil (Draad *et al.*, 1998), increase of fluid discharge rate in fire fighting devices, improved marine propulsions and possible medical applications like prevention of hemorrhagic shock (Kamenva *et al.*, 2004), improvement of flow through arterial stenoses (Unthank *et al.*,

Figure 3.1: Trans Alaskan Pipeline system (TAPS) extended over 800 miles.

1992), fluid mechanics of dilute polymer solutions has been an active area of interest. One of the successful applications is the 800 mile long Trans Alaskan oil pipeline (figure 3.1) where addition of polymers has substantially reduced the expenses of oil transport (White & Mungal, 2008). Use of polymers on submarines showed that speed can by increased by 10-15 % but the benefits are overshadowed by logistics costs (Council, 1997). Even in nature, it was observed that the fish slime which has an important contribution in drag reduction during fish locomotion, contains polymers (Povkh *et al.*, 1979).

3.1.1 Onset of DR

Early studies of DR showed that skin friction reduces only when the flow is turbulent. No noticeable change in the skin friction is observed when the flow is laminar. This implies that mutual interaction of polymer dynamics and turbulence results in drag reduction. It has also been observed that the onset of DR depends on the number of monomers in the macromolecule of the polymer in the flow (White & Mungal, 2008). Based on experimental observations and theoretical considerations (Hershey & Zakin, 1967; Lumley, 1969) it has been shown that DR starts when the polymer relaxation time λ (i.e. average time taken for a stretched polymer to restore its coiled configuration) is greater than time scale of wall turbulence $\lambda > \frac{\mu}{\rho U_\tau^2}$ where μ is fluid viscosity, ρ is fluid density and $U_\tau = \sqrt{\tau_w/\rho}$ is wall friction velocity and τ_w is wall shear stress. Therefore the onset of DR happens when the ratio of the two time scales, defined as wall shear Weissenberg number $We_\tau = \frac{\lambda \rho U_\tau^2}{\mu}$ exceeds unity. Berman (1977) showed that the onset We_τ ranges from 1 to 8 depending upon properties of the polymer and the solvents. Theoretical studies (Goldshtik *et al.*, 1982) showed that the onset We_τ are 1 and 5-6 for Maxwell model and Oldroyd B model respectively with a ratio of solvent viscosity to solution viscosity=0.9.

Although the reason for the onset of DR has not been fully resolved, two

schools of thought have emerged since its discovery, one emphasizing on viscous effects (Lumley, 1969; Lyvov *et al.*, 2004; Ryskin, 1987) whereas the second group advocates elastic effects (Joseph, 1969; Tabor & de Gennes, 1986). The first category argues that when the polymer relaxation time becomes greater than the characteristic time scale of wall turbulence, polymers adjacent to the wall are substantially stretched which is known as coil stretch transition. Due to polymer stretching elongational viscosity increases almost by four orders of magnitude (Metzner & Metzner, 1970; Landahl, 1973; Hinch, 1977). The effect of this increase is predominant adjacent to walls due to high extensional strain rates. The increased extensional viscosity is believed to suppress turbulent fluctuations, increase the buffer layer and finally reduce wall friction. On the other hand, the proponents of elastic theory claim that the randomly fluctuating strain rates in turbulent flows cannot cause full stretching of polymer chains. Consequently no coil stretch transition would be happening in the flow. Experimental studies (Smith & Chu, 1998) also showed that moderate stretching of polymers is the norm even under rapid strain rates. Hence moderately stretched polymers cannot result in an appreciable change of viscosity. Therefore, the onset of DR occurs when the stored elastic energy of the partially stretched polymers becomes comparable to the turbulent kinetic energy. With decreasing length scales the elastic energy increases whereas turbulent kinetic energy decreases. When the elastic energy becomes comparable with the turbulent kinetic energy, the classical Kolmogorov energy cascade is then terminated prematurely and the scales below this cutoff scale act elastically (Joseph, 1990). This causes an increase of the buffer layer and subsequent DR. In the previous studies by Sreenivasan & White (2000) and Gennes (1990) it was found that the elastic energy of polymers per unit volume was dependent on polymer stretching and number of monomers of polymers in unit volume or concentration. It was argued that for solutions with very low polymer concentrations, the scale at which elastic energy is equal to turbulent energy is less than Kolmogorov scale. So no effect of DR is observed at very low polymer concentration. With increase of polymer concentration the cutoff scale increases and minute stretching of polymers leads to DR. Onset of DR happens adjacent to the pipe wall, not in the core region (Sreenivasan & White, 2000; Cadot *et al.*, 1998). Numerical simulations of channel flow with polymer solutions (Min *et al.*, 2003, 2004) showed that elastic effects should be considered in correct prediction of onset of DR.

3.1.2 Maximum Drag Reduction (MDR) Asymptote

DR is typically found to increase with increase in flow rate, polymer concentration (Virk *et al.*, 1970), polymer molecular weight (White & McEligot, 1970) and decrease in pipe diameter (Dodge & Metzner, 1959). However, there is an upper bound on DR called the Maximum Drag reduction asymptote (MDR) or Virk's asymptote (figure 3.2). For a given polymer concentration, the friction factor($f = \Delta p/(1/2\rho U^2 L/D)$, where Δp is the pressure drop over a length L ,ρ is the fluid density, D as pipe diameter and U being the mean velocity) settles down to MDR asymptote and remains there even in case of further increase of Re. Also, for a given Re the friction factor does not go below MDR on further addition of polymers to the Newtonian solvent.

An alternative way to plot friction factors, also known as Prandtl-Kármán

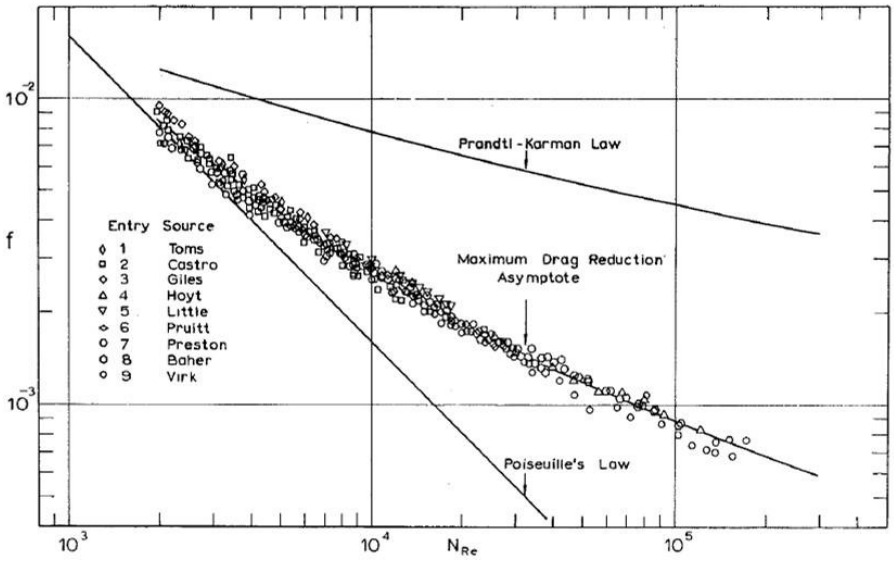

Figure 3.2: Friction factor vs. Reynolds number with MDR asymptote (Virk *et al.*, 1970).

coordinates is to plot $1/\sqrt{f}$ versus log (Re$\sqrt{f}$)(figure 3.3). The ordinate $1/\sqrt{f}$ can be interpreted as ratio of bulk velocity to wall shear velocity ($U_{bulk}/\sqrt{2}U_\tau$) and abscissa $Re\sqrt{f}$=$\sqrt{2}(dU_\tau)/\nu$ is the ratio of pipe diameter to turbulent length scale (ν/U_τ). Prandtl Kármán coordinates are often used for pipe flow since most of the polymer dynamics takes place in the near wall region where wall shear velocity and turbulent length and time scales (ν/U_τ^2) are relevant parameters. As shown in figure 3.3 for this choice of coordinates , the DR regime shows higher values of$(1/\sqrt{f})$ than turbulent flow eventually reaching the upper MDR bound.

Till date, no universally accepted theory is available for explaining the MDR asymptote. Initially it was thought that at MDR, polymer chains in high concentration polymer solutions mutually overlap and make the strain rate dependent stretching mechanism ineffective (Sreenivasan & White, 2000). However experimental investigations showed that MDR is reached at concentrations much lower than the overlap concentration. There are two phenomenological explanations: (a) MDR takes place when polymer effects are felt through the entire spectrum of turbulence, resulting the buffer layer thickness to spread across the whole boundary layer (Sreenivasan & White, 2000; Virk, 1975) and (b) MDR occurs when Reynolds stresses are strongly suppressed and polymer stresses sustain turbulence in the flow (Min *et al.*, 2004; Ptasinski *et al.*, 2001; Warholic *et al.*, 1999).

3.1.3 Velocity statistics and Reynolds stress:

The DR phenomenon is sometimes divided into two regimes : LDR (low) and HDR (high). DRs greater than 40 % is termed as HDR (Warholic *et al.*, 1999; Dubief *et al.*, 2004.). Experimental and numerical investigations in the LDR regime have revealed that the log law region of mean streamwise velocity shift

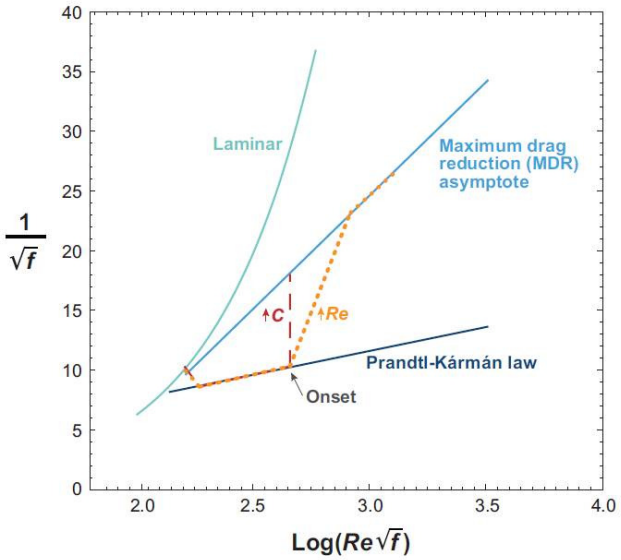

Figure 3.3: Different trajectories of laminar, fully turbulent and MDR are illustrated. The red dash line symbolizes the upper bound on drag when Re is fixed and polymer concentration is varied. The yellow trajectory symbolizes the saturation of DR capacity when Re is increased keeping the concentration varied (White & Mungal, 2008).

more upward with increasing DR but stay parallel to the Newtonian case (figure 3.4). However in recent studies it has been claimed that the upward shift is not exactly parallel to the logarithmic profile, rather an increase in the slope with the DR (White *et al.*, 2012; den Toondner *et al.*, 1997; Escudier *et al.*, 1999). With increase of DR there is an increase in peak of streamwise velocity fluctuations ($\overline{u'^2}$) and a reduction of wall normal ($\overline{v'^2}$) and spanwise ($\overline{w'^2}$) velocity fluctuations as well as Reynolds stress ($-\rho\overline{u'v'}$). Strong reduction of transverse velocity fluctuations indicate that the polymers affect the vortices preferentially which are responsible for fluctuations in wall normal and spanwise direction (Dubief *et al.*, 2004.).

In case of HDR there is an increase in slope in the log region of the mean streamwise velocity profile, a decrease of the peak of streamwise velocity fluctuations and an increase in the contribution of the polymer shear stress to the maintenance of turbulence (figure 3.4). According to previous studies (Virk *et al.*, 1970; Virk, 1975) the mean velocity profile during MDR can be divided into three radial zones: (a) the viscous sublayer which is the layer adjacent to the wall. This layer is similar to Newtonian cases implying the absence of polymer dynamics in this layer. The normalized mean streamwise velocity profile is: $u^+=y^+$ where $y^+<15$. Here u is normalized by the wall shear velocity $U_\tau=\sqrt{\tau_w/\rho}$ and the height from the wall is normalized by the turbulent length scales near the wall ν/U_τ.

(b)The elastic sublayer is the zone where the DR mechanisms take place. In this radial zone, increase of axial streamwise velocity fluctuation and decrease of radial velocity fluctuations, turbulent shear stress and u-v correlation coefficient

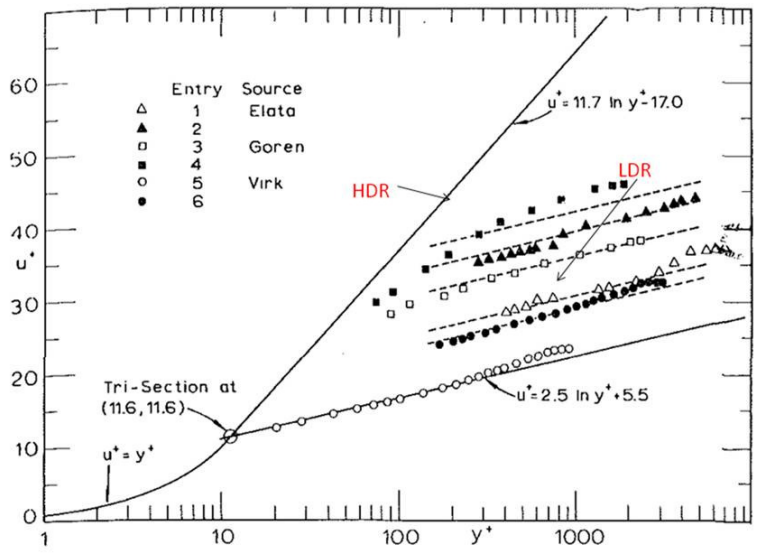

Figure 3.4: Mean velocity profiles during drag reduction (Virk *et al.*, 1970)

take place. The reduction in the u-v correlation coefficient signifies the reduction in radial transport of axial momentum and turbulent kinetic energy. With increasing DR the peak of the streamwise velocity fluctuations shifts away from the wall (Warholic *et al.*, 1999). Here the normalized mean streamwise velocity profile is u^+=11.7lny^+−11.70 for 15<y^+<60.

(c) The outermost region is known as Newtonian plug region where the turbulence features during DR are similar to Newtonian turbulence. Outside the elastic sublayer, due to less shear polymer stretching is minimal. In this region, the velocity profile is similar to the Newtonian log law: u^+≈2.5lny^++5.5 for y^+>60. However it must be noted that the plug region is minimized in the MDR region and the elastic sublayer is extended almost to the central axis of the pipe.

One of the main features of polymer DR is the reduction of Reynolds stress which is responsible for the momentum transfer from the mean flow to the turbulence. Therefore Reynolds stress is an important quantity during DR studies. In experiments determination of Reynolds stress ($-\rho\overline{u'v'}$) is generally done by LDV based single point measurements or instantaneous velocity fields obtained by PIV measurement techniques. The total shear stress ($\overline{\tau}$) can be written as the sum of the mean shear ($\mu\ \frac{\partial U}{\partial y}$), the Reynolds shear stress and the polymer shear stress ($\overline{\tau_{xy}^p}$): $(\overline{\tau})=(\mu\ \frac{\partial U}{\partial y})-\rho\overline{u'v'}+(\overline{\tau_{xy}^p})$

The instantaneous flow velocity $u(x,y,z,t)$ can be decomposed into mean velocity ($\overline{u(x,y,z)}$) and fluctuating component ($u(x,y,z)'$). Subsequently the role of polymer shear stress can be indirectly estimated if the remaining two stress components ($\mu\ \frac{\partial U}{\partial y}$) and $-\rho\overline{u'v'}$ are measured from experiments. Warholic *et al.* (1999) found total extinction of Reynolds stress for high DR>64 % over most of the channel section except y/H<0.1 while for lower DR regimes Reynolds stress is present in the center of the channel. Other studies (Dubief *et al.*, 2004.; Min *et al.*, 2004; Ptasinski *et al.*, 2001) showed that although Reynolds stress

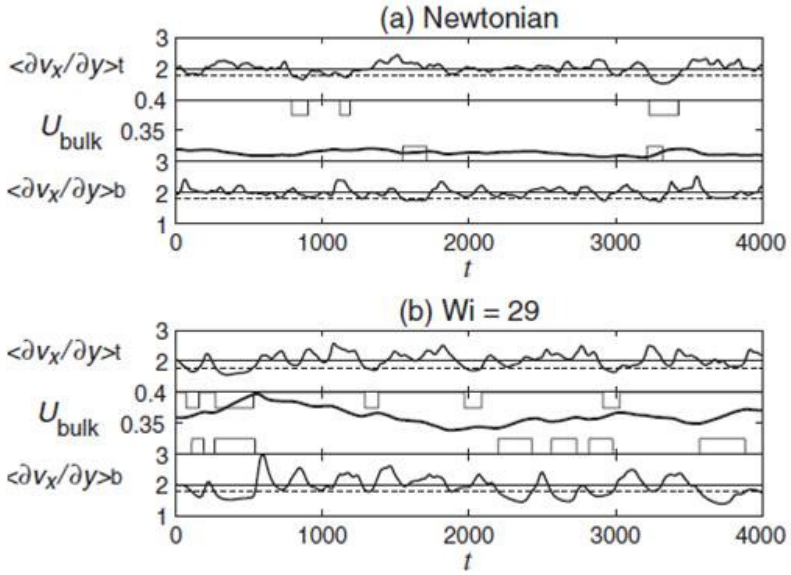

Figure 3.5: Mean shear rates at top (t) and bottom (b) walls of channel are presented. Threshold of shear stress is considered 1.8. Below this threshold, if the shear stress drops for time period of t=50, then that duration is hibernating period. Comparison of top figure (a) Newtonian and (b) drag reduction regime of Wi =29 shows that hibernating periods are more frequent in the drag reduction regime. In the hibernating periods, noticeable increase in bulk velocity is noticed. (Xi & Graham, 2010).

is strongly suppressed, it has a finite contribution in the flow.

3.1.4 Hibernating and Active turbulence

Recent numerical studies (Xi & Graham, 2010) in turbulent channel flow of drag reducing polymers showed that the turbulent activity varies over time. The time when the turbulence activity is high i.e. Reynolds stress and wall shear are high and streamwise velocity is low is called active period (figure 3.5). During the active period streamwise vortices are highly three dimensional with abundant low speed streaks. On the contrary, the period when the centerline velocity is high with lower wall shear is called hibernating period. During hibernating turbulence only weak streamwise vortices are present with almost no streamwise variation and a comparatively much smaller number of low speed streaks. The interpretation given by (Xi & Graham, 2010) is that in the active periods the polymer chains are substantially stretched resulting in a reduction of Reynolds stresses and hence the hibernating period starts. In the hibernating period polymer molecules regain the original configuration. Eventually turbulent fluctuations start to grow and the active period starts resulting in a stochastic cycle of active and hibernating turbulence. It is argued that hibernating periods are few and far between in Newtonian turbulence (Webber *et al.*, 1997). In non Newtonian fluid flows during active events polymer chains are substantially stretched in spanwise and transverse directions which mainly contribute to streamwise vortex suppression (Xi & Graham, 2010). This leads to

reduction in the duration of active events even though the duration of hibernating periods are not affected by polymer interaction and shown to be insensitive to Weissenberg number. Therefore, inspite of increase in the fraction of duration of hibernating events increase over We, there is no significant change on addition of more polymers or higher molecular weight or longer molecular chain polymers. Thus at MDR, the saturation point of the DR capacity due to polymers is achieved.

Subsequent studies (Xi & Graham, 2012) explored potential connections between edge states and MDR. It is shown that edge states at low Re are unaffected by viscoelasticity. The edge states are weakly three dimensional and minimum stretching of polymers takes place. The mean velocity profile in the edge states matches with experimentally observed mean velocity profiles at MDR. Strong similarity of flow structures e.g. extremely weak vortices, almost streamwise invariant streaks and extremely low Reynolds stress during both hibernating events and edge states has been observed leading to a suggestion that hibernating events are excursion towards the edge state. Hence a possible connection between edge states and the MDR asymptote has been proposed.

3.1.5 Early turbulence and transition delay

In the seventies of the twentieth century several investigators observed an increased drag (with respect to the laminar value) for polymer solutions at low Re i.e. in regimes where for Newtonian fluids no turbulence can be sustained. This phenomenon was coined as early turbulence (Forame *et al.*, 1972; Zakin *et al.*, 1977). This phenomenon was believed to happen when large shear rate is achieved due to pipe of sufficiently small diameter and large solvent viscosity. In a previous study (Ram & Tamir, 1964) it was shown that the onset of early turbulence is a function of shear stress and not Re. It was also observed that the critical Re for onset of early turbulence decreases with increasing molecular weight, concentration and capillary diameter(Ram & Tamir, 1964). Early transition sets in irrespective of inlet disturbances (Hansen *et al.*, 1974). Pressure measurements show that smooth transition takes place to turbulence with reduced drag. No large pressure fluctuations due to intermittent puffs or slugs in Newtonian cases are observed (Zakin *et al.*, 1977). In the work of Zakin *et al.* (1977) a deviation from the laminar pressure scaling was observed at Re 1400. It has been observed that even when no pressure rise can be detected, the increase of the turbulent intensity from the laminar level and the flattening of the velocity profiles are two salient features to track the onset of early turbulence.

Studies of transition in Non Newtonian pipe flow have been focused on the effect of polymers on transition delay or enhancement. Theoretical studies (Porteous & Denn, 1972a) using the Maxwell model showed that elasticity in the polymer solutions can reduce the critical Re below which there will be no linear growth of disturbances. On the other hand calculations with rod like suspensions predicted transition delay (Bark & Tinoco, 1978). These behaviors are related to coiled and stretched polymer configuration respectively. Experimental studies (Virk & Wagger, 1990) classified drag reduction behavior of two types : Type A for coiled configuration and type B for stretched configuration where transition delay was observed. In extensive experimental studies carried out by Draad *et al.* (1998) it was reported that for a pipe setup with natural transition Re $\approx$ 60000 for water, fresh polymer solutions with stretched confor-

mation exhibited natural transition at Re≈8000 and degraded as well as coiled configuration polymer showed transition at Re ≈ 30000. Decrease in natural transition number for polymers was not clear and attributed to a non optimal shape of the contraction of the settling chamber or a possible destabilization of the boundary layer in the entry region due to elastic effects (Porteous & Denn, 1972a,b). For stretched polymers the friction factor smoothly deviated from the laminar profile without showing any characteristic jump present during Newtonian transition. However mechanical degradation of the same polymer solution showed the jump in friction factor. Regarding artificially triggered transition polymers showed stabilizing effect i.e. transition happened at higher Re than water(Draad *et al.*, 1998). The stabilizing effect decreases with the increase of salt content in the polymer solution resulting more coiled configuration of the polymers.

3.2 Discussion

Based on the discussions in the previous sections of this chapter, it can be summarized that the reasons for onset of DR have been mainly attributed to either enhancement of elongational viscosity effects or elastic effects due to stretching and coiling of the polymer chains. In spite of substantial experimental and numerical observations on Reynolds stress, velocity profile and velocity fluctuations no universally acceptable theory for MDR asymptote exists. Numerical simulations of Xi & Graham (2010) have suggested that alternating active and hibernating turbulence events observed in minimal flow units may be linked with MDR. Besides DR, early deviation from laminar profile at Re below onset of Newtonian turbulence i.e. early turbulence was reported in pipe flow of dilute polymer solutions. Onset of early turbulence was observed to be dependent on shear stress. Stability analysis showed that elasticity reduces the natural transition number whereas polymer solutions show transition delay when the flow is artificially perturbed.

In the present thesis different transition scenarios with varying polymer concentration and flow geometry are studied. Subsequently the DR capacity of solutions of varying polymer concentrations is measured. Attempts are made to explore plausible causes behind MDR. Experimental investigations on hibernating and active turbulence events at MDR state is also carried out. Experimental observations on transition delay during artificial triggering and early turbulence have also been reported. The experimental results and discussion is presented in chapter 6 of this thesis.

Chapter 4

Experimental setup

4.1 Introduction

This chapter contains a description of the experimental setup used for studies of the transition to turbulence in Newtonian and Non Newtonian pipe flow. In section 4.2 the construction and design of the pipe setup used for Newtonian fluids are described. In addition the instrumentation for temperature control, pressure drop measurements and flow visualization techniques are also described in this section. In section 4.3 the Non Newtonian pipe flow setup and the characterization of Non Newtonian fluids i.e. rheometry are discussed. The rheometry of the Non Newtonian fluids has been carried out in the Lab of Professor Christian Wagner at the University of Saarbrucken. Overall, this chapter contains information on the subtleties required in successful implementation of experiments in Newtonian and Non Newtonian pipe flow.

4.2 Newtonian Pipe flow setup

4.2.1 Pipe

Figure 4.1 is the schematic of the experimental setup used for studying transition in Newtonian pipe flow. The setup consisted of a 6 m long glass pipe of 1 cm diameter. The flow system was pressure driven. Flow velocity can be changed by varying the height of the reservoir placed before the pipe entrance. At the pipe exit, the working fluid was collected in another container and recirculated back to the reservoir by a pump.

In order to allow us to study the response of the laminar flow to external perturbations, flows should be laminar upto sufficiently high Re. Therefore disturbances that originated from the setup e.g. the pipe entrance, pipe joints etc. had to be minimized. In particular, the pipe inlet had to be designed carefully to increase the 'natural transition number'. In order to minimize inlet disturbances, a settling chamber was used before the pipe entrance (figure 4.2). The settling chamber was made from Plexiglas. The chamber consisted of a 200 mm long cylinder with a diameter of D =100 mm. There were three screens within the cylinder. The screens were used to break down turbulence to dissipative scales. The three screens were made of stainless steel and the mesh size was 1

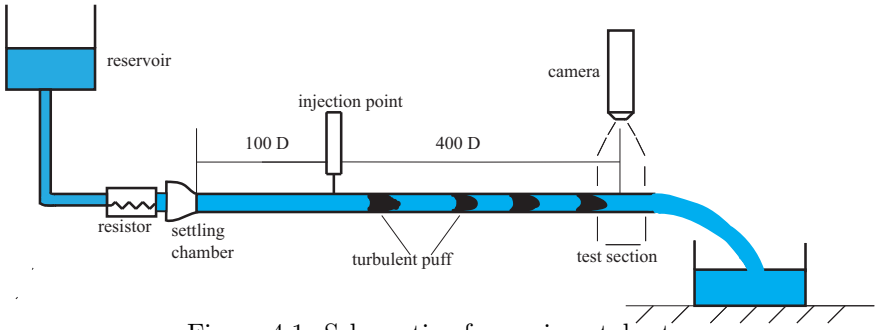

Figure 4.1: Schematic of experimental setup

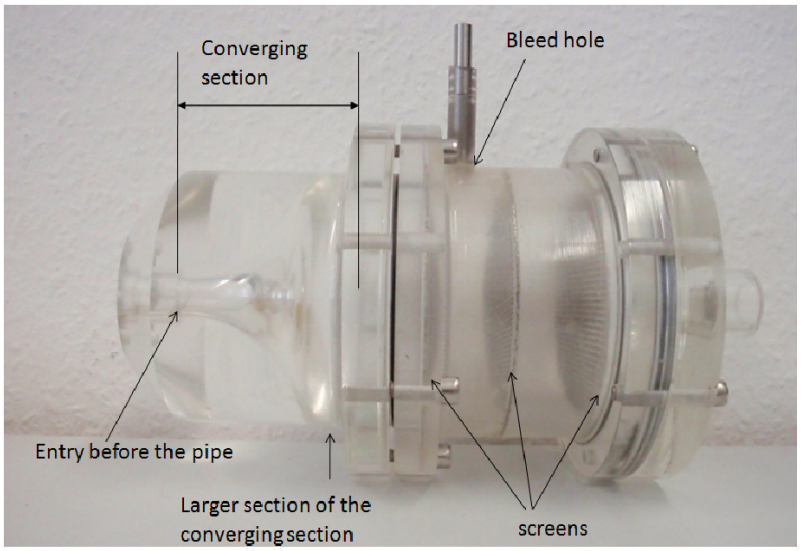

Figure 4.2: Settling chamber used in our pipe setup

mm, denoted as 'fine' screens. Regular cleaning of these meshes was done for better performance of the settling chamber.

The settling chamber had a converging section at the pipe entry. The contraction of the converging section was essential in suppressing flow non-uniformities. Using Bernoulli's theorem (Ward-Smith, 1980) it can be shown that the velocity fluctuations with respect to mean flow velocity is proportional to the fourth power of the diameter ratio (diameter of smaller section/ diameter of larger section). In our case the outer section was 10 cm whereas the smaller section was 1 cm. So the efficiency of suppression of the axial velocity fluctuations is 10^4.

For optimum performance of the settling chamber no air bubble should be trapped in the settling chamber. This could be achieved by the following procedure. Once the pipe was fully filled with water, the reservoir was set to the maximum height ($\approx$2 m) to generate high pressure. Then the pipe exit section was blocked with a rubber stop and the bleed hole in the settling chamber (figure 4.2) was opened to remove the entrapped air. Smaller bubbles got dissolved in the fluid once the pipe flow resumed for some time. Once the settling chamber was devoid of bubbles, attention could be diverted to other parts of the experimental setup.

Pipe sections were connected with specially machined connectors (figure 4.3)

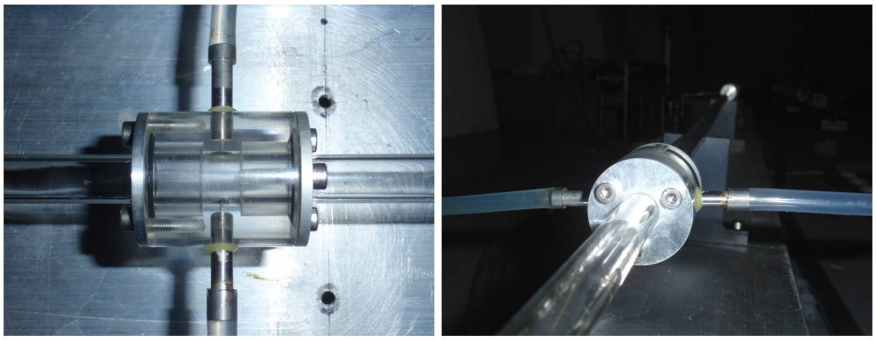

(a) (b)

Figure 4.3: (a) Top view and (b) Side view of a connector

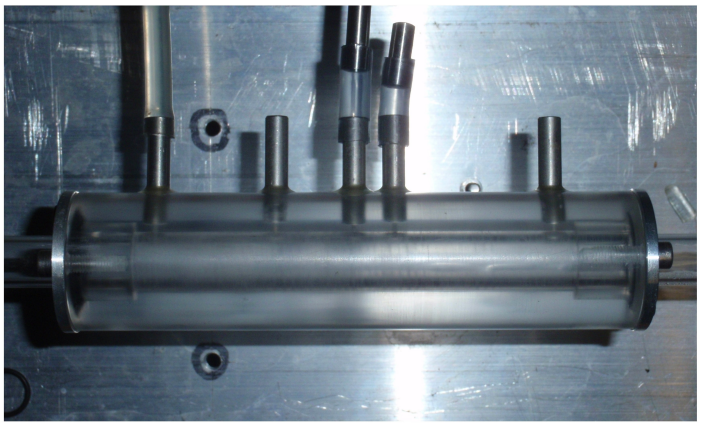

Figure 4.4: Connector with multi holes on side walls

with the same inner diameter that had 0.5 mm holes which could be used either for pressure drop measurement or for jet injection to disturb the flow. O rings were used when pipes were inserted in the connectors. Circular Aluminum plates were used on both sides of the connector to compress the O rings. Figure 4.4 shows a connector with multi holes where pressure drop measurements could be carried over lengths of 3 D and 10 D respectively. The junctions were carefully machined to avoid disturbances in the flow. Care was taken to avoid any gaps at the joints. A flat aluminium profile formed the base of the pipe and provided a flat horizontal level. The pipe was held at a fixed distance of 10 cm above base profile using aluminum supports that were screwed to the base and allow for horizontal alignment of the pipe. In the absence of external perturbations, flow remained laminar up to Re=8000. Measurements of flow velocity and the time required of turbulence to arrive at the pipe exit showed that at the natural transition Re, turbulence was triggered at the pipe inlet and not inside the pipe itself.

When the flow changed from laminar to turbulent, the drag increased and consequently the flow rate in gravity driven pipe was reduced. This undesired

effect was minimized by circulating the water through a big flow resistance (in our case a tube of small diameter) before entering the pipe. Since $\approx$ 96 % of the pressure drop occured over this entrance resistance, the mean flow was virtually unaltered by the increase of drag during transition in the pipe. Detailed flowrate measurements showed that in the present setup the Reynolds number decreased by less than 10 when the flow was changed from laminar to intermittent. If the flow was in a steady state (i.e. laminar or intermittent at a fixed turbulent fraction), so either before or shortly after such a reduction, instantaneous pressure measurements (Validyne DP45 low pressure transducer) showed that fluctuations in the flow rate and hence in Re were smaller than Re $\pm$ 1.

Distilled water was used as the working fluid. Prevention of algae growth is very important in these experiments as the liquid properties as well as pipe surface roughness properties may change due to algae or biofilm growth. Biofilm formation can cause reduction of internal pipe diameter leading to erroneous calculation of Re. Algae growth was prevented by adding 300 ppm of sodium hypochlorite. Viscosity change due to addition of sodium hypochlorite was negligible. The distilled water was kept for one day in a separate container to avoid the formation of air bubbles. Presence of bubbles is undesirable as it may trigger turbulence and hamper the study of puff generation and generate unwanted fluctuations in pressure drop measurement.

The mean flow velocity was determined by weighing the mass of discharged fluid over a period of time (typically 60 s). The flow velocity was regulated by altering the height of a reservoir tank connected to the pipe. The reservoir tank had a large surface area (90x40 cm^2) to minimize the drop in water level during one pump cycle. To maintain constant pressure head a pump was employed at the pipe end that periodically recirculated the water to the reservoir. To increase the accuracy even further a second pump of lower capacity could be placed in the reservoir tank itself which continuously circulated water to a smaller bucket which constantly overflowed thereby maintaining constant height and supplied the fluid for the pipe.

4.2.2 Temperature control

For any controlled study of laminar turbulent transition regime, maintenance of constant Re is essential. Re is inversely proportional to viscosity which is strongly dependent on temperature. In order to reduce temperature fluctuations that alter the liquid viscosity, the water was circulated through a heat exchanger (figure 4.5 b). While the working fluid passed through the smaller copper tubes in the cylinder, temperature controlled water was pumped through the large surrounding tube using a commercial thermostat (Lauda RK20) which was set to 20 ± 0.01^oC. In the outer portion of the cylinder a bleed valve was present. Bubbles should be taken out through this valve for faster heat exchange between the working fluid and the fluid running through the tubes in the outer periphery. After a brief period of running the pipe, the working fluid was uniformly heated. The temperature of the water was continuously monitored by a PT100 thermal probe which showed typical variations of 0.1 K over 3-4 h. Repeated measurements showed that Re variations were less than $\pm$0.5% over a 3-4 h period. In addition to the heat exchanger, the pipe was insulated by polystyrene foam. The largest variations in Re were caused by long term

(a)

(b)

Figure 4.5: Heat exchanger: (a) the box where liquid was heated to the desired temperature (b) the metal cylinder where heat exchange between heated fluid and working fluid of the pipe took place.

temperature drifts (typically take place on order of hours) where a change by 0.1 K results in a change of about ΔRe=6.

4.2.3 Pressure measurement and flow visualization technique

Pressure drop measurements were carried out to determine the friction factor of the flow. A Validyne DP45 very Low Differential Pressure Transducer (figure 4.6) was used to measure pressure differences with a resolution of 0.5 % of the full range of the measurable pressure difference. The range of measurable pressure drop was from less than 1 mm to 225 cm of water column. Different diaphragms could be inserted into the sensor depending on the required pressure range. For the most sensitive diaphragm the maximum pressure was 1.4 cm of water column whereas the least sensitive one can measure up to 2.25 m of water column. This type of pressure sensor was extremely helpful where dynamic response at low pressure drops is required. In order to select the correct pressure range, initially the maximum pressure drop over a certain distance was estimated using the Blasius friction factor formula for turbulent flows (f=$0.3164/Re^{0.25}$). The two ports of the pressure sensor were connected via pvc tubing to two pressure tabs of the pipe. Once the flow was started the steel membrane got deflected accordingly due to the pressure difference on the two sides. This deflection was quantified through a voltage demodulator. The two sides of the sensor were connected to the pipes through tubes attached to 1 mm holes in the pipe connections. On the two metal cases '+' and '-' signs were engraved. The metal case with the '+' sign was placed on the upstream side whereas the '-' sign was on the downstream side.

The pressure sensor was calibrated before the measurements. Calibration of the sensor was carried out within the prescribed optimum range for pressure difference measurement. The steel diaphragms were extremely delicate and needed careful handling. Regular cleaning of the diaphragms was carried out to prevent rust on the membrane surface. The tubes attached to the sensor should be free of bubbles as to avoid erroneous readings. In order to free any trapped bubble within the metal casing the bleed valves on the surface of the casings were opened until all the air was removed.

Figure 4.6: A Validyne pressure sensor connected to a pipe setup

In addition to pressure measurements flow structures could be visualized by adding neutrally buoyant anisotropic particles (Mearlmaid AA) of 10 to 50 micron size. These particles have the form of flat platelets which align with the shear (Savas, 1985; Gauthier *et al.*, 1998) and hence turbulent flow can be easily distinguished from laminar flow. Images were taken with a CCD camera (Matrix Vision Bluefox 121G)of 1 mega pixel resolution and 10 Hz frequency. A pipe segment of about 10 D length was captured in each frame.

4.2.4 Perturbation method

In order to trigger turbulent flow structures, the laminar flow was disturbed using a controlled perturbation scheme. Different types of controlled perturbations have been used in the past, like pressure pulses from loudspeakers (Wygnanski *et al.*, 1975), jet injection in the pipe (Darbyshire & Mullin, 1995) or devices like iris diaphragm which can block the flow temporarily (J.Rotta, 1956; Wygnanski & Champagne, 1973; Durst *et al.*, 2003) or simultaneous injection and suction (de Lozar & Hof, 2009). However it was shown (de Lozar & Hof, 2009) that except for a brief period after the introduction of perturbation in the flow, the turbulent structures in the transitional regime (turbulent puffs) were independent of puff perturbation. It was also shown (Hof *et al.*, 2003) that the minimum perturbation amplitude to trigger turbulence depended on Re as well as the pulse width (duration). We therefore selected a jet perturbation where the amplitude and the duration could be very accurately controlled. However since amplitudes were <1 % of the pipe mass flow and pulses were only several ms long the perturbations effect on the overall flow rate is negligible. Water was injected through a 1 mm hole in the pipe wall via a commercial fuel injection valve. The solenoid valves were very fast and allow to time the jets with an accuracy of 1 μs. An injection driver unit was required for controlled injection. The valve was opened by TTL voltage signal of 5 volts through signal generator express in Labview . The flow could also be perturbed periodically, for this purpose the voltage signal was a periodic square wave(figure 4.7). The time period was t_{pert} and the valve opening time was t_{valve}. The valve opening time (t_{valve}) was adjusted through Injector Driver Unit from 0.1-10 seconds and t_{pert} could be controlled by selecting frequency of the voltage signal. The perturbation

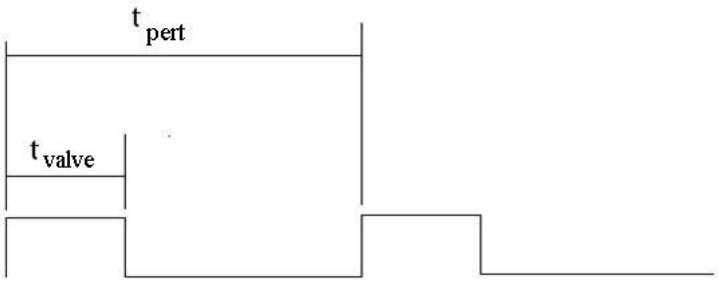

Figure 4.7: A square wave signal where t_{pert} is time period and t_{valve} is the time for which the valve remains open

amplitude was strong enough to transform into a puff (Darbyshire & Mullin (1995),Hof *et al.* (2003)). As shown in figure 2.1 at Re≈2000 such a disturbance resulted in a localized turbulent puff which developed its typical shape in less than 50 advective time units.

4.3 Experimental setup of Non Newtonian pipe flow

4.3.1 Pipe setup

The experimental setup was similar to the Newtonian pipe flow setup (figure 4.1). The pipe had a diameter of 4±0.01 mm and a length of 3.6 meters (900 L/D) comprising of 1.2 m long pipe segments made of precision bore glass. Using an inlet with a smooth contraction from 20 mm to 4mm flows remained laminar upto Re 6500. The temperature was kept constant at 20±0.2^{o}C for three to four hours.

4.3.2 Working fluid

Polyacrylamide (5-6 million g/mol molecular weight) manufactured by Sigma Aldrich was used for preparing Non Newtonian solutions. Polymers were weighed using a precision scale (resolution of 0.01 mg) for preparing solutions of desired concentration. The polyacrylamide was then gently sprinkled over 30 liters of distilled water. The solution was kept for two days to fully dissolve. Generally magnetic stirrers were used for small amounts of polymer solutions and large quantities of solution were stirred manually. In order to avoid large shear rate, in the later case, a cylindrical rod was used and this method was found to be much more gentle than commercial mixing devices. For high polymer concentrations, care was taken to prevent lump formation on the floor and corners of the container. Lump formation should be strictly avoided so that the solution could dissolve the amount of polymers fully to obtain the desired concentration. One of the complications in carrying out the experiments is polymer degradation caused by mechanical stresses. Degradation of polymers is undesirable as it leads to breakdown of polymer chains leading to reduction of molecular weight and change in drag reduction properties. Particularly, the high shear rates in the pump can cause severe degradation of the polymers. During lifetime measurements, to minimize degradation no pumps were used to recirculate the fluid,

instead, the solution was collected in a container placed at the pipe exit. The collected solution was then manually put again into the reservoir making the whole process more time consuming than for Newtonian fluids.

4.3.3 Puff detection during lifetime measurements

In order to create turbulent puffs the flow was perturbed by a jet of 50 ms duration injected through a 1mm diameter radially through the pipe wall. At the pipe exit, the arrival of puffs could be determined by visual inspection of the outflow angle. In the transition stage the laminar flow assumes a parabolic profile. In case of the turbulent puffs, redistribution of momentum causes lower centerline velocity and faster velocity adjacent to walls . Due to this difference in centerline velocity, turbulent puffs have a different outflow angle than laminar flow (Hof *et al.*, 2006, 2008; J.Rotta, 1956). Monitoring the flow angle at the pipe exit allowed to determine whether the puff has survived till the pipe exit.

4.3.4 Rheometry

In complex fluids the viscosity typically changes with shear rate and therefore a Rheometer is required to determine the shear rate dependent viscosity. Since dilute polymer solutions are viscoelastic they exhibit elastic properties also. The elastic nature of the fluids is quantified through a parameter named relaxation time (λ) which is specified as the time required by a stretched polymer chain under shear to regain its random coiled configuration. Determination of viscosity and relaxation times is very important in estimating Reynolds and Weissenberg number respectively. To determine these properties of the fluid, rheometry was carried out in the lab of Professor Christian Wagner at university of Saarland. Measurements were carried out at the same temperature of 20^oC with a controlled shear rate Rheometer (MARS, Thermo Fischer Scientific, Karlsruhe, Germany) equipped with a double cone geometry ($2^o/60$). This geometry is suitable to measure viscosities down to $\mu\approx$ 1 mPa-s. The solutions were tested before and after the experiments in the pipe and in addition we tested samples that were prepared in smaller quantities (250ml). All these solutions gave similar results within the experimental resolution of $\pm$5% and in agreement with former studies (Zell *et al.*, 2010). We did not observe any notable degradation of the polymer. The viscosity was measured at shear rates $5< \gamma^{\bullet} < 100\ s^{-1}$ and no shear thinning was observed i.e. the viscosity was constant. The results are shown in figure 4.8. The viscosity μ increases with the concentration and from the dilution series (figure 4.8 b) we can extract an overlap concentration of c_{ov} = 1150ppm. The overlap concentration (c_{ov}) is the polymer concentration at which viscosity of the polymer solution becomes twice the viscosity of the solvent. Since polymers have no influence on the drag in laminar flow, pressure drop measurements at laminar flow conditions were performed . Assuming a parabolic profile for the laminar state the wall shear rate is calculated. Since the shear stress is already estimated from the pressure drop measurements, viscosity can be calculated by dividing shear stress by shear strain rate. Rheological data and viscosity calculated from pressure drop measurements were in agreement within $\pm$ 5 %.

Due to the low viscosity of dilute polymer solutions elasticity and relaxation times is very low in magnitude. Resolutions of ordinary rheometers are not

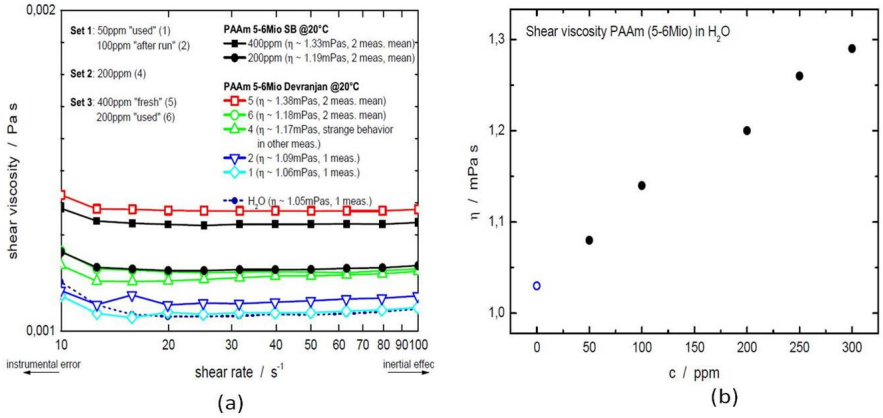

Figure 4.8: (a)Viscosity measurements of different polymer concentration solutions at shear rate ranging from 0 to 100 /s ; cyan diamonds : 50 ppm; blue inverted triangle : 100 ppm; both green symbols : 200 ppm; black solid square : 400 ppm; red hollow square : 500 ppm (b) Shear viscosity vs. polymer concentrations

low enough to measure relaxation times of dilute polymer solutions. Therefore the second rheological characterization was performed with a self build Capillary Break-up Elongational Rheometer (CaBER)(Anna & McKinley, 2001). A droplet of the sample was placed between two steel plates from which the upper one is displaced by a linear motor until the capillary bridge becomes unstable to the Rayleigh-Plateau instability. In the following thinning process a parallel filament is formed that shrinks exponentially in time. The characteristic time scale from the thinning process λ_c (Fig 4.9) can be related to the polymer relaxation time λ. Simple models predict λ=3λ_c but it has been shown that in reality the relation is far more complex (Zell *et al.*, 2010; Clasen *et al.*, 2006). However, the CaBER is still most sensitive to the elasticity of diluted aqueous solutions and the time scale λ_c is commonly used to define a Weissenberg number Wi (Rodd *et al.*, 2005). The relaxation time λ_c scales with a power law with an exponent of 0.8 with the concentration n, $\lambda_c \approx n^{0.8}$ which was in good agreement with previous measurements (Zell *et al.*, 2010).

4.3.5 Particle Image Velocimetry (PIV)

PIV is a non intrusive optical measurement technique used for determining instantaneous velocity field. Based on the working fluid, tracer particles e.g. glass beads, polystyrene or aluminum particles of size ranging from 10 to 100 μm are used in the flow and assumed to faithfully follow the fluid motion. The particles should be of optimum size so that they follow the flow with good precision and scatter sufficient amount of light for image acquisition. An area of investigation is illuminated by laser for very short exposure time and at very high frequencies. The particles in the illuminated flow field scatter light to the camera lens placed perpendicular to the plane of investigation. High speed CCD or CMOS cameras are used for image acquisition of the flow field. After the data acquisition, two successive frames with very short time difference between

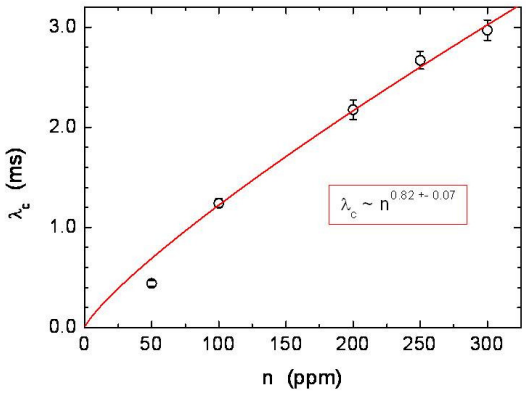

Figure 4.9: Characteristic relaxation time of the polymer solutions in the CaBER experiments. The relaxation time λ_c scales with a power law with an exponent of 0.8 with the concentration.

their acquisition are analyzed using cross correlation techniques to determine the velocity vectors.

PIV measurements were carried out to obtain quantitative measurements of streamwise and spanwise velocity fluctuations. The PIV system was supplied by La Vision, Goettingen, Germany. For flow visualization glass particles of 10 to 50 micron size were used. For PIV measurements refraction index matching with the fluid in the pipe is essential for acquiring good images. A customised plastic box was used as the test section. The transparent plastic box was filled to capacity with the same polymer solution to maintain same refractive index. Two black semicircular metallic segments were wrapped around the test pipe section in such a way that laser light can illuminate the horizontal plane passing through the central axis of the pipe. The top segment had an opening through which the planar view could be acquired by the high speed camera. Before image acquisition the camera was calibrated. Tests were carried out to verify whether the camera was focusing the central plane. Frequency of the image acquisition had to be estimated properly so that the movement of glass particles in successive images could be used for image correlation. In our measurements the images were captured at 50 or 100 Hz for 2-3 seconds depending on the Re. The images were then postprocessed by the software provided by La Vision to get the desired quantities of the flow field.

Chapter 5

Newtonian pipe flow measurements

5.1 Introduction

In the transition stage of pipe flow at Re ≈2000, turbulence only occurs in localized patches (Reynolds, 1883; J.Rotta, 1956) also referred to as equilibrium puffs (Wygnanski & Champagne, 1973; Wygnanski *et al.*, 1975), which are separated by laminar fluid. Only when the Reynolds number is further increased turbulent patches begin to spatially expand. A better understanding of the processes underlying localization and localized states in shear flows (Schneider *et al.*, 2010) is an essential requirement to allow further theoretical progress. In addition edge states (Mellibovsky *et al.*, 2009; Willis & Kerswell, 2009; Duguet *et al.*, 2010) separating laminar from turbulent flow and which are potentially relevant for the transition process remain bounded in axial direction even at much higher Re. This indicates that even beyond the intermittent regime localization is relevant to some aspects of the flow.

Laminar turbulent intermittency can be identified in a number of canonical shear flows, but unlike in pipe , for Torsional Couette flow (figure5.1 a), plane Couette flow (PCF) (figure 5.1 b) and Taylor-Couette flow (TCF) (figure 5.1 c) regular spatio-temporal structures consisting of tilted laminar-turbulent stripes have been reported. Cros & Gal (2002) showed that in torsional Couette flow nucleation of turbulent spirals is initiated by generation of structural defects in a periodic roll pattern. Then with the increase of rotation, turbulent spirals are arranged almost periodically around the circumference, especially during their initial appearance. Eventually turbulent spots appear in the flow with increase of Re and capture the whole domain. In PCF and TCF by decreasing Re, during reverse transition from fully turbulent flow to laminar state, an well defined pattern of regularly spaced inclined turbulent stripes are observed in the flow domain (Prigent *et al.*, 2003). In the case of TCF, the localized turbulent stripes are traditionally known as turbulent spirals (Coles, 1965).

The existence of a distinct preferred wavelength has led to the speculation of a wavelength instability preceding turbulence (Cros & Gal, 2002; Prigent *et al.*, 2002*b*; Barkley & Tuckerman, 2005). In pipes, on the other hand, many earlier investigations of the intermittent regime (J.Rotta, 1956; Wygnanski & Cham-

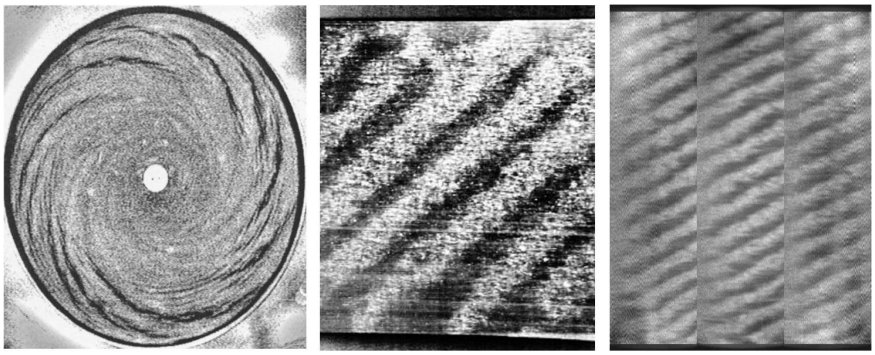

(a) (b) (c)

Figure 5.1: (a) Periodic rolls called SR III in Torsional Couette flow at Re=106700 (Cros & Gal, 2002) (b) Plane Couette Flow R=716 (Prigent *et al.*, 2002*b*)(c) Taylor Couette flow Re_i = 703 Re_o =-699 (Prigent *et al.*, 2002*b*)

pagne, 1973) were focused on quantities like intermittency factors and turbulence fraction which for observation times typically realized in experiments and simulations ($\approx$ a few hundred D/U), are strongly dependent on initial conditions as well as imperfections, such as disturbances created at the pipe entrance.

In this chapter, we aim to determine an upper bound on turbulence fractions and friction factors, which unlike above quantities do not depend on the specifics of the experimental setup. The nature of the resulting puff spacing which naturally occur after a sudden Re reduction from a fully turbulent flow is discussed in this chapter. Also we presented the quantitative measurements of spatial interaction in the transition regime of pipe flow. The flow is periodically perturbed and subsequently corresponding rate of puff generation is studied. Beyond a certain frequency the perturbed flow segments start to interact mutually and lead to lower rate of puff generation. The distance corresponding to this frequency is termed as interaction distance. Finally the resulting puff spacing from reduction experiments and interaction distances obtained from periodic perturbation experiments are compared to typical wavelength in intermittent Couette and TCFs.

5.2 Periodic perturbation

The first set of experiments is concerned with determining the distance at which puffs start to interact. When two puffs are located too close to each other, the downstream puff decays (Hof *et al.*, 2010). Determination of the interaction distance of turbulent puffs has implications on the drag since puffs located to each other at distances lower than the interaction distance will annihilate each other downstream and eventually reduce drag. To find the exact distance where this interaction starts, periodic perturbations were applied to the flow at a fixed position and the rate of puff triggering as response of the injected disturbance was observed at a downstream distance.

The perturbation consisted of a water jet injected by a solenoid valve, placed 100D downstream of the pipe entrance, which was run at frequencies ranging from f =0.2 Hz to f =2.5 Hz. The valve opening time, frequency and water discharge were independently controlled. The duration of each jet was t_{jet} =0.11 s $\approx$ 2.5 D/U and the amount of water injected was 0.15 ml per discharge

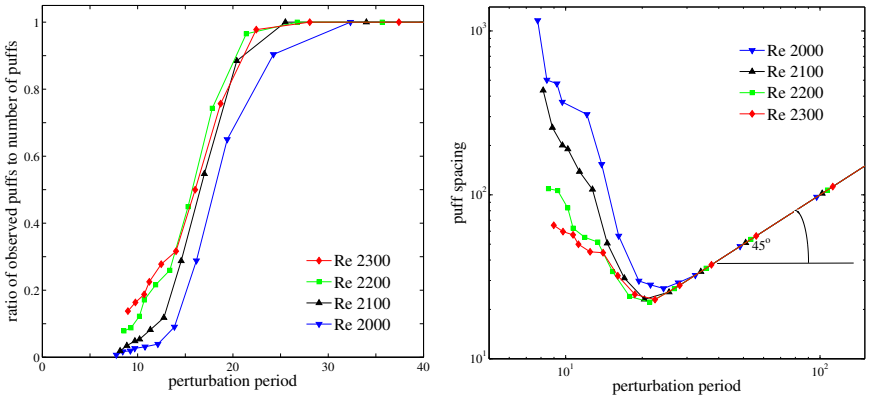

Figure 5.2: (a) Ratio of number of puffs to number of perturbations vs. perturbation period. (b)Distance between puffs vs. perturbation period.

which corresponded to less than 1 % of the pipe discharge at Re=2000. At the distance of 400D downstream of the perturbation point, the number of induced puffs, N_{puffs}, was counted during 300 s ≈7500D/U. For each frequency of the input disturbance, the experiments were repeated five times to extend the observation period to t_{obs} ≈37500 D/U. In the following, the temporal spacing of perturbations is converted into an axial spacing of pulses by multiplication with the mean velocity U, assuming that perturbations are advected with the mean flow speed. This assumption is supported by a previous studies (e.g. de Lozar & Hof (2009)) where it was shown that at Re 2000 the puff speed agrees with the mean velocity to within 2 %.

For large axial spacing (small frequencies) each perturbation results in a single puff. However once the puff spacing is below ≈ 20-25 D, new generated puffs interact and annihilate each other and the ratio of created puffs to perturbations drops below 1. The ratio of the number of observed puffs to the number of perturbation pulses is shown in figure 5.2(a) as a function of the perturbation period. Figure 5.2(b) shows the distance between the generated puffs in response to the perturbation period. From figure 5.2(a) and 5.2(b), it is evident that the rate of puff generation is in synchrony with the rate of injected perturbation for large axial spacing and that the puff spacing is identical to the spacing preselected by the perturbation (highlighted by the slope of 45^o in the log-log plot figure 5.2 b). Once puffs are created at too short distances ($<$ 20-25D), the number of puffs observed downstream drops resulting in an increase in puff spacing. The minimum of each curve in figure 5.2(b) corresponds to the perturbation frequency generating the maximum number of puffs which can sustain themselves in a given length of the pipe. The corresponding distance will be referred to as the optimum spacing as it provides the maximum turbulent fraction. For times between perturbations shorter than the minimum one (high frequencies), the generation of puffs decreases quite sharply for the lower Re. For instance, at Re=2000, only one puff each 1000D is observed at high perturbation frequencies (1/f=7D/U). At these frequencies perturbed regions typically annihilate each other and only rarely merge to form a single puff. This decrease of generated puffs is smaller for the higher Re where the distance between puffs seems to saturate for large frequencies.

Next we investigated whether the generation of puffs depends on the intri-

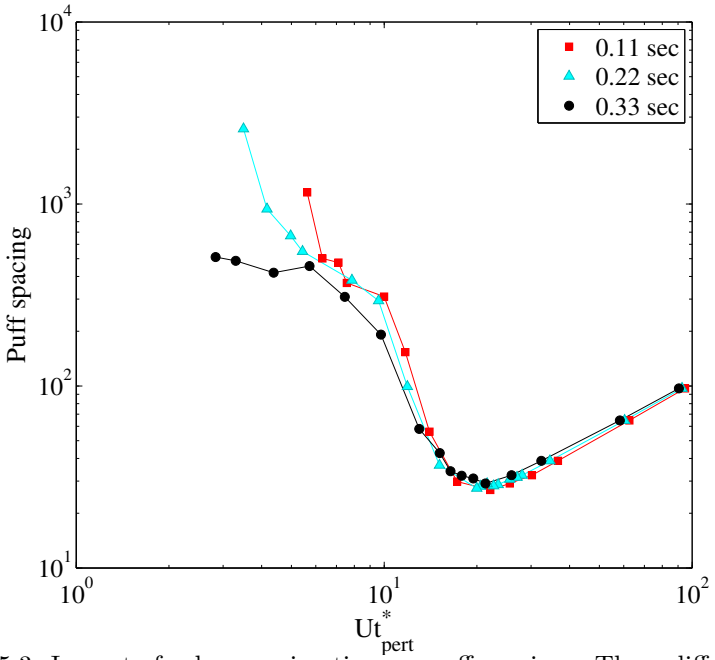

Figure 5.3: Impact of valve opening time on puff spacings. Three different valve timings (0.11, 0.22 & 0.33 sec) were used. In the x-axis t^*_{pert} is the time between pulses taking valve opening time into account (see text)

cacies of the jet injection method, i.e. the water injected per perturbation and the valve opening time. The puff spacing is found to remain unchanged when the jet discharge is varied from 0.15 ml discharge^{-1} to 0.25 ml discharge^{-1}. The impact of the jet duration on puff spacing has also been investigated. Here the valve opening time was varied from t_{valve} =0.11 s to 0.22 s and to 0.33 s for Re=2000. From figure 5.3 it is evident that all curves collapse when plotted as a function of the time between perturbation pulses, i.e. the time between the end of one jet and the beginning of the next one ($t^*_{\mathrm{pert}} = t_{\mathrm{pert}}$-$t_{\mathrm{valve}}$). This highlights that the relevant time is not the period of the perturbation but the time for which the flow is unperturbed. Since the minimum of all curves is the same, the optimum puff spacing is independent of the details of the perturbation.

Subsequently we measured friction factors over the puff regime of Re 1900-2400. Since a perturbed flow in this regime is neither fully laminar nor fully turbulent, there has to be a highest turbulent packing fraction in the transition regime. From the periodic perturbation experiments, an optimum puff spacing was already obtained. Since optimum puff spacing signifies highest turbulent packing fraction, the corresponding friction factor will be the upper bound for friction factor in this regime. In the following the friction factor was measured for three cases: for a flow without perturbation, when the flow is tripped by obstacle of two different sizes and for the periodic perturbation described earlier. The friction factor is defined in a pipe as $f = \Delta p/(1/2\rho U^2 L/D)$, where Δp is the pressure drop over a length L ,ρ is the fluid density, D as pipe diameter and U being the mean velocity. When the flow is not perturbed, the friction factor closely follows the Hagen-Poiseuille law $f = 64/Re$ (figure 5.4b) till Re $\approx$

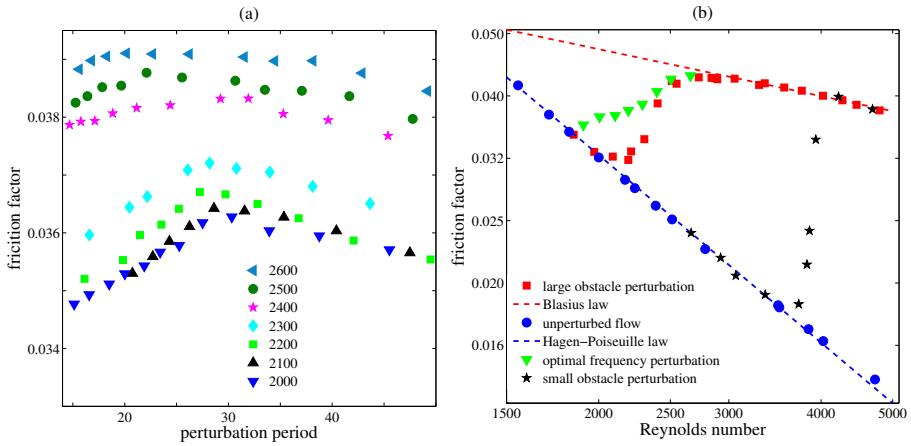

Figure 5.4: (a) Friction factor vs. perturbation period. (b) Friction factor vs. Reynolds number using different perturbation types as indicated in the legend.

8000 (not shown in figure 5.4 b). For a fully turbulent flow, the friction factor lies on the Blasius curve $f = 0.3164Re^{-0.25}$. On the other hand, in the transitional regime the friction factor strongly depends on initial conditions as well as experimental imperfections. To demonstrate this dependence, friction factors resulting from two different obstacles are shown in figure 5.4(b) (red squares and black stars). The large obstacle is a small cubic magnet of 4 mm whereas the small obstacle is a 2mm thick iron wire of 2cm long. Both the obstacles are held to a fixed position at 150 D from the pipe entrance in the pipe by a strong magnet placed beside the pipe. For the small obstacle, transition sets at ΔRe $\approx$1500 higher than the large obstacle. Depending on the type of perturbation, the perturbation amplitude and the observation point any transitional friction factor (i.e. points between the Hagen-Poiseuille and the Blasius curves) can be observed for Re>2000.

In order to investigate the dependence of the friction factor on initial conditions, we studied the pressure drop for varying frequencies of the jet perturbation. The flow was again periodically perturbed as described earlier and 100D downstream of the perturbation point the pressure drop was measured over a length of 770D (the pipe length was increased by 5 m for this purpose) with a Validyne DP45 pressure sensor. The pressure drop over this length lies in the optimal working range of the DP45 sensor resulting in accuracy better than one percent for the pressure readings. Generally the pressure measurements were carried out for 30 seconds and the mean value of the time series was used for friction factor calculation. Starting from small perturbation frequencies, i.e. large spacing, the friction factor is found to first increase with frequency and then reaches a maximum at the optimum puff spacing (figure 5.4 a). Beyond this point the perturbed regions start to interact resulting in a lower density/packing fraction of puffs. The maximum packing fraction data provide an upper bound for the friction factor for a given Re, shown by the green triangles in figure 5.4 b. These data therefore provide a well-defined connection between the Hagen-Poiseuille law and the Blasius law. While the maximum packing fraction is clearly differentiated for Re $<$ 2300 (figure 5.4a) the curves become flatter when

increasing the Re until the point that the curves are almost flat and only a very weak interaction can be detected (Re=2500). The fading of the maximum indicates that a fully turbulent flow state is approached. Beyond Re 2500 turbulent domains start to grow, split and merge resulting turbulent state to occupy the pipe domain almost completely at downstream distance. Previous studies (Moxey & Barkley, 2010) showed that the puff splitting phenomena is common from Re 2350 onwards. As a result, the dependence of turbulence fraction on initial perturbation frequencies is masked by downstream turbulence dynamics from Re 2400 onwards. This is in qualitative agreement with recently suggested transition points to fully turbulent flow at Re=2550-2600 (Moxey & Barkley, 2010; de Lozar & Hof, 2009), although from our data no criticality can be inferred. Contrary to common intuition that the more fluid is perturbed the higher the turbulent fraction, the present measurements identified the existence of an upper limit on turbulent fraction in this regime and hence friction factor.

5.3 Reduction experiments

In the following we would like to investigate if in analogy to TCF and PCF, 'large wavelength instability' scenario (Prigent *et al.*, 2002*b*; Barkley & Tuckerman, 2005) can also be observed in pipe flow. In the above studies, it has been suggested that when Re is reduced from the fully turbulent regime, an instability occurs which gives rise to periodic laminar-turbulent patterns. If the same holds for pipe flow, it is expected that upon reduction of Re from the fully turbulent regime, laminar gaps open up at regular intervals giving rise to a periodic laminar turbulent pattern. The technique of Re reduction in studying the laminar-turbulent pattern in the transition regime is of interest as it eliminates the dependence on the nature of perturbation. In order to allow an abrupt Re reduction, a bypass tube with a valve was installed. Tube arrangements before the pipe entrance had to be suitably adjusted to reduce the resistance to raise the flow at Re 4500. We therefore initially created a uniform turbulent flow at Re=4500 by putting an obstacle into the pipe directly behind the entrance and subsequently reduced the Re to the intermittent regime by opening the valve of the bypass tube resulting in reduction of flow rate in the main pipe. By pressure measurements we verified that the friction factor lies on the Blasius curve (5.4 b) and hence that the flow is initially turbulent throughout the pipe. Next a bypass valve was opened allowing half the total discharge to flow through a parallel pipe (not shown in figure 4.1). By doing so, Re in the pipe decreases to the desired value. Care was taken to avoid air pockets or elastic components in the setup which would cause damped oscillations in the flow rate during the reduction. Damped oscillations are highly undesirable as it may cause momentary backflow and reduction of Re beyond the desired one. On reduction, when the outflow angle decreased gradually without making to and fro adjustment it was ensured that there was no backflow and hence no damping agents. Flow visualization and monitoring of the outflow angle at the pipe exit showed that the flow changes smoothly between both Re during approximately 4 s ($\approx$100D/U).

For flow visualisation Mearlmaid particles of 50 micron size were added in the flow. Images were captured at 10Hz with a CCD camera (Matrix Vision Blue Fox 121G) placed 500D downstream of the entrance. Figure 5.5(a) shows typical snapshots for a laminar and a turbulent flow. Pixel intensity values of

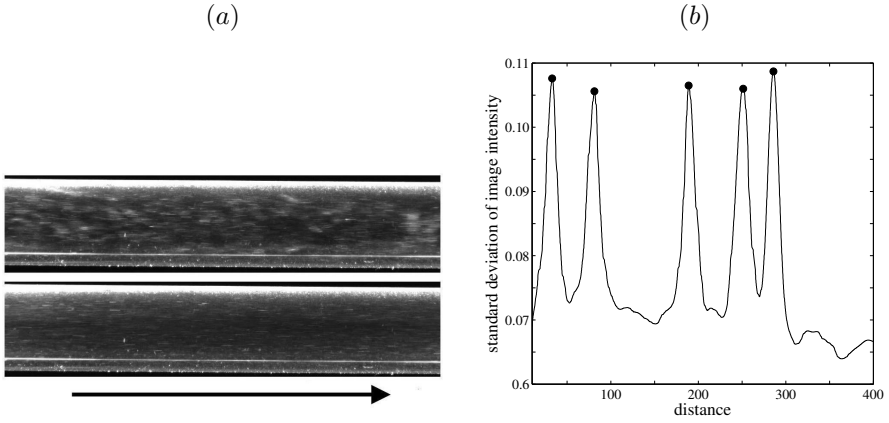

Figure 5.5: (a) Flow visualization at $Re = 2000$ in turbulent(upper image) and laminar flow (lower image). Images display a pipe segment of 5-6 D long. Flow direction is from left to right. (b) Standard deviation of image intensity vs. reconstructed pipe position at $Re = 2100$. Summits of the peaks (black dots) indicate the position of a turbulent spot.

the images were read with a MATLAB program. The flow visualization particles were aligned with the axial flow in laminar state. So the pixel intensity of the images of laminar state was uniform. However in turbulent states flow particles emitted more light in presence of eddies causing a non uniform pixel intensity of the turbulent state images. Hence, the standard deviation in the image intensity of turbulent flow is greater than that of laminar flow, which allows for a simple identification of the turbulent regions. The laminar turbulent pattern in the pipe was reconstructed using the Taylor's hypothesis at the Reynolds numbers of the experiments.

Generally it was found that after reduction, the flow rapidly (<100D/U) adjusts to the new Re resulting in a fixed pattern of equilibrium puffs separated by laminar flow. Consequently, initial 4 s (100 time units) of each signal were disregarded to allow the flow to establish the equilibrium pattern allowing a measurement time of 400 D/U. Once established, this pattern shows little dynamics on the time scale of the experiment for Re < 2400. This was confirmed by a second set of measurements where the waiting time was increased to 300 D/U resulting in a remaining measurement time of 200 D/U (data not shown). Both sets of measurements (200D/U and 400D/U) resulted in the same size distributions (within experimental error). The dynamics of puffs only appear to be relevant on much longer time scales, puff splitting in pipes of similar length has been observed (Nishi *et al.*, 2008) for Re>2450 and the probability of an isolated puff to decay during 500 time units at Re=2000 is around 5×10^4 (Hof *et al.*, 2006, 2008; Avila *et al.*, 2010). A sample signal at Re 2100 is presented in figure 5.5(b). The data have been postprocessed by smoothing the original signal. The peaks in figure 5.5(b) represent the presence of turbulent puffs and the intermediate valleys correspond to the laminar regions. The summits of the peaks were traced and represent the puff positions. Distances between the two peak positions were taken as puff spacing. After 600 time units all the fluid,

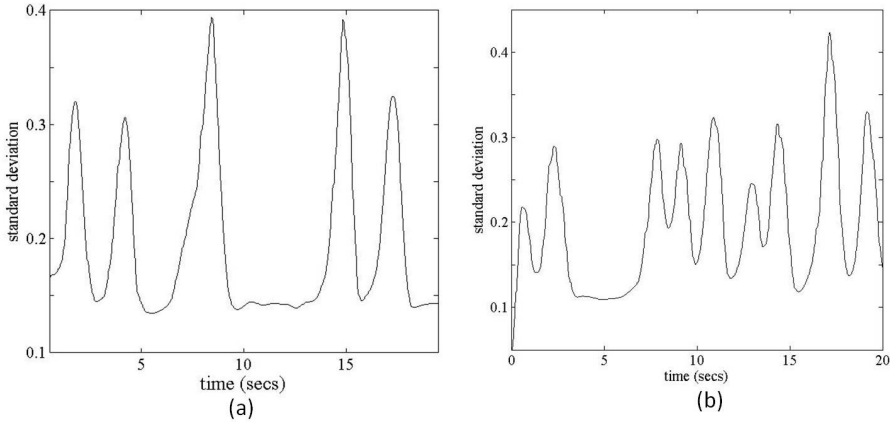

Figure 5.6: (a) Standard deviation of puff images at Re 2000 (b) at Re 2400

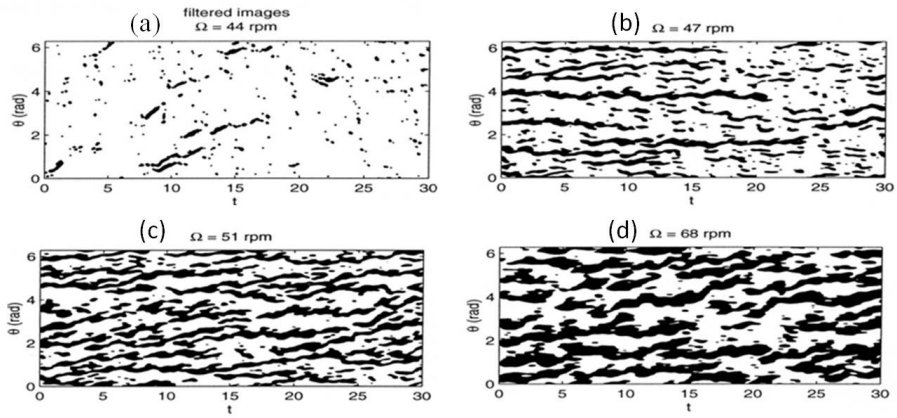

Figure 5.7: Spatio temporal diagram of Torsional couette flow at different Re (a)590300 (b)596500 (c)104700 and (d)139600 (Cros & Gal, 2002)

which initially had been in the fully turbulent state, has advected past the pipe exit and the entire flow is laminar.

For each Re 30-50 experiments were performed and this resulted in a sample size of about 200 puff spacing. In general, the puff spacing decreased with increasing Re. Typically 4-5 puffs appeared for Re=2000 whereas the number of puffs for Re=2400 was 8-10 for the same time interval (figure 5.6). Time series signal of the standard deviation of the images at Re 2000 and Re 2400 are presented in figure 5.6(a) and 5.6(b) respectively. Qualitative comparisons of the figures 5.6(a) and 5.6(b) shows gradual increase of turbulent fraction with increase of Re. Increase of turbulent fraction with increase of Re is also observed in Torsional Couette flow (figure5.7). It is worth mentioning that while the number of puffs increases with Re in pipe flow, in TCF the number of spirals is constant all along the transition (Prigent *et al.*, 2002*a*). In torsional Couette system the number of spirals first increased with Re , but then all disappeared

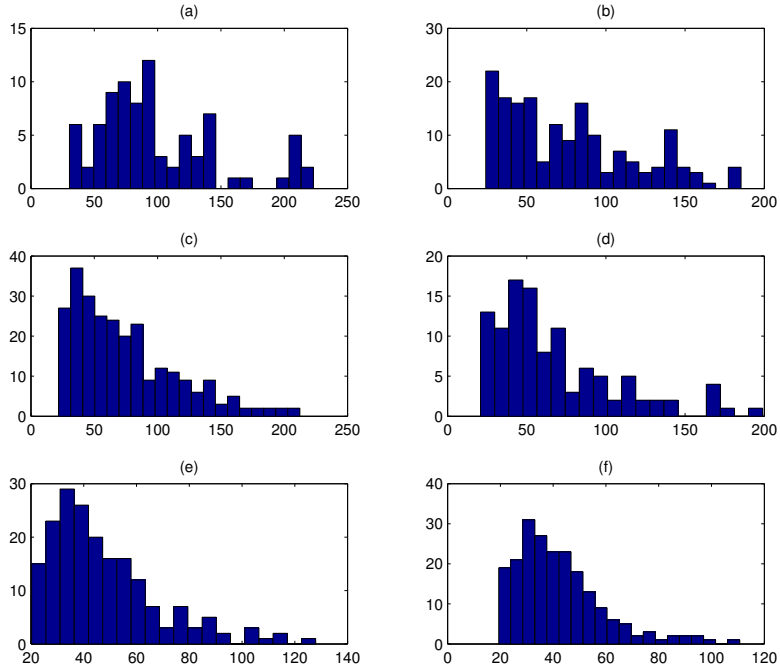

Figure 5.8: Histograms of puff spacing at (a)Re 1900 (b)Re 2000 (c)Re 2100 (d)Re 2200 (e)Re 2300 (f)Re 2400

with the onset of turbulent spots occupying the flow domain (Cros & Gal, 2002).

From figures 5.5b, 5.6a, 5.6b it is evident that the laminar turbulent domains are not periodically spaced unlike previously studied shear flows. Histograms of puff spacings for different Re were computed showing no preferential spacing (figure 5.8). From figure 5.8 it is evident that for a given observation time, the range of puff spacing decreases with increase of Re. It is obvious from the fact that with the increase of Re especially at Re 2300 or 2400, more puffs appear in a given time thereby eliminating the possibility for puffs to arrive at greater distances like Re 2000. In previous studies of PC flow (Manneville, 2009), pipe flow (Moxey & Barkley, 2010) it was shown that the standard deviation of laminar lengths decrease with Re. We also computed standard deviation of the puff spacings obtained from reduction experiments (figure 5.9). It is visually evident that standard deviation of puff spacing is decreasing, which is in accordance with numerical simulation results of Moxey & Barkley (2010). In addition to our studied regime of Re 1900-2400 it has been shown by Moxey & Barkley (2010) that the standard deviation of turbulent region spacings saturates after Re 2600 suggesting the onset of uniform turbulence.

From the data we determined the cumulative probability P(d) that two adjacent puffs are separated (peak to peak distance) by a distance d or larger. For a spatially periodic pattern such cumulative distribution should show a sharp drop at the wavelength of the pattern. Instead, as shown in figure 5.10(a), the data fall on exponential tails. The fact that the spacing between the puffs is irregular is visually evident from figure 5.5(b). The exponential distributions

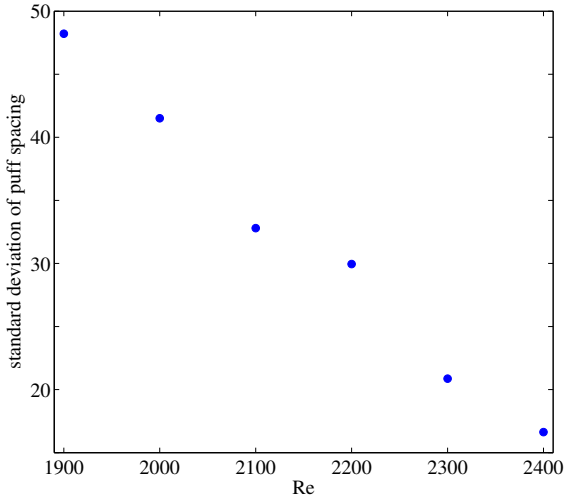

Figure 5.9: Standard deviation of puff spacings with Re.

(figure 5.10(a)) do not cross zero but reach $P(d)$=1 at some value d=$d_{min} > 0$, where d_{min} is the minimum puff spacing. The distribution takes the form of:

$$P(d) \propto e^{\frac{-d}{\delta}} \text{ for } d > d_0 \tag{5.1}$$

where d_0 is related to the distance from which the exponential distribution applies and δ is the characteristic scale of the exponential distribution. Note that δ+d_0 is the mean distance between the puffs. The statistical analysis of an exponential distribution which only applies from a distance d_0 has been performed using techniques described in Avila *et al.* (2010). In general exponential distributions signify a memoryless process. This probability function implies that the spacing between two puffs is always larger than d_0 but otherwise arbitrary and that it is not influenced by the spacing between puffs further up and downstream. Therefore the existence of a preferred spacing or wavelength is ruled out.

For the lower Re (Re = 1900-2200), the exponential distribution applies from the minimum puff distance ($d_0 = d_{min}$) showing that the appearance of a puff is not influenced by any upstream or downstream puff. Note that for $Re = 2300$ and 2400, there is a slight initial rounding indicating that size distributions only become random for puff spacings slightly larger than d_{min}. The deviations from the exponential distributions at long distances, on the other hand, can be attributed to the finite size of the pipe. To rule out any effects of initial Re on the reduction experiments, a second set of experiments was carried out where the Re was reduced from a turbulent flow at Re=6000. Excellent agreement is found with the reduction experiments from Re=4500 (see the inset in figure 5.10a). Note that the deviations at the end of the tails carry little statistical weight and can be attributed to finite sample size. This indicates that the size distribution of the observed flow pattern does not depend on the initial intensity of the turbulence but only on the Re established after reduction. Independence of puff dynamics on initial Re from where reduction is carried out is also illustrated in numerical simulations of lifetime studies of puffs (Avila *et al.*, 2010). The characteristic distance δ, from 5.1, clearly decreases with Re (figure 5.10b). As

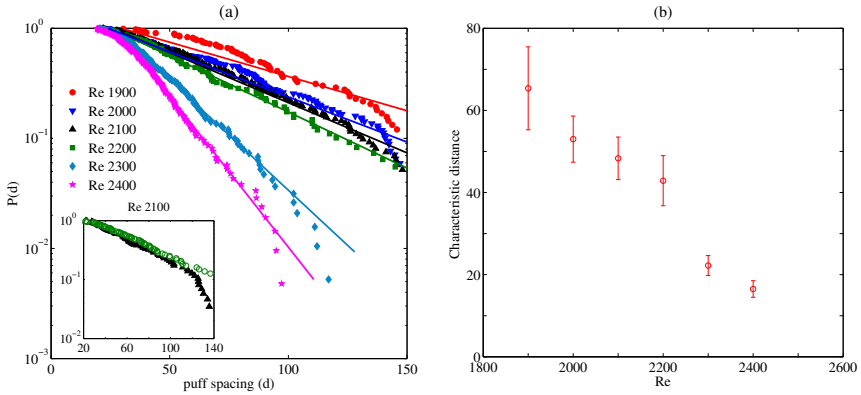

Figure 5.10: (a) Probability that puffs are separated by a distance greater than d after reducing the Reynolds number from $Re = 4500$. At the initial Re the flow is fully turbulent. The inset compares experiments with two initial Reynolds numbers (black triangles for $Re = 4500$ and green circles for $Re = 6000$). Note that deviations for d >100 were due to the finite sample size. (b) Characteristic distance δ from equation 5.1 as function of the Reynolds number.Error bars correspond to 95 % confidence interval.

expected, turbulent spots are more closely spaced with the increase of the Re. While the quality of the data does not allow to determine the exact functional dependence the characteristic distances appear to approach zero for Re$>\approx 2500$, where maximum puff packing should be achieved. This point is very close to where turbulence is observed to fill the domain ($Re_c = 2550 - 2600$) and to the Reynolds number where the puff interaction diminishes (figure 5.4(a)).

5.4 Discussion

The experiments presented in this chapter establish the existence of a minimum distance between turbulent patches in pipe flow. In the first set of experiments, an optimum distance corresponding to the densest packing fraction of puffs has been determined with the aid of a periodic perturbation. Specifically we measured the maximum achievable friction factor in the transition regime as a function of Re. Typically the friction factor in this regime strongly depends on initial conditions and previously reported values vary from one experiment to another. Our data give an upper bound for the sustainable friction factor and provide a well-defined link between the Hagen-Poiseuille and the Blasius law. In the second set of experiments, where no periodicity was imposed externally, a minimum spacing has been observed. In figure 5.11 we compare the minimum distance from the reduction experiments with the optimum distance from the periodic perturbation experiments as a function of the Reynolds number. Both data sets overlap indicating that the minimum spacing is a property intrinsic to the flow, independent of initial conditions or flow perturbations.

The existence of a minimum spacing in pipe flow can be explained following the arguments presented in Hof *et al.* (2010) where it has been pointed out that

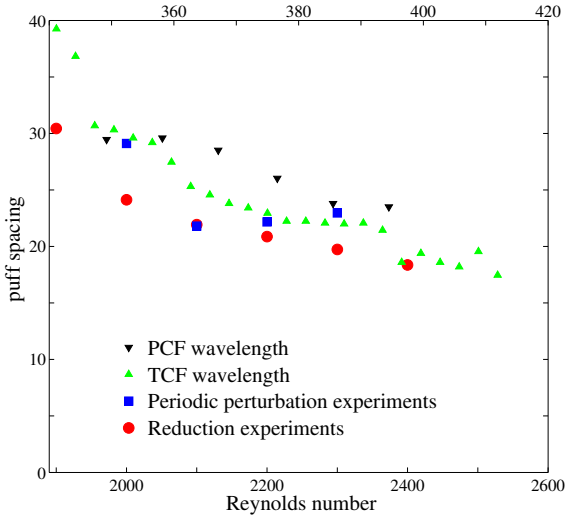

Figure 5.11: Comparison of minimum puff spacing (Reduction experiments) and optimum puff spacing (Periodic perturbation experiments) with laminar turbulent wavelengths in transition regimes of Taylor-Couette and Plane-Couette flow from Prigent *et al.* (2002*b*). The upper x axis represents the Re used for TC flow and PC flow and the lower x axis represents the Re used in our experiments.

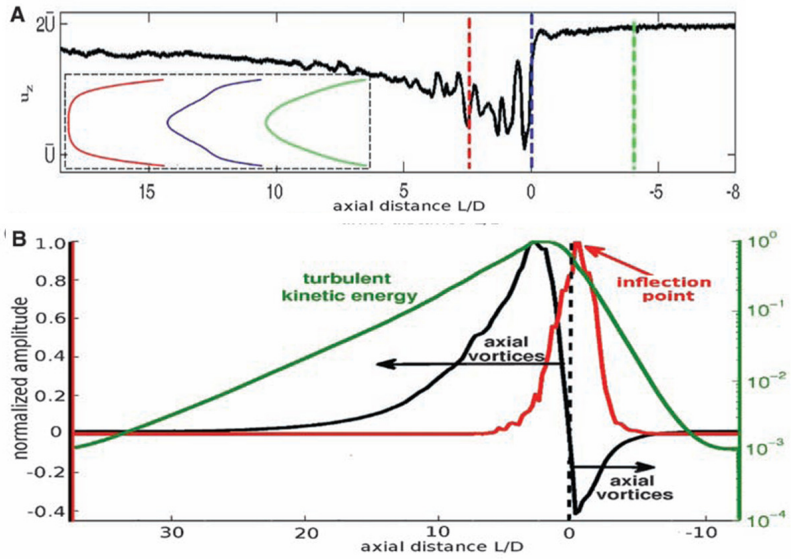

Figure 5.12: (a) Center line axial velocity: inset figure describes the azimuthally averaged velocity; upstream parabolic profile (green), velocity profile with inflection point (blue) just upstream of the trailing edge and turbulent velocity profile (red) (b) Numerical simulations of a turbulent puff show the magnitude of the inflection point (red). 2D upstream of inflection point turbulent kinetic energy curve (green) becomes maximum and vorticity transport (black) (Hof *et al.*, 2010)

the instability mechanism sustaining a puff relies on an inflection point at the rear of the puff. The process of the puff sustaining mechanism is illustrated in figure 5.12. Figure 5.12a shows the centerline axial velocity. The flow is from right to left. At the upstream laminar turbulent interface the centerline velocity (blue curve in inset of fig. 5.12a) drops well below the laminar level. The velocity profile continues for 5-10 D and gradually returns back to laminar profile at approximately 20 D downstream the rear end. In the inset of figure 5.12a the azimuthally averaged velocity profiles are shown. The upstream profile (green) is parabolic and the downstream profile ≈3 D from the trailing edge (red) has a turbulent plug profile. Hence the velocity profile has to adjust over a very short distance. The fluid at the center line has to decelerate and the fluid adjacent to the boundary has to accelerate to maintain mass conservation. This creates an inflection point in the velocity profile (blue) just downstream of the trailing edge. The presence of inflection point in the velocity profile satisfies Rayleigh's criterion (Rayleigh, 1880*b*). In figure 5.12b it has been shown that the strongest inflection point matches with the site of vorticity generation. At ≈2 D downstream of the inflection point, turbulent kinetic energy becomes highest. The localized nature of turbulence has been highlighted by rapid exponential decrease of energy in up and downstream distances. This emphasizes that turbulence in a puff is indeed supported by the inflection point mechanism. When an upstream puff appears too close, the profile at the rear of the downstream puff is not parabolic anymore and the inflection point is reduced. Eventually the downstream puff decays if the disruption by the upstream puff is strong enough.

The nature of the instability at the rear end of the puff has also been discussed by Shimizu & Kida (2009) and Duguet *et al.* (2010). The self sustaining cycle of puffs proposed by Shimizu & Kida (2009) is as follows: (a) Due to near wall interaction low speed streaks accompanied by streamwise vortices are generated. These low speed streaks move upstream relative to the puff and penetrate the trailing edge. (b) Just upstream of the puff trailing edge strong shear layers are formed due to low speed streaks travelling upstream and laminar flow travelling downstream. Subsequently Kelvin-Helmholtz instability sets in and the shear layer gets rolled up and generates new fluctuations. (c) Most of these fluctuations travel downstream faster than the puff and penetrate the trailing edge and increase turbulence activity in the turbulent puff. Thus the cyclic process goes on. Similar arguments were given in an earlier study by Bandyopadhyay (1986) emphasizing the relevance of Kelvin- Helmholtz vortices created at the rear interface to the puff sustenance.

It should be pointed out that the active region of a turbulent puff is ≈10D long (Hof et al. 2010). Further downstream the fluctuations have disappeared and the profile gradually recovers the parabolic shape until the preceding puff is encountered. This aspect is similar to the observations in stripe patterns in PCF (Barkley & Tuckerman, 2007). The turbulent eddies are localized in the turbulent stripes which approximately have a width of 10 wall spacing. Between two stripes the flow relaminarizes but does not quite reach the fully developed laminar profile. A comparison (figure 5.11) of the minimum puff spacing in pipes measured in the present study to the wavelength measured in PCF and TCF laminar turbulent patterns (Prigent *et al.*, 2002*b*) surprisingly shows that the wavelength closely matches the interaction distance found in pipes when the Reynolds number is rescaled so that the intermittent region

for the different flows overlap. The wavelength has been calculated from the spanwise and streamwise spacings measured by (Prigent *et al.*, 2003). Banded laminar-turbulent patterns with similar wavelengths have been reported in TCF, PCF, torsional Couette flow and plane Poiseiulle flow (Barkley & Tuckerman, 2007). Our measurements extend this similarity to the case of pipe flow where the typical length scale does not appear as a wavelength but as a minimum or optimum distance. We hope that this observation will stimulate further studies to clarify similarities and differences between these flows. Our results indicate that in pipes the spacing between adjacent turbulent regions is a consequence of nearest neighbor interaction process and that no long range instability as suggested for PCF and TCF Prigent *et al.* (2002*b*, 2003) is required. It should also be pointed out that as a recent study shows (Avila *et al.*, 2011) the spreading and splitting of puffs take place on time scales much larger than those available in typical pipe experiments. It is therefore possible that in the asymptotic time limit more regular puff spacing is reached, which may be closer to the maximum packing fraction. If so this flow pattern would result from nearest neighbor interaction and not manifest a least stable wavelength of an instability.

Chapter 6

Non Newtonian pipe flow measurements

6.1 Introduction

Despite many studies that focused on the transition to turbulence in Non Newtonian pipe flow and on the onset of drag reduction there is neither quantitative nor qualitative agreement on the effect of polymers on the transition point. While several studies (White & McEligot, 1970; Chung & Graebel, 1972; Pereira & Pinho, 1994) observed delay in transition, others (Paterson & Abernathy, 1972) reported a decrease in natural transition Re. More recent findings obtained in Newtonian pipe flows like the transient nature of localized turbulent puffs to date have not been investigated in flows of dilute polymer solutions. Since lifetimes of puffs are accurately known for Newtonian flows, this quantity potentially offers a robust way to quantify the influence of polymers on the transition point. In addition we will investigate the DR capacity of polymer solutions as Re is increased above the transition point and the approach of the friction factor to the MDR asymptote.

6.2 Results

6.2.1 Lifetime measurements in dilute polymer solutions

Experiments were carried out to quantify the transient nature of puffs in pipe flow for non Newtonian fluids. Dilute polymer solutions of polyacrylamide (PAAM) of 50, 100, 125, 150 and 175 ppm were used. Puff decay measurements were carried out at 760 D from the point of perturbation. For each Re 200 measurements were carried out to generate a reasonable sample size and to reduce statistical uncertainty. For each run one turbulent puff was created with the injection perturbation described in chapter 4.2.4. The puff survival rate was determined by visual inspection at the pipe outlet 760 D from the perturbation point (see chapter 4.3.3 for details). Figure 6.1 shows the probability of puff survival for a Newtonian fluid (blue line) (Hof *et al.*, 2008) and three different polymer concentrations of 50, 100 and 175 ppm. It is evident from figure 6.1 that all probability distributions are 'S' shaped and P=1 is only approached

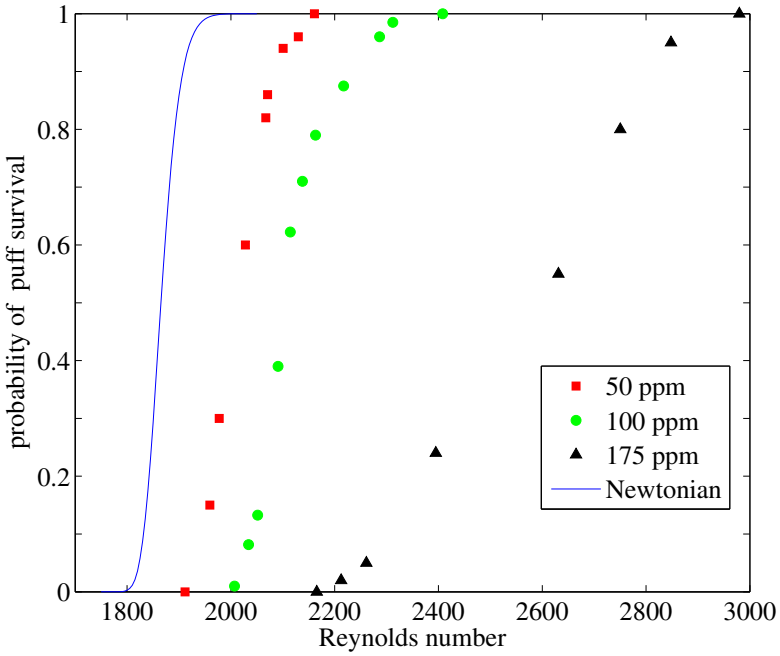

Figure 6.1: Probability of a puff survival at different concentrations of polyacrylamide in water

asymptotically. This implies that also in polymer solutions lifetimes of localized structures remain finite. In comparison to Newtonian fluid (blue curve) probability curves of polymer solutions get shifted more rightward with increase of polymer concentrations. Hence the transition is delayed with increasing polymer concentrations. The puff regime (in Newtonian flows $\approx 1700 \leq Re \leq 2400$) is pushed to higher Re. For 175 ppm localized puffs are still observed at Re as large as 3000 where Newtonian fluid flows are fully turbulent. Therefore the polymer dynamics appear to be be disrupting the puff sustaining mechanisms and postpone the transition to fully turbulent flow.

In figure 6.2 the characteristic lifetimes of puffs (see equation 2.1) in polymer solutions are compared with those in Newtonian flow. The formation time t_o was estimated as 70 D/U similar to the Newtonian cases (Hof *et al.*, 2008). Figure 6.2 shows that the lifetime of puffs at a given Re is shortened in the presence of polymers. This is consistent with the drag reduction behavior of the polymers where vortices and turbulent fluctuations are suppressed. It is likely that the eddies at the trailing edge of the puffs which help in puff sustenance are suppressed due to polymer stretching eventually leading to lower lifetimes in comparison to Newtonian fluids.

Memorylessness : Memorylessness is an essential feature of puff decay in Newtonian flow (see chapter 2.3.1). We here want to examine whether the puff decay in polymer solutions is still memoryless and hence follows equation 2.1 or if qualitative differences arise. In order to test the memorylessness property, lifetimes of puffs were measured at three different distances simultaneously. If the decay process is memoryless, decay rates should only depend on Re and not

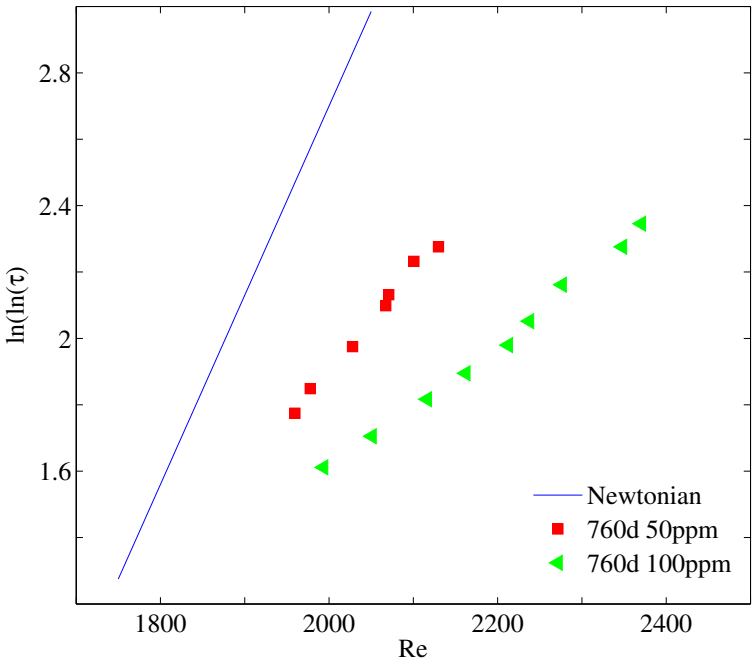

Figure 6.2: Characteristic lifetime of puffs in water and two polymer solutions of 50 and 100 ppm

on the age of the puff (i.e. the distance from the perturbation point). It must be noted that the three measurements at three different distances were simultaneously carried out to avoid any aging effects of polymer solutions due to shear. Aging effect or polymer degradation can change the drag reducing properties of the fluid considerably leading to inconsistent observations. For this experiment we placed two pressure sensors at 332 D and 595 D to detect the presence of puffs. By monitoring the pressure signals of the two pressure sensors by Labview software, puff survival rates were measured. It was assumed that consecutive puffs had a spacing of at least 20-25 D. This ensured that no interaction between puffs would take place. The polymer solution was collected in a container at the pipe exit. Then the accumulated solution was again transferred manually to the reservoir to maintain constant height as well as constant Re. At the pipe exit of 760 D from the perturbation injection point, the survival rate of the puff was determined by inspection of the outflow. Since the centerline velocity of puffs is lower than that for laminar flow, puffs will leave the pipe exit at a different angle than the laminar flow (see chapter 4.3.3). So if the flow angle changes after some time of perturbation injection in the flow it implies that the puff has survived till that distance.

Figure 6.3 shows the lifetime measurements of the 100 ppm solution at three different distances. With increasing distance or observation time the probability for a puff to survive decreases. Based on probability measurements the characteristic lifetime was calculated and presented in figure 6.4. If the process is memoryless the decay rate τ should be constant in time. Figure 6.4 shows

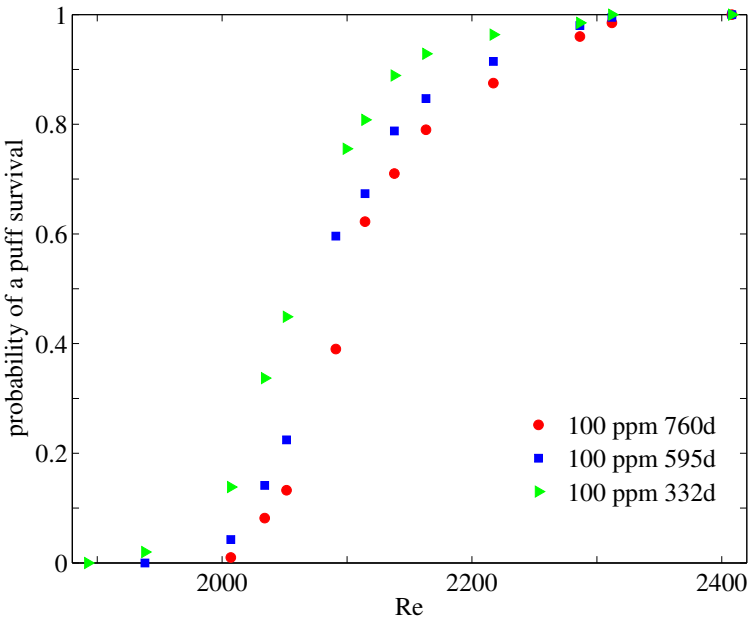

Figure 6.3: Lifetime measurements at three different distances for 100 ppm

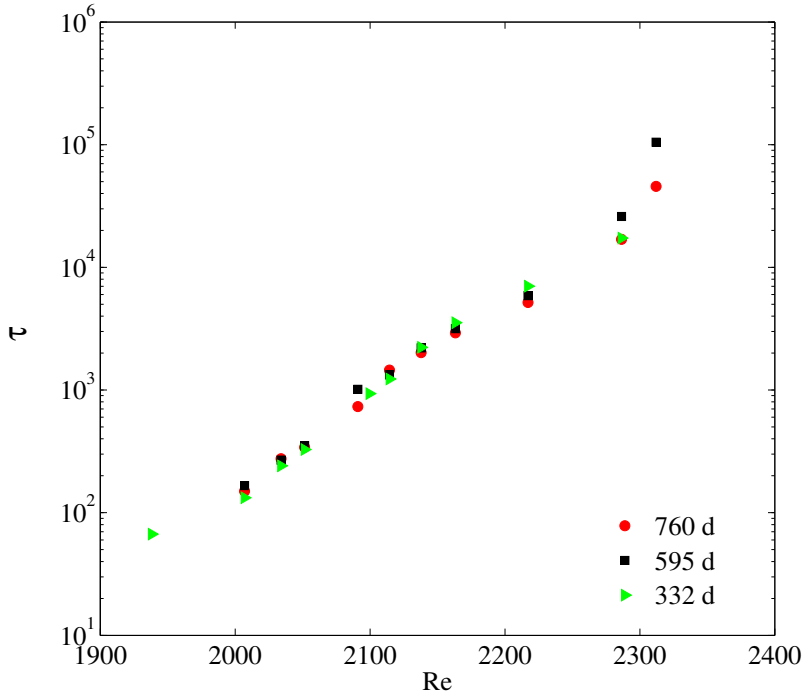

Figure 6.4: Characteristic lifetime of puffs estimated from measurements at different distances

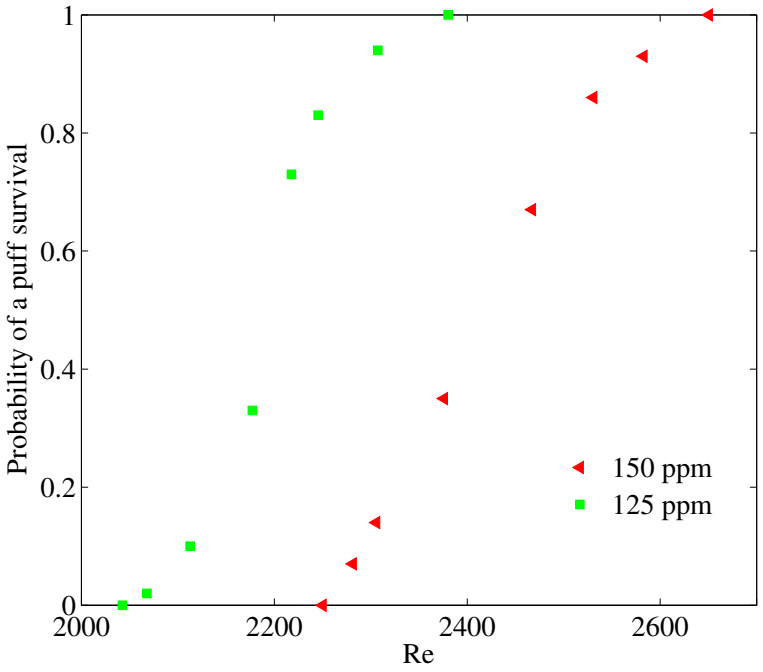

Figure 6.5: Lifetime measurements of 125 ppm and 150 ppm solutions

that characteristic lifetime τ estimated from measurements at three different distances overlap on each other. This implies that the polymer stretching dynamics has no impact on the memoryless nature of the puff decay process. So even if polymers can delay the arrival of puffs to higher Re, the memorylessness property of puff decay process is preserved.

Subsequently lifetime measurements were carried out with several different polymer concentrations (the data for 125 and 150 ppm is shown in figure 6.5). A measure of the effect of the polymer concentration on transition can be obtained by plotting the Re at which the probability of a puff to survive for 760 D becomes 50 % and this is presented in figure 6.6. The Re marking this 50 % survival rate increases faster than linear with concentration manifesting the transition delay. This confirms the earlier claims (White & McEligot, 1970; Chung & Graebel, 1972; Pereira & Pinho, 1994) that the transition threshold increases and provides a quantitative measure of this effect. This is also in line with previous nonlinear stability calculations using an Upper convected Maxwell (UCM) model in plane Poiseuille flow which showed that polymeric flows have a stabilizing effect compared to Newtonian cases (Draad *et al.*, 1998) and that transition is postponed when Weissenberg number (We) exceeds 1. With the increase of polymer concentration the relaxation time as well as the shear rate increase (since higher polymer concentration solutions are more viscous resulting higher flow velocity at a given Re compared to lower concentration solutions), hence leading to an increase in We.

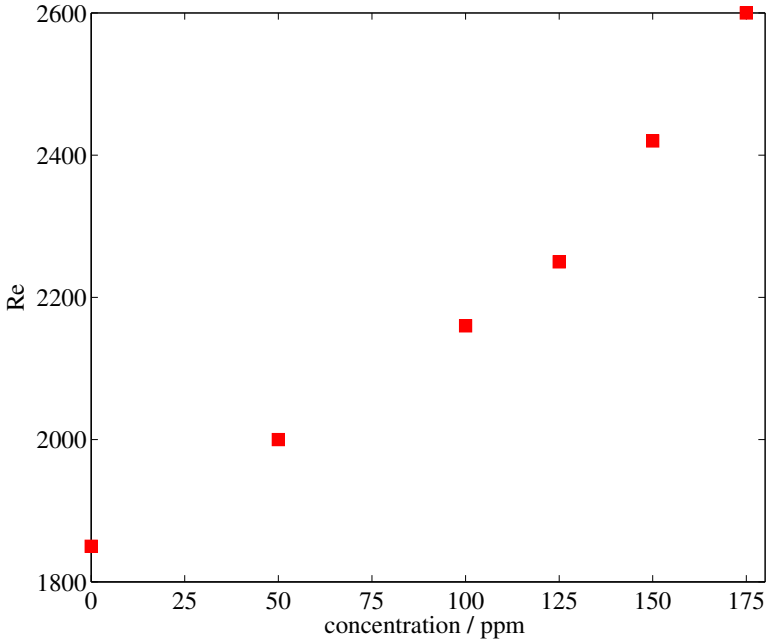

Figure 6.6: Influence of polymer concentration on Reynolds number at which probability of puff survival becomes 50 percent

6.2.2 Drag reduction and transition in low concentration polymer solutions

Subsequently we measured the pressure drop across a 120 D long section and a 3 D long section of the pipe. These quantities were used to determine the friction factor and fluctuation levels respectively. For measuring the friction factor, a long distance (here 120 D) is preferable as it smoothes out spatial variations in the flow. On the other hand to measure fluctuations in the time series of the pressure signal a short distance of 3 D was selected. Pressure signals were measured for 30 seconds (which for water in a 4mm dia pipe flow at Re =2000 corresponds to 3750 advective units D/U). The standard deviation of the pressure signal is a good tool to identify the transition point in the flow because the spatio-temporal variations encountered at transition lead to a sharp increase in fluctuation levels.

Figure 6.7 shows the friction factor measurements as a function of Re for a 50 ppm paam solution and for water. If the flow is perturbed (obstacle in the form of a 1mm thick and 2 cm long thick wire at the entrance), the drag of the solution for Re $\geq$2000 is reduced when compared to the Newtonian turbulence friction scaling (Blasius law, f=$0.079Re^{-0.25}$ as red line in figure 6.7, measurements in water represented in open squares). The blue and the green line in the figure 6.7 are the Hagen- Poiseuille and the Maximum Drag reduction (MDR) asymptote respectively. The latter is also called Virk's asymptote given by f=$0.58Re^{-0.58}$.

Comparisons of friction factors of water and 50 ppm paam solution show that natural transition (i.e. when the flow is unperturbed) sets in at Re$\approx$ 6000 and Re$\approx$ 3800 respectively whereas triggered transition (when the flow is perturbed

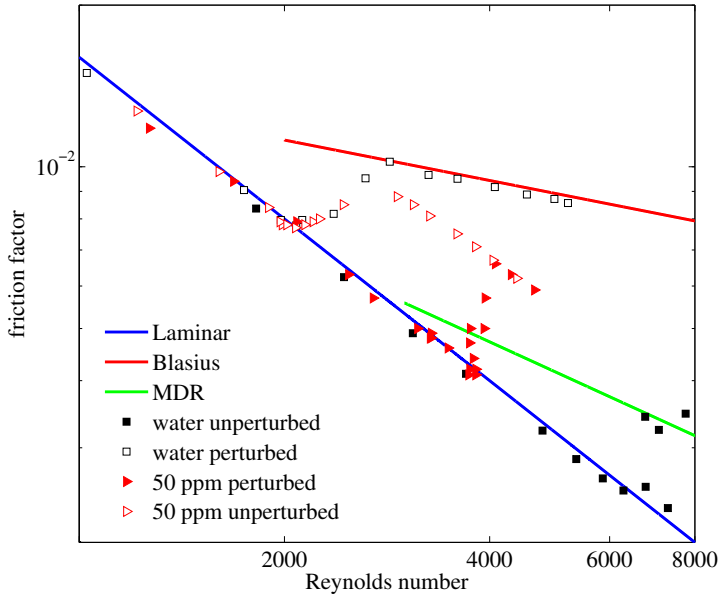

Figure 6.7: Friction factor measurements at 50 ppm and water in perturbed and unperturbed conditions

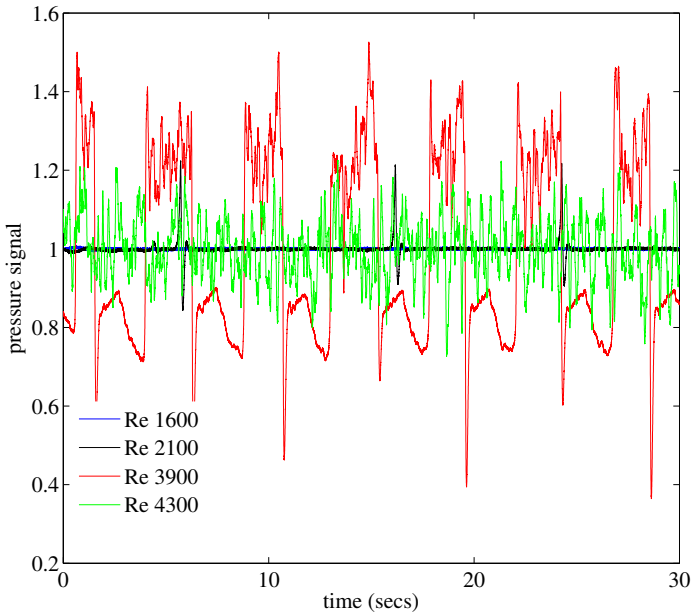

Figure 6.8: Pressure signal at different flow conditions in 50 ppm: (a)laminar flow at Re 1600 (b)intermittent flow with turbulent puffs at Re 2100 (c)intermittent flow with turbulent slugs at Re 3900 (d)uniformly turbulent flow at Re 4300. For better comparison all the signals are superimposed on each other by rescaling the mean value of the signals to 1

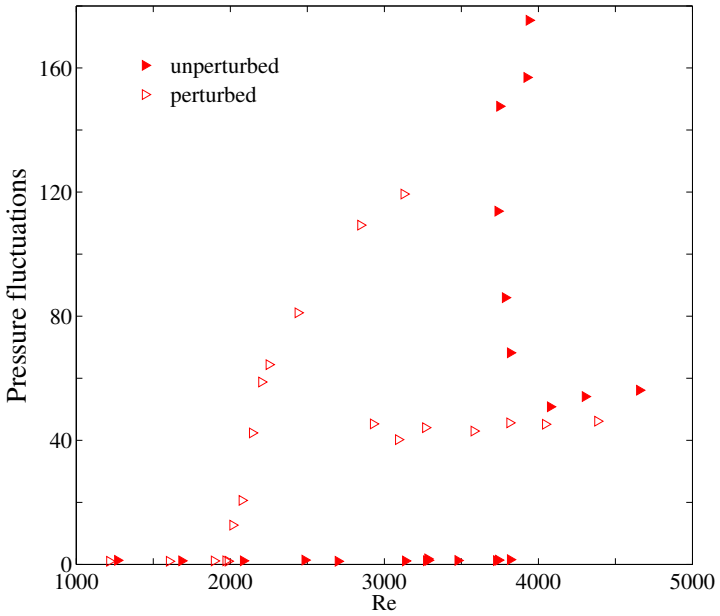

Figure 6.9: Standard deviation of pressure signal of 50 ppm

by placing a thin wire at 120 D from the pipe entrance) sets in at about Re≈2000 for both cases. From figure 6.7 it can be observed that the transition Re to turbulence for 50 ppm solution is different depending on the perturbation in the flow. Except the difference in onset Re of natural and triggered transition with respect to water, the pressure signals in case of 50 ppm (figure 6.8) solutions are similar to that of water. This is reminiscent of transition in Newtonian cases where transition sets in depending upon the perturbation amplitude. This type of transition is called subcritical bifurcation where hysteresis i.e. different Re for onset of transition for different flow conditions is observed. Like in the Newtonian case, transition in the 50 ppm solution is still hysteretic, however the hysteresis loop has decreased and already ends at Re ≈ 3800. Therefore the transition scenario in the 50 ppm paam solution is similar to Newtonian case as subcritical bifurcation is also exhibited in this case (fig. 6.7).

Time series of pressure signals of different conditions: laminar flow(blue curve), flow with puffs in perturbed condition (black curve), flow with slugs in unperturbed condition (red curve) and fully turbulent flow in 50 ppm solution are plotted in figure 6.8. The standard deviation of the pressure signal acquired over 3 D for 30 seconds for different Re is plotted in figure 6.9. The standard deviation of the signal is normalized by the noise level of the sensor in the absence of flow. As soon as the puffs appear in the flow due to perturbations, the flow alternates between laminar and turbulent states. Because of the large pressure fluctuations the standard deviation of pressure is very large. When the flow becomes uniformly turbulent the pressure fluctuations saturates to lower values, but substantially higher than the laminar levels. In unperturbed state, when transition sets in at higher Re≈ 3900 slugs appear in the flow, the fluctuation level is also higher than fully turbulent flow. This method provides

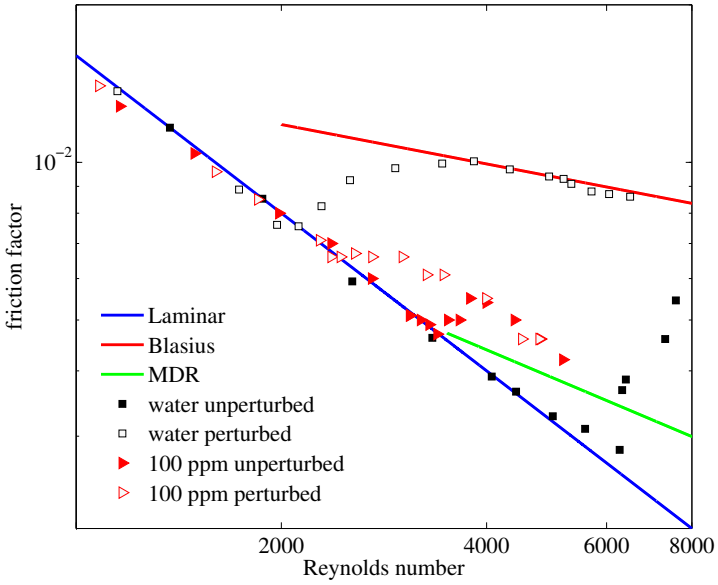

Figure 6.10: Friction factors of water and 100 ppm Paam solutions

a more accurate way to determine the onset of turbulence than friction factor measurements.

The same kind of measurements was carried out for a 100 ppm solution. Figure 6.10 shows the friction factor for perturbed and unperturbed condition of 100 ppm solution and water. The transition is still hysteretic and when compared to 50 ppm the natural transition set in at earlier Re≈3000 and triggered transition was delayed beyond Re ≈2100. As expected with increase of polymer concentration in the flow, DR was higher than 50 ppm. Also the friction factor seems to reach MDR at lower Re values if the downward trend is extrapolated to MDR curve (red triangles both filled and unfilled). Figure 6.11 shows the comparisons of the pressure fluctuations of 100 ppm solution and water. The hysteresis loop in case of water i.e. the difference between the Re at which natural transition takes place and the Re at which triggered transition sets in is much larger than 100 ppm which on the other hand is smaller than that of 50 ppm. So in case of 100 ppm also the bifurcation is similar to hydrodynamic case however flow cannot be held laminar beyond Re ≈ 3000.

6.2.3 Deviation from Newtonian stability

It will be a natural tendency to carry on the lifetime measurements with increasing polymer concentration in the flow and measure the transition delay in the flow. However when 200 ppm solution was used there were no puffs or slugs in the flow. Due to lack of intermittency in the flow it was difficult to track the transition point by visual inspection. This has been reported in earlier studies (Escudier *et al.*, 1999) where it was claimed that for highly drag reducing polymer solutions, from a friction factor vs. Re curve it was difficult to track the transition point as it smoothly deviates from the laminar friction factor curve. Naturally lifetime measurements were not possible anymore.

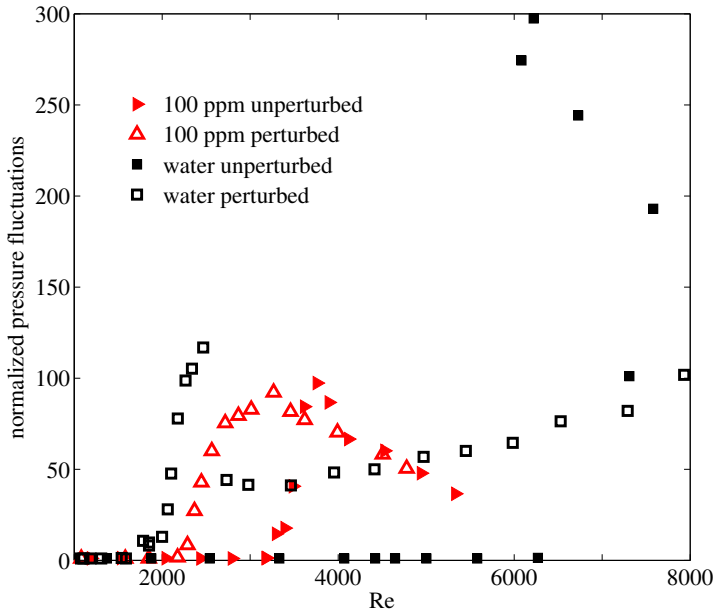

Figure 6.11: Standard deviations of pressure signals in water and 100 ppm Paam solutions

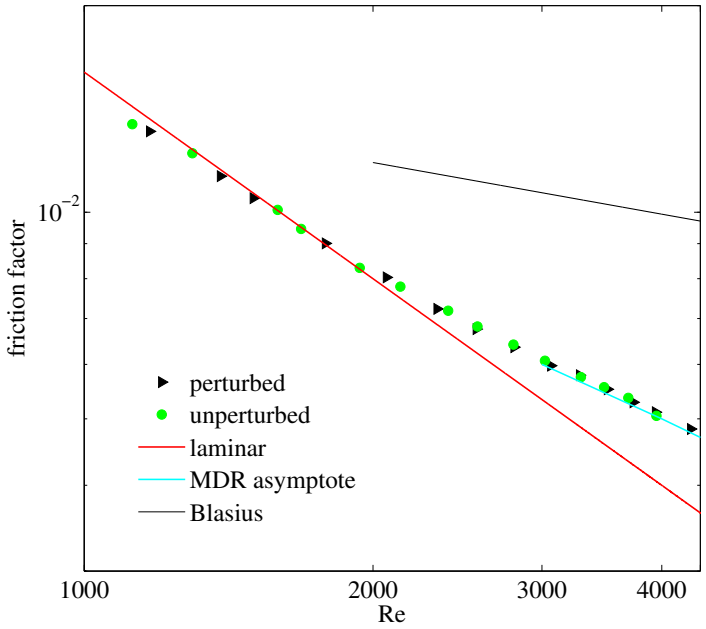

Figure 6.12: Friction factors of 300 ppm solutions

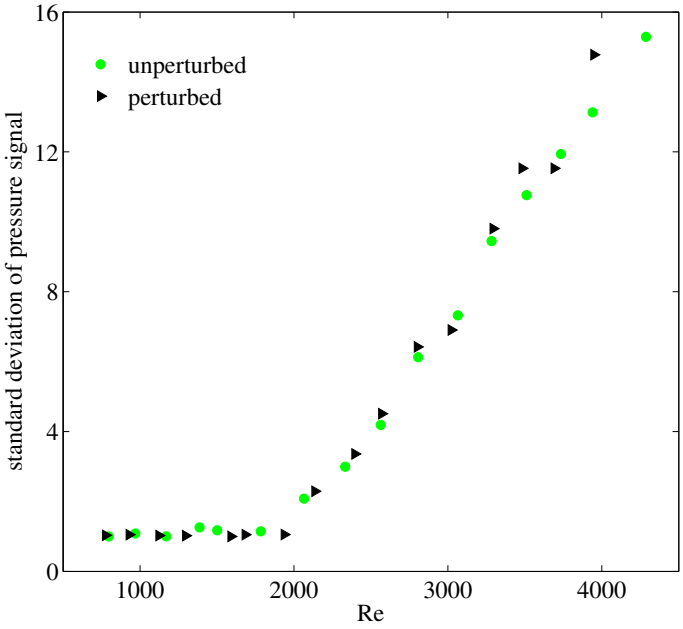

Figure 6.13: Standard deviation of pressure signals in 300 ppm

Figure 6.12 shows the friction factor in 300 ppm solution of both perturbed and unperturbed cases. In both cases the friction factor makes a smooth digression from laminar profile towards the MDR asymptote. Unlike 50 or 100 ppm solutions there is no considerable rise of friction factor from the laminar profile and subsequent decrease of friction factor towards the Virk's asymptote. The most striking fact is that friction factors in both the perturbed and unperturbed cases are similar to each other and shows no dependence on perturbation. Since there is no distinction between triggered transition and natural transition, hysteresis behavior is lost within limit of our experimental resolution. Earlier it was observed that the hysteresis loop in 100 ppm is smaller than 50 ppm. Comparison of the two friction factor diagrams (fig. 6.7 and fig. 6.10) may lead to the conjecture that with the increase of polymer concentration in the flow hysteresis behavior might disappear at certain concentrations. At 300 ppm solution the conjecture is confirmed when it's observed that the hysteresis really vanishes with increase of polymer concentration. It is worthwhile to mention that fresh 200 ppm solutions also showed no hysteresis. However, 200 ppm solutions of 3 to 4 days old exhibited intermittent flows and puffs appeared in the flow. Due to this ambiguity in transition behavior, it's difficult to distinguish the critical polymer concentration from where Newtonian transition scenario changes. Nevertheless, the classical subcritical bifurcation scenario is absent in 300 ppm solution and a new type of instability sets in this regime of polymer concentration solutions. We don't know if it's a linear instability or not. It should be noted that transition point could slightly vary due to minor differences in the mixing procedure, difference in chemical features from one batch of polymers to another or slight variation in the polymer quantity actually mixed in the polymer solutions. Hence transition points in different runs could vary by as

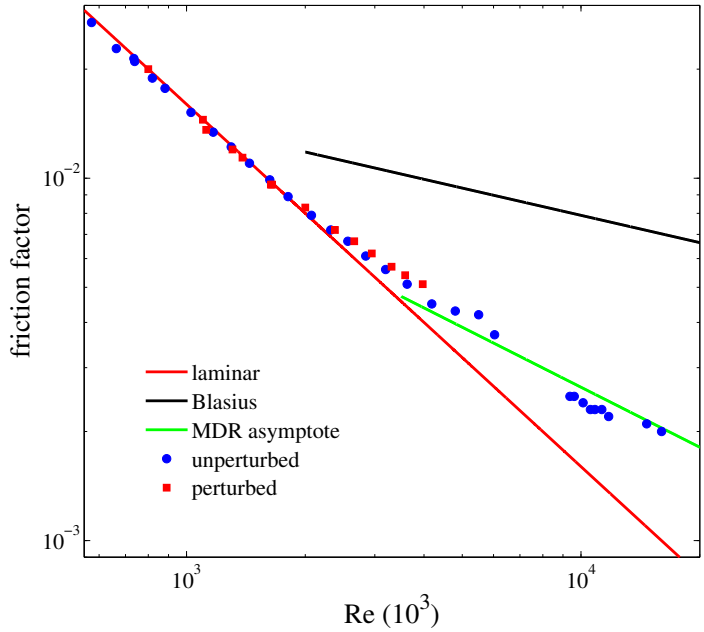

Figure 6.14: Friction factor of 500 ppm solution

much as 10 % due to these subtle differences. Still, in every run the absence of hysteresis definitely confirms the deviation from the Newtonian subcritical bifurcation.

At these high drag reducing polymer flows, due to lack of puffs or slugs it is difficult to track transition by visual inspection at the pipe exit. To resolve these situations, measurements of pressure fluctuations are very useful in tracking the transition point. Figure 6.13 shows the pressure fluctuations diagram of 300 ppm solution. From figure 6.13 it is clear that pressure fluctuations rise from laminar level at Re $\approx$ 2000 in both perturbed and unperturbed conditions. Unlike previous pressure fluctuation diagrams of 50 ppm and 100 ppm, in 300 ppm solution there is no abrupt rise of pressure fluctuations as there is no more spatial intermittency in the flow which can cause high standard deviation in the pressure signal. Another contrasting fact discernible from figure 6.13 in comparison to figures 6.9 and 6.11 is that the pressure fluctuations show a monotonic increase with the Re and doesn't saturate at some values in uniformly turbulent state.

Similar measurements are carried out for 400, 500 and 600 ppm solutions. These set of solutions also showed the same type of transition as the 300 ppm solution i.e. deviation from Newtonian transition. Figure 6.14 shows the friction factor measurements in 500 ppm solution. Friction factor was measured till Re 15000. In figure 6.14 also there is a smooth deviation from the laminar friction factor. Once the friction factor reaches MDR, it will remain on MDR. Figure 6.15 shows the pressure signal at different Reynolds number for 500 ppm. At all Re flows are fluctuating throughout unlike at lower polymer concentrations (50 ppm, see figure 6.8) turbulent structures are not localized but appear globally. The fluctuation level of the pressure signals are increasing with the increase

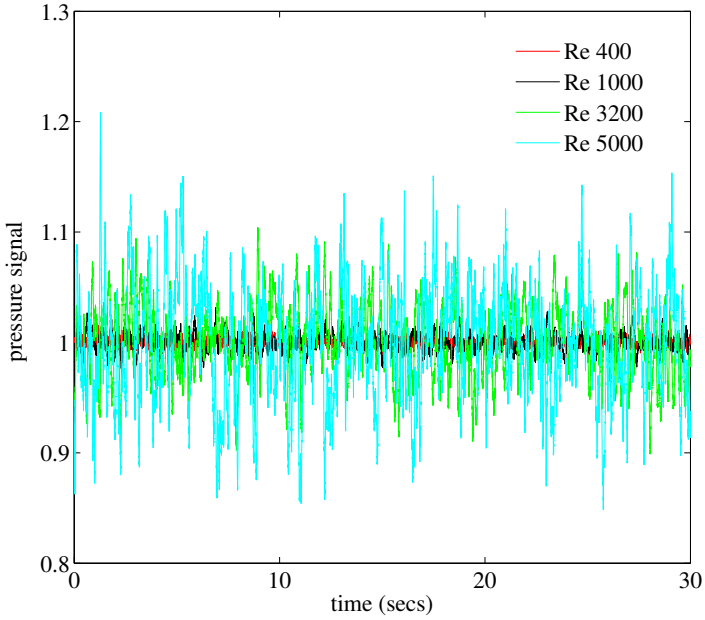

Figure 6.15: Pressure signal in 500 ppm solution at different Re ≈(a)400 (b)1000 (c)3200 (d)5000. Pressure signals are rescaled to convert the mean value of the signals to 1.

of Re. Based on figure 6.15, standard deviation of the pressure fluctuations is calculated and shown in figure 6.16. Pressure fluctuations show deviation from laminar level at very early Re ≈800. Deviation from laminar level at low Re 800 is drastically different from hydrodynamic turbulence. This behavior is previously observed (Forame *et al.*, 1972; Zakin *et al.*, 1977) and coined as 'early turbulence' due to its appearance at Re lower than hydrodynamic cases (see chapter 3.1.5 for further detail). Since this deviation from laminar behavior at Re≈800 is not evident from the friction factor diagram 6.14, we needed a more reliable measure of the onset of turbulence. In earlier studies (Escudier *et al.*, 1999; Park *et al.*, 1989), streamwise velocity fluctuations were measured to track transition in the flow. To measure streamwise velocity fluctuations PIV or LDV techniques can be useful. So in another set of 500 ppm solution, simultaneously PIV and pressure measurements were performed. Figure 6.17 shows a comparison of streamwise velocity fluctuations and pressure fluctuation measurements. In both cases due to ambient noise non zero fluctuations of a constant level are measured for laminar flow. Both signals start to rise above the noise level at Re ≈1000. Even though the transition point varies from the other set of measurements (figure 6.16 and figure 6.17) due to already discussed reasons like slight differences in mixing procedure, transition points are comparable and much lower than values for hydrodynamic turbulence. Hence both the velocity as well as the pressure signals are equally well suited to determine the transition points. Since pressure readings can be obtained more easily transition points for all other concentrations were measured in this way.

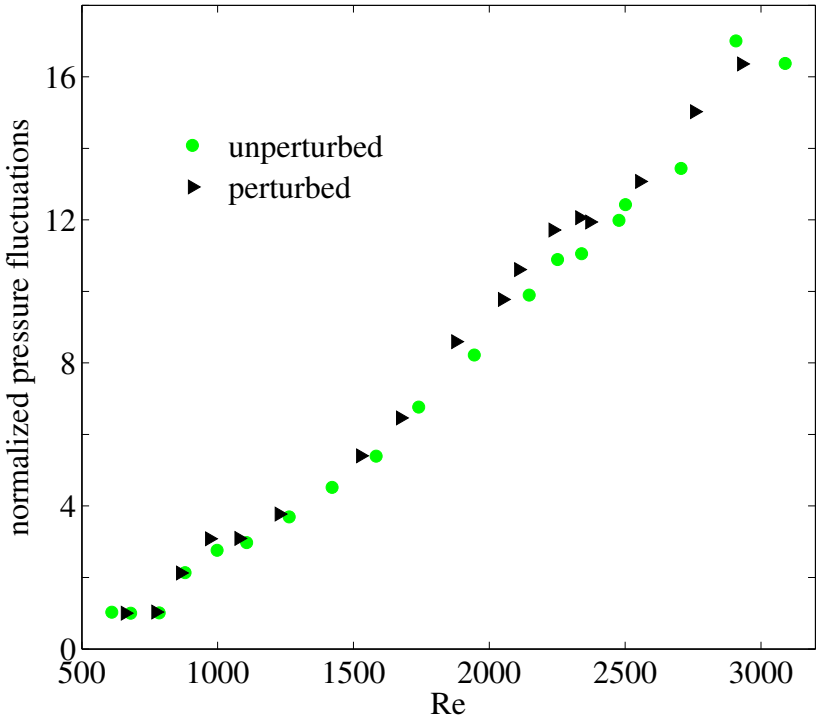

Figure 6.16: Pressure fluctuations at 500 ppm solution in perturbed and unperturbed condition

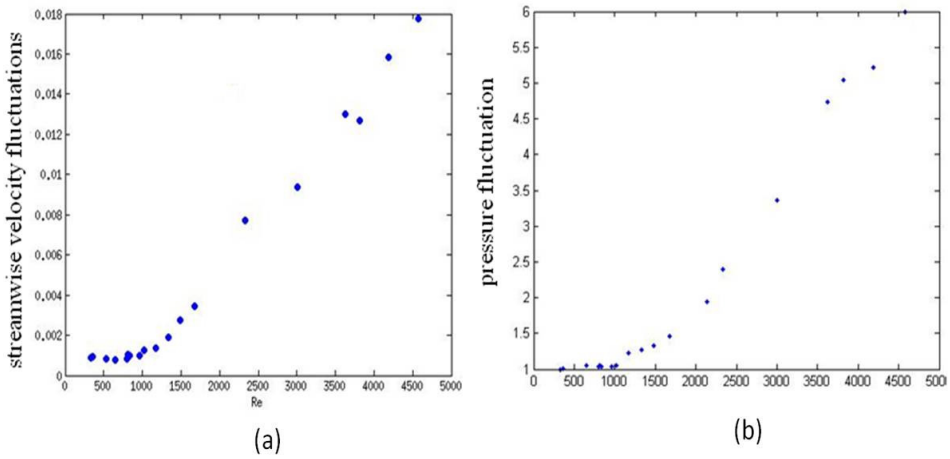

Figure 6.17: Comparisons of (a) velocity fluctuations and (b) pressure fluctuations measured simultaneously by PIV and pressure sensor in 500 ppm

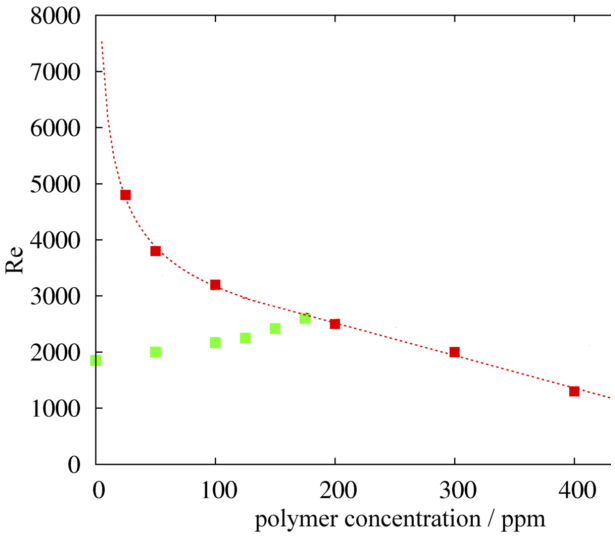

Figure 6.18: The transition threshold to elasto-inertial turbulence is plotted for different concentrations (red squares). The red line is a guide to the eye. The green points mark the transition delay to ordinary turbulence. Consequently for concentrations below 200ppm the elasto-inertial instability sets in at Reynolds numbers where ordinary turbulence can already occur whereas in the D=4mm pipe above 200ppm only the elasto-inertial instability is found

6.2.4 Elasto inertial instability

Based on the lifetime studies and pressure fluctuations measurements in the 4 mm pipe, the natural transition point for different polymer concentrations are plotted in figure 6.18. The red squares in figure 6.18 signify the Re above which deviation from laminar flow occurs. With the increase of polymer concentration there is an an increase in relaxation times and hence viscoelastic effects. With increasing viscoelastic effects natural transition Re can be lowered at Re as low as 800. This instability at lower Re compared to Newtonian transition regime is clearly a combined effect of inertia and elasticity. Hence the instability is called as elasto-inertial instability. The reduction of naturally triggered transition Re due to polymers is consistent with previous experimental observations where the natural transition Re is lowered from 60000 in case of water to 8000-12000 for fresh polymer solutions (Draad, 1996). On the other hand, the green squares symbolize the triggered transition in the flow when intermittent puffs arrive in the flow. In contrast to the natural transition Re, in case of triggered transition Re is increased with the increase of polymer concentration. So viscoelasticity has a stabilizing effect in case of triggered transition.

In the existing literature there were contrasting results on transition to turbulence in pipe flow. Depending upon the pipe geometry and polymer concentration either transition delay or an earlier onset of turbulence has been reported. The present study clarifies this seeming contradiction. Our study shows that polymers delay the transition to Newtonian turbulence i.e. the 'turbulent state' is suppressed. At high shear flows an elasto inertial instability sets in causing a different type of turbulence. In small tubes where shear rates are high and for sufficient concentrations this instability will set in at low Reynolds numbers, before any Newtonian turbulence exists. Hence we clarified that there are two different types of turbulence and while ordinary turbulence becomes suppressed with polymer concentration the threshold to elasto inertial turbulence decreases.

6.2.5 Role of critical shear rate

We next investigated the dependence of the transition point on the shear rate. In addition to 4 mm pipe used above, pipes of D=2 mm and D=10 mm were used. The shear rate ($\gamma^{\bullet}$) at a given Re for laminar state is inversely proportional to square of the pipe diameter. The critical shear rate is estimated assuming the flow to be laminar and parabolic until the instability sets in. Following calculation establishes the inverse square dependence of shear rate on pipe diameter: $\gamma^{\bullet}=\frac{\partial u}{\partial y}=\left|\frac{\partial(U_{max}(1-(r/R)^2}{\partial y}\right|$ where U_{max} , R are centerline velocity and pipe radius respectively. On the other hand at the same Re, $U_{max} \propto 1/R$. Therefore shear rate is inversely proportional to square of pipe radius.

In the preceding sections it is observed that Newtonian like transition occurs until 175 ppm and above 200 ppm polymer concentration, Newtonian type transition disappears. In case of 400 ppm or 500 ppm solutions deviation from laminar level occurs at Re where hydrodynamic turbulence doesn't exist. For a 500 ppm solution in a 10 mm pipe, unlike 4 mm pipe, the instability is still subcritical with a large hysteresis loop (figure 6.19). For the 10 mm pipe the natural transition for water is Re ≈10000. In the case of 500 ppm the natural transition is lowered to Re 6000 and the triggered transition takes place a little above Re≈2000. Since the shear rate for the 1 cm pipe is 6.25 times smaller than in the 4 mm pipe, a different bifurcation scenario is encountered here. From figure 6.22 it can be observed that the critical shear rate for both cases of transition in case of 500 ppm solution is almost same. The critical shear rate which causes deviation from subcritical bifurcation in the 4 mm pipe for 500 ppm is encountered at much higher Re in case of 10 mm pipes. At this high Re inertial effects are already dominant resulting in appearance of slugs. At lower Re or at low shear rates since the polymers are not sufficiently stretched, hydrodynamic or inertial turbulence becomes dominant. Therefore in both triggered and natural transition, puffs and slugs appear intermittently.

Then we did measurements in a 2 mm diameter pipe. Since in a 2 mm pipe shear rate will be 4 times greater than that in a 4 mm pipe at same Re, it is expected that the deviation from Newtonian transition will take place at lower polymer concentrations. We started with 25 ppm polymer solutions. Figure 6.20 shows the pressure fluctuations measurement of 25 ppm solutions. Deviation from laminar profile starts as early as Re 1000. Also it is observed that the fluctuations start from the laminar level independent of perturbation. Again from figure 6.22 it is clear that the critical rate for 25 ppm solutions in 2

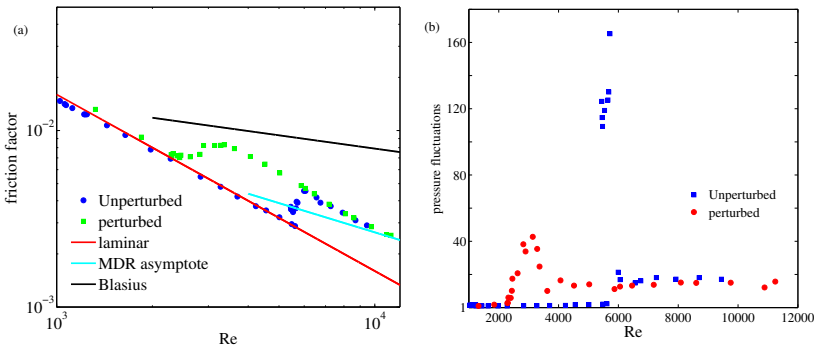

Figure 6.19: (a)Friction factor and (b)pressure fluctuations in 500 ppm solution in 10 mm pipe

mm and 4 mm pipes is same although the bifurcations are of different nature. Additional measurements were carried out with 300 ppm solutions in 2 mm pipe. From figure 6.21 pressure fluctuations studies show that transition sets in at Re as early as 400. This observation suggest that this instability will occur at even lower Re for smaller pipe diameters and higher polymer concentrations opening up possibilities of better mixing in micro fluidic devices where mixing is a tricky issue due to low Re.

Figure 6.22 shows that the critical shear rate for transition is decreasing with polymer concentration. Elastic energy of the polymer solution increases with number of monomers per unit volume i.e. polymer concentration (Gennes, 1990). Therefore it can be justifiably said that even at lower shear rates , cumulative elastic energy due to minute stretching of individual polymer molecules in a high polymer concentration flows is strong enough to create instability in the flow. This same argument can be used for reduction in the onset of natural transition Re with increase of polymer concentration (figure 6.18) Based on the critical shear rate, the critical Weissenberg number is calculated based on the shear rate in figure 6.23. Figure 6.23 shows that for 4 mm pipe the critical Wi is increasing with ppm upto 300 ppm and then a decreasing trend once the deviation from subcritical bifurcation sets in from 300 ppm. The exhibited trend is not conclusive enough for further claims.

6.2.6 Relevance of active and hibernating turbulence

Recent numerical simulations (Xi & Graham, 2010) claimed that during drag reduction regime there are periods of 'active' and 'hibernating' turbulence when wall shear stress increases and decreases respectively. It was argued that the hibernating periods are insensitive to polymer dynamics. Hence MDR effect occurs when the turbulent dynamics comprises mostly hibernating periods with active periods few and far between. However the pressure signal time series presented in figure 6.15 shows uniform intensity. No distinction can be observed where the pressure signal seems to be of decreasing magnitude and increasing magnitude with time. Therefore the claim, that MDR results from the saturation in the fraction of hibernation periods over the whole time duration need to be reexamined.

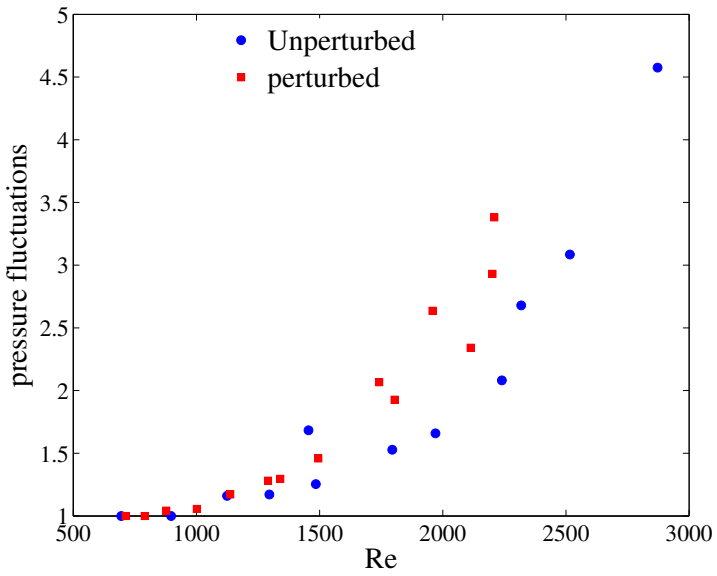

Figure 6.20: Pressure fluctuations in 25 ppm solution in 2 mm pipe

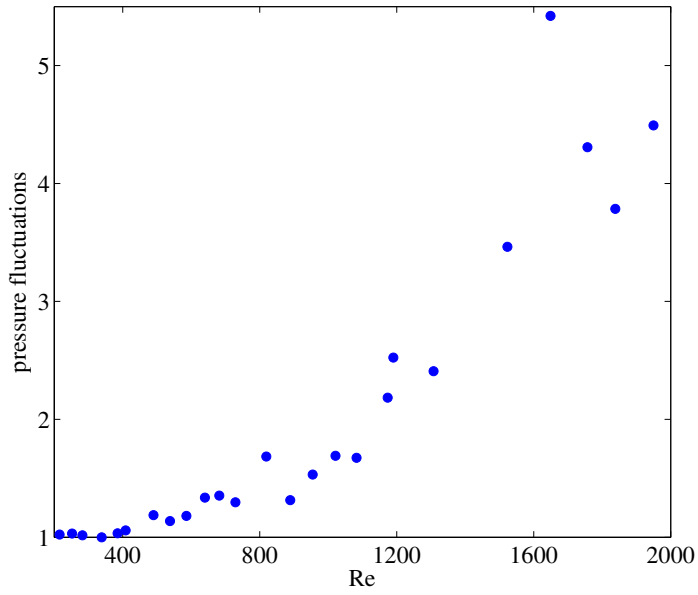

Figure 6.21: Pressure fluctuations in 300 ppm solution in 2 mm pipe

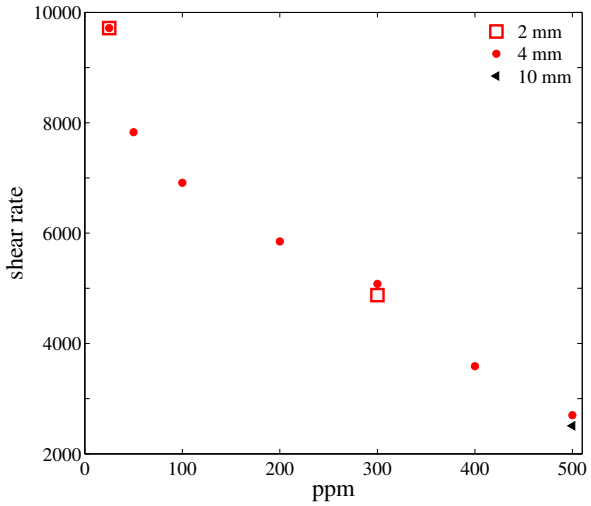

Figure 6.22: The red symbols mark the critical shear rate for the onset of elasto-inertial turbulence in the 4mm pipe (same as red symbols in figure 5.24). In addition critical shear rates were determined in a D=10mm and a D=2mm pipe. In these cases transition occurs at the same critical shear rate. Hence unlike ordinary turbulence the onset of elasto-inertial turbulence is not governed by Re but instead by the shear rate

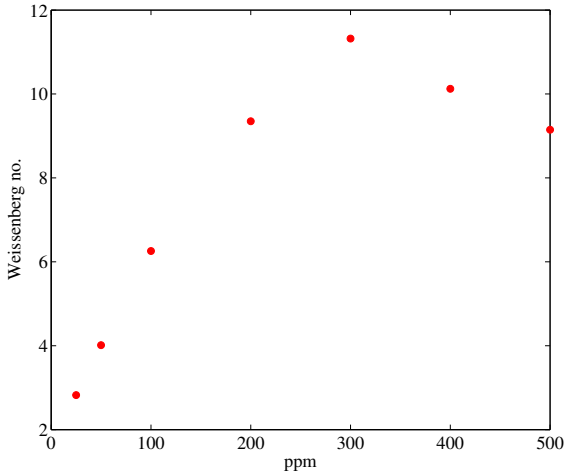

Figure 6.23: Dependence of critical Weissenberg number on polymer concentration

6.2.7 MDR: an asymptotic state of elasto-inertial instability

When elasto-inertial instability sets in at lower Re compared to Newtonian transition regime , the friction factor directly approaches the MDR asymptote without any intermediate jump from the laminar level due to puffs or slugs in the flow. Previous studies (White & Mungal, 2008) on DR claims that MDR state is a modified version of hydrodynamic turbulence with reduced Reynolds stress and appearance of polymeric stress. From our experimental studies it has been observed that once the elasto inertial instability sets in at early Re, an uniformly fluctuating state (figure 6.15)arises with increase of Re without any excursion towards intermittent puff or slug regime. We therefore propose that MDR state is not just a modified version of Newtonian turbulence weakened by polymer actions, rather an asymptotic state of elasto-inertial instability.

Chapter 7

Summary

7.1 Newtonian pipe flow

7.1.1 Results

Experiments on localized puffs in Newtonian pipe flow were carried out. In earlier studies on other shear flows like PC flow and TC flow (Prigent *et al.*, 2002*b*; Barkley & Tuckerman, 2005), upon reduction from fully turbulent regime to transition regime regularly spaced laminar turbulent stripes appeared in the flow. The existence of a preferred spacing has led to the speculation that a wavelength induced instability sets in preceding turbulence. Reduction experiments were carried out in pipe flow. No preferred puff spacing has been observed. However puffs are observed to appear at a vast range of distances. The appearance of a puff at a given distance from downstream puff follows an exponential process i.e. it doesn't depend upon the preceding puff. The mean puff spacing decreases with Re. Linear interpolation of the mean distance with Re suggests that the mean puff spacing ceases to zero at approximately Re 2550-2600.

Subsequently periodic perturbation experiments were carried out. It has been observed that above certain frequency of perturbations, puffs are so closely spaced that their mutual interaction starts causing decay of the puffs eventually. The corresponding puff spacing is termed as interaction distance and is observed to be independent of perturbation duration and amplitude. The interaction distance decreases with increase of Re. It has been observed that above Re 2400 the influence of interaction distance on puff generation is diminished due to puff splitting and merging. The interaction distance corresponds to the maximum turbulent packing fraction in the transition regime. Elimination of turbulence at low Re using the puff interaction process has been exhibited in previous works of Hof *et al.* (2010). Comparison of the minimum puff spacing and interaction distance in pipe flow with laminar turbulent spacings of PC and TC flow were observed to be of similar length scale. Overall from our experiments it has been concluded that instead of a single wavelength instability, nearest neighbor interaction process results the puff spacing. It has been proposed that in an asymptotic time limit even if the regularly spaced puff spacing ultimately appears, it will still result from the nearest neighbor interaction process instead of long range wavelength instability.

7.1.2 Future scope

We believe that this study will stimulate further investigations on the similarity and differences in the localization process of different shear flows. Investigations on the existence of interaction distance in plane Poiseuille flow is an interesting problem also. Previously coupled amplitude equation also known as complex Ginzburg-Landau equation was used to show the large scale finite wavelength instability in TC and PC flow (Prigent *et al.*, 2002*b*). It would be an interesting project to simulate the laminar turbulent dynamics in the pipe transition using Ginzburg-Landau equation.

7.2 Non Newtonian pipe flow

7.2.1 Results

Lifetime measurements were extended to Non Newtonian pipe flow using different polymer concentrations of polyacrylamide (paam). By lifetime measurements transition delay is quantified. With increasing polymer concentration transition delay is exhibited at higher Re. Hence viscoelastic effects of polymer solution is stabilizing against triggered transition . With increasing polymer concentration lifetime of puffs are reduced due to greater polymer actions. Memorylessness of puff decay process is preserved even in presence of polymer actions in the flow.

Friction factor measurements were done for different polymer concentrations. At low polymer concentration flows Newtonian like transition is observed. Transition delay as well as reduction in natural transition Re is exhibited i.e. the hysteresis loop compared to water is reduced. Reduction in natural transition Re implies that viscoelasticity has a destabilizing effect in unperturbed flows. The drag reducing capacity increased with Re and ultimately saturated at MDR asymptote.

With increasing polymer concentration puffs or slugs were not observed in the transition regime. Also the transition from the laminar flow happened at same Re irrespective of perturbed or unperturbed conditions. Hence hysteresis is lost and deviation from Newtonian transition occurs in the flow. At high concentrations like 500 ppm, early transition is noticed as early at Re 800. Previous studies have confirmed that this phenomena is early transition.

Further experiments in different pipe geometry ensured that critical shear rate is the driving parameter in causing instability in the flow. If the critical shear is reached at high Re greater than 2000 , inertial effects become dominant and Newtonian like transition is observed. If the critical shear rate is observed at Re less than onset of Newtonian elastic effects become dominant. Then elasto inertial instability sets in. In that case no localised turbulence is observed and the friction factor directly approaches the MDR asymptote. We propose that MDR is an asymptotic state of this elasto inertial instability.

7.2.2 Future scope

Determination of the critical polymer concentration at which deviation from Newtonian bifurcation happens should be more meticulously done. The influence of pipe geometry on this critical polymer concentration can be also

studied. Flow devices where erratic pressure fluctuations during the transition regime needs to be fully eliminated, can utilize the optimum amount of polymer concentration to ensure a smoother transition from laminar state.

As critical shear rate is the driving parameter for elasto inertial instability, smaller pipe geometry can induce instability at a lower Re. This provides an opportunity for enhanced mixing in micro-fluidic devices.

MDR is proposed as an asymptotic state of elasto inertial instability. In order to strengthen our claims, other viscoelastic fluids like surfactant solutions can be also experimentally studied. Preliminary investigations showed the deviation from Newtonian instability at certain concentrations (see Appendix A). However more detailed studies are essential to confirm our claims.

Appendices

Appendix A

Surfactant drag reduction

A.1 Introduction

Surfactants are known to be DR agents on addition of minute amount in the solvent (Mysels, 1949) . Just like polymers, for surfactants there is a saturation limit for DR, also known as Zakin's asymptote (Zakin *et al.*, 1996). This asymptote is lower than polymer MDR and given by the formula f=$0.32Re^{-0.55}$. Pipe flow of surfactant solutions also shows reduction in Reynolds stress and decrease in radial and spanwise turbulence intensities (Chara *et al.*, 1993; Myska *et al.*, 1996) . Drag reduction studies of surfactant solutions (Savins, 1967a) have claimed that viscoelasticity of the surfactant solutions is responsible for DR. However surfactants are less popular compared to polymers as greater DR can be achieved with lower polymer concentration (Zakin & Bewersdorff, 1998). However unlike polymers, surfactants can regain their original configuration after mechanical degradation due to high shear. The surfactants are effective as DR agents only when the molecules are rod shaped and lose their efficiency in spherical shapes. There exists a critical wall shear stress independent of pipe diameter above which the surfactant solutions lose their DR property (White, 1967; Savins, 1967a). However the process is reversible i.e. the solution exhibits DR behavior once the shear rate is lowered. DR behavior of surfactants is also affected by temperature. Beyond a critical temperature, the surfactants lose DR property.

Inspite of many differences with polymer DR there are certain similarities with polymer DR. Our aim was to investigate whether elasto inertial instability sets in pipe flows of surfactant solutions also to result in final asymptotic states of MDR.

A.2 Setup

For our experiments Cetyl try methyl ammonium chloride (CTAC) is used as surfactant and Sodium salicylate is used as counterions to generate the rod like structures of the surfactant molecules in the surfactant solution. The different surfactant concentrations are 75 ppm, 150 ppm and 400 ppm respectively. The experimental setup is similar to that of Non Newtonian case. We used a pipe of diameter 2mm and a length of 2 meters.

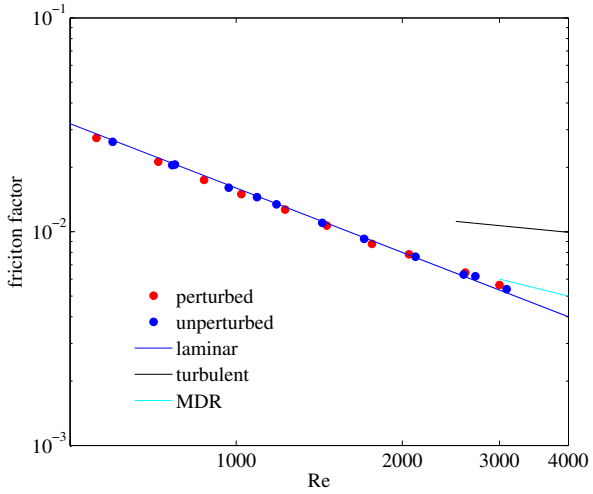

Figure A.1: Friction factor measurements (perturbed and unperturbed condition) of pipe flow of 75 ppm surfactant solution in a 2 mm pipe

A.3 Results

Figure A.1 shows the friction factor measurements for 75 ppm surfactant solution. The friction factor diagram shows that the friction factor rises smoothly from the laminar profile without any characteristic jump in the transition zone like Newtonian cases. Also there?s no dependence on perturbation in the flow implying the deviation from subcritical bifurcation.

Figure A.2 represents the friction factor measurements of 150 ppm surfactant solution flow in a 2 mm diameter pipe. The friction factor stayed on the laminar curve in the measured regime (Re¡ 2500). Figure A.3 shows the time series of pressure signals at different Re. The mean values of the pressure signals (measured in volts) are rescaled to 1 and different signals are superimposed on each other for easier comparison. However a major discrepancy with time series signal of polymer flows is possibility of high oscillations in the signal over time instead of uniformly increasing fluctuations over time. There is a possibility of time periodicity in the flow of surfactant solutions. Moreover, shear banding in surfactant solutions may lead to another type of elastic instability (Britton & Callaghan, 1999) . So much more detailed measurements need to be carried out to extend our claims to surfactant solutions. Figure A.4 shows the pressure fluctuation diagram for 150 ppm. Pressure fluctuations rise from laminar level at a very low Re $>$ 500 showing signatures of early turbulence.

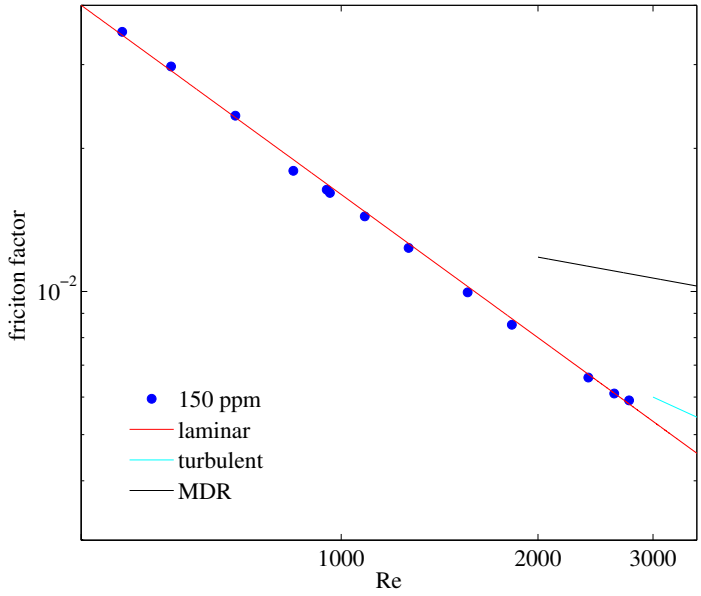

Figure A.2: Friction factor of pipe flow of 150 ppm surfactant solution

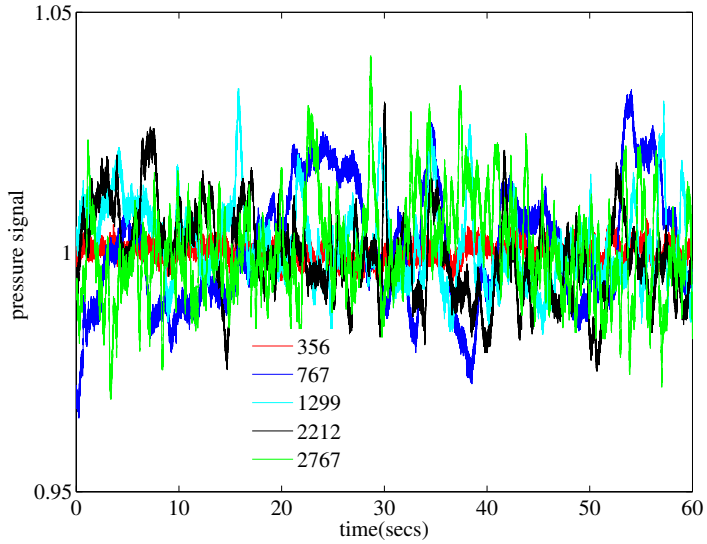

Figure A.3: Pressure signals at different Re of 150 ppm surfactant solution in 2 mm pipe flow

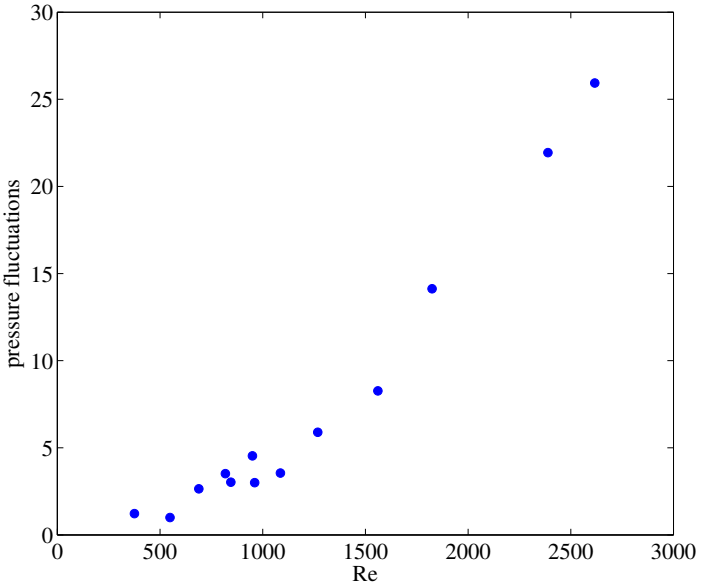

Figure A.4: Standard deviation of pressure signal of pipe flow of 150 ppm surfactant solution

Bibliography

Anna, S.L. & McKinley, G.H. 2001 Elasto-capillary thinning and breakup of model elastic liquids. *J. Rheol.* **45**, 115.

Auerbach, D., Cvitanovic, P., Eckmann, J.P., Gunaratne, G. & Procaccia, I. 1987 Exploring chaotic motion through periodic orbits. *Phys. Rev. Lett.* **58**, 2387–2389.

Avila, K., Moxey., D., Lozar, A. De, Avila, M., Barkley, D. & Hof, B. 2011 The onset of turbulence in pipe flow. *Science* **333**, 192–196.

Avila, M., Willis, A. P. & Hof, B. 2010 On the transient nature of localized pipe flow turbulence. *J. Fluid Mech.* **646**, 127–136.

Bandyopadhyay, P.R. 1986 Aspects of the equilibrium puff in transitional pipe flow. *J. Fluid Mech* **163**, 439–58.

Bark, F.H. & Tinoco, H. 1978 Stability of plane poiseuille flow of a dilute suspension of slender behavior. *J. Fluid Mech.* **87**, 321–333.

Barkley, D. & Tuckerman, L. S. 2005 Computational study of turbulent laminar patterns in couette flow. *Phys. Rev. Lett.* **94**, 014502.

Barkley, D. & Tuckerman, L. S. 2007 Mean flow of turbulent-laminar patterns in plane couette flow.,. *J. Fluid Mech.* **576**, 109–137.

den Berg, T. H.van, van Gils, D.P.M., Lathrop, D.P. & Lohse, D. 2007 Bubbly turbulent drag reduction is a boundary layer effect. *Phys. Rev. Lett.* **98**, 084501.

Berman, N. S. 1977 Flow time scales and drag reduction. *Phys. Fluids* **20**, 168–174.

Bird, R.B., Armstrong, R.C. & Hassager, O. 1987 *Dynamics of polymeric liquids*. A Wiley-Interscience Publication.

Boberg, L. & Z.Brosa, U. 1988 Onset of turbulence in a pipe. *Naturforschung A Phys. Sci.* **43**, 697–726.

Borrero-Echeverry, D., Tagg, R. & Schatz, M.F. 2010 Transient turbulence in taylor-couette flows. *Physical Review E* **81**, 025301.

Bottin, S. & Chate, H. 1998 Statistical analysis of the transition to turbulence in plane couette flow. *Eur. Phys. J.* **B6(1)**, 143–55.

Bottin, S., Daviaud, F., Manneville, P. & Dauchot, O. 1998 Discontinuous transition to spatiotemporal intermittency in plane couette flow. *Europhys. Lett.* **43**, 171–176.

Brautlecht, C.A. & Sethi, J.R. 1933 Flow of paper pulps in pipe lines. *Ind. and Eng. Chem.* **25**, 283–288.

Brecht, W. & Heller, H. 1939 *Das Papier*.

Britton, M.M. & Callaghan, P.T. 1999 Shear banding instability in wormlike micellar solutions. *Eur. Phys. J. B* **7**, 237–249.

Brosa, U. 1989 Turbulence without attractor. *J. Stat. Phys.* **55**, 1303–1312.

Brosa, U. & Grossmann, S. 1999a Minimum description of the onset of pipe turbulence. *Eur. Phys. J. B* **9**, 343–354.

Cadot, O., Bonn, D. & Douady, S. 1998 Turbulent drag reduction in a closed flow system:boundary layer versus bulk effects. *Phys. Fluids* **10**, 426–435.

Chara, Z., Zakin, J.L., Severa, M. & Myska, J. 1993 Turbulence measurements of drag reducing surfactants. *Experiments in fluids* **16**, 36–41.

Choi, K.S. & Karniadakis, G.E. 2003 Mechanisms on transverse motions in turbulent wall flows. *Annu. Rev. Fluid Mech.* **35**, 45–62.

Chung, J.S. & Graebel, W. P. 1972 Laser anemometer measurements of turbulence in non-newtonian pipe flows. *Physics of fluids* **15(4)**, 546–554.

Clasen, C., Plog, J., Kulicke, W., Owens, M., Macosko, C., Scriven, L., Verani, M. & McKinley, G.H. 2006 How dilute are dilute solutions in extensional flows? *J. Rheol.* **50**, 849.

Clever, R.M. & Busse, F.H. 1992 Three-dimensional convection in a horizontal fluid layer subjected to a constant shear. *J. Fluid Mech.* **234**, 511–27.

Clever, R.M. & Busse, F.H. 1997 Tertiary and quaternary solutions for plane couette flow. *J. Fluid Mech.* **344**, 137–53.

Coles, D. 1965 Transition in circular couette flow. *J. Fluid Mech.* **21**, 385–425.

Council, National Research 1997 *Submarine platform technology. In technology for the United States Navy and Marine Corps, 2000-2035: Becoming a 21st century force.Vol. 6; Platforms, pp85-114.*. Washington, DC: Natl. Acad. Press.

Cros, A. & Gal, P. L. 2002 Spatiotemporal intermittency in the torsional couette flow between arotating and a stationary disk. *Phys. Fluids* **14**, 3755–3765.

Cvitanovic, P. 1988 Invariant measurement of strange sets in terms of cycles. *Phys. Rev. Lett.* **61**, 2729–2732.

Darbyshire, A.G. & Mullin, T. 1995 Transition to turbulence in constant-mass-flux pipe flow. *J. Fluid Mech.* **289**, 83–114.

Dodge, D. W. & Metzner, A.B. 1959 Turbulent flow of non newtonian systems. *AiChE Journal* **5(2)**, 189–204.

Draad, A.A. 1996 *Laminar-turbulent transition in pipe flow for Newtonian and Non Newtonian fluids*. TU Delft, Netherlands.

Draad, A.A., Kuiken, G.D.C. & Nieuwstadt, F.T.M. 1998 Laminar-turbulent transition in pipe flow for newtonian and non-newtonian fluids. *J. Fluid Mech.* **377**, 267–312.

Drazin, P.G. 2002 *Introduciton to hydrodynamic stability*. Cambridge University Press.

Dubief, Y., White, C.M., Terrapon, V.E., Shaqfeh, E.S.G., Moin, P. & Lele, S.K. 2004. On the coherent drag-reducing turbulence-enhancing behaviour of polymers in wall flows. *J. Fluid Mech.* **514**, 271–80.

Duguet, Y., Willis, A. P. & Kerswell, R. R. 2010 Slug genesis in cylindrical pipe flow. *J. Fluid Mech.* **663**, 180–208.

Durst, F., Heim, U., Unsal, B. & Kullik, G. 2003 Mass flow rate control system for time-dependent laminar and turbulent flow investigations. *Meas. Sci. Technol.* **14**, 893–902.

Eckhardt, B., Schneider, T. M., Hof, B. & Westerweel, J. 2007 Turbulence transition in pipe flow. *Annu. Rev. Fluid Mech.* **39**, 447–468.

Ehrenstein, U. & Koch, W. 1991 Three-dimensional wavelike equilibrium states in plane poiseuille flow. *J. Fluid. Mech.* **228**, 111–48.

Escudier, M.P., Presti, F. & Smith, S. 1999 Drag reduction in the turbulent flow of polymers. *Journal of non Newtonian fluid mechanics* **81**, 197–213.

Faisst, H. & Eckhardt, B. 2003 Travelling waves in pipe flow. *Phys. Rev. Lett.* **91**, 224502.

Faisst, H. & Eckhardt, B. 2004 Sensitive dependence on initial conditions in transition to turbulence in pipe flow.,. *J. Fluid Mech.* **504**, 343–352.

Forame, P.C., Hansen, R.J. & Little, R.C. 1972 Observations of early turbulence in the pipe flow of drag reducing polymer solutions. *AiChE Journal* **18 (1)**, 213–217.

Forrest, G. 1931 Friction losses in cast irop pipe carrying paper stock. *Paper trade Journal* **22**, 298.

Gauthier, G., Gondret, P. & Rabaud, M. 1998 Motion of anisotropic particles: application to visualization of three-dimensional flows. *Phys. Fluids* **10**, 2147–2154.

Gennes, P.G. De 1990 *Introduction to polymer dynamics*. Cambridge university press.

Goldshtik, M.A., Zametalin, V.V. & Shtern, V. N. 1982 Simplified theory of the near-wall turbulent layer of newtonian and drag-reducing fluids. *J. fluid Mech.* **119**, 423–441.

Grossmann, S. 2000 The onset of shear flow turbulence. *Rev. Mod.Phys.* **72**, 603–618.

el Hak, M. Gad 1980 *Flow Control: Passive, Active, and Reactive Flow Management.*. Oxford Univ. Press.

el Hak, M. Gad & Tsai, H.M. 2005 *Transition and turbulence control*. World Scientific, Singapore.

Hamilton, J.M., J.Kim & Waleffe, F. 1995 Regeneration mechanisms of nearwall turbulence structures. *J. fluid Mech.* **508**, 317–348.

Hansen, R.J., Little, R.C., Reischman, M.M. & Kelleher, M.D. 1974 Stability and laminar to turbulent transition pipe flows in drag reducing polymer solutions. *In proceedings of first International conference on Drag reduction, edited by N.G. Coles (BHRA Fluid engineering, Cranfield, United Kingdom , 1974)* pp. B4–B5.

Heisenberg, W. 1924 Ueber stabilitaet und turbulenz von fluessigkeitsstroemen. *Ann. Phys. Leipzig* **74(4)**, 577–627.

Henningson, D.S. & Reddy, S.C. 1994 On the role of linear mechanisms in transition to turbulence. *Physics of fluid* **6**, 1396–1398.

Hershey, H.C. & Zakin, J.L. 1967 A molecular approach to predicting the onset of drag reduction in the turbulent flow of dilute polymer solutions. *Chem. Eng. Sci.* **22**, 1847–56.

Hinch, E.J. 1977 Mechanical models of dilute polymer solutions in strong flows. *Phys. Fluids* **20**, 20–30.

Hof, B., Juel, A. & Mullin, T. 2003 Scaling of the turbulence transition threshold in a pipe. *Phys. Rev. Lett.* **91**, 244502.

Hof, B., de Lozar, A., Avila, M., Tu, X. & Schneider, T.M. 2010 Eliminating turbulence in spatially intermittent flows. *Science* **327**, 1491–1494.

Hof, B., de Lozar, A., Kuik, D. J. & Westerweel, J. 2008 Repeller or attractor? selecting the dynamical model for the onset of turbulence in pipe flow. *Phys. Rev. Lett.* **101**, 214501.

Hof, B., Vandoorne, C. W. H., Westerweel, J., Nieuwstadt, F. T. M., Faisst, H., Eckhardt, B., Wedin, H., Kerswell, R. & Waleffe, F. 2004 Experimental observation of nonlinear travelling waves in turbulent pipe flow. *Science* **305**, 1594–1598.

Hof, B., Westerweel, J., Schneider, T. M. & Eckhardt, B. 2006 Finite lifetime of turbulence in shear flows. *Nature* **443**, 59–62.

Hoyt, J.W. 1990 Drag reduction by polymers and surfactants. *American Institute of Aeronautics and Astronautics, Washington, D.C.* .

Hoyt, J.W. & Soli, G. 1965 Algal cultures: ability to reduce turbulent friction in flow. *Science* **149**, 1509.

Joseph, D.D. 1969 Eigen value bounds for the orr- sommerfeld equation part 2. *J. fluid Mech* **36**, 721–34.

Joseph, D.D. 1990 *Fluid Dynamics of Viscoelastic Liquids.*. New York: Springer Verlag.

J.Rotta 1956 Experimenteller beitrag zur enstehung turbulent stroemung im rohr. *Ing-Arch* **24**, 258–251.

Kadanoff, L.P. & Tang, C. 1984 Escape from strange repellers. *Proc. Natl. Acad. Sci. USA* **81**, 1276–1279.

Kamenva, M.V., Wu, J.Z. & Uraysh, A. 2004 Blood soluble drag-reducing polymers prevent lethality form hemorrhagic shock in acute animal experiements. *Biorheology* **41**, 53–64.

Kaneko, K. 1985 Spatiotemporal intermittency in coupled map lattices. *Progr. Theo. Phys.* **74**, 1033–1044.

Kantz, H. & Grassberger, P. 1985 Escape from strange repellers. *Physica D* pp. 75–86.

Kawahara, G., Uhlmann, M. & Veen, L.V. 2012 The significance of simple invariant solutions in turbulent flows. *Annual Rev. Fl. Mech.* **44**, 203–25.

Kerswell, R. 2005 Recent progress in understanding the transition to turbulence in a pipe. *Nonlinearity* **18**, 17–44.

Khanafer, K. M., Bull, J. L., Jr., G. R. Upchurch & Berguer, R. 2007 Turbulence significantly increases pressure and fluid shear stress in an aortic aneurysm model under resting and exercise flow conditions. *Ann. Vasc. Surg.* **21**, 67.

Kuik, D.J., Poelma, C. & J.Westerweel 2010 Quantitative measurement of the lifetime of localized turbulence in pipe flow. *J. Fluid Mech.* **645**, 529–539.

Landahl, M.T. 1973 Drag reduction by polymer addition. *Proc. 13th Intl. Congr. Theor. Appl. Mech. Moscow (ed. E becker and G. K. Mikhalov)* pp. 177–199.

Landau, L. & Lifshitz, E. 1959 *Fluid dynamics*. Pergamon,Newyork.

Lindgren, E.R. 1957 The transition process and other phenomena in viscous flow. *Ark. Fys.* **12**, 1–169.

Lindgren, E.R. 1969 Propagation velocity of turbulent slugs and streaks in transition pipe flow. *Phys. Fluids* **12**, 418–25.

de Lozar, A. & Hof, B. 2009 An experimental study of the decay of turbulent puffs in pipe flow. *Phil. Trans. R. Soc. A* **367**, 589–599.

Lumley, J.L. 1969 Drag reduction by additives. *Annu. Rev. Fluid Mech.* **1**, 367–84.

Lyvov, V.S., Pomyalov, A., Procaccia, I. & Tiberkevich, V. 2004 Drag reduction by polymers in wall bounded turbulence. *Phys. Rev. Lett.* **92**, 244503–4.

Manneville, P. 2009 Spatiotemporal perspective on the decay of turbulence in wall bounded flows. *Phys. Rev E* **79**, 025302.

Mellibovsky, F., Meseguer, A., Schneider, T. M. & Eckhardt, B. 2009 Transition in localized pipe flow turbulence. *Phys. Rev. Lett.* **103**, 054502.

Meseguer, A. & Trefethen, L.N. 2003 Linearized pipe flow to reynolds number 10^7. *J. Comp. Phys.* **186**, 178–197.

Metzner, A.B. & Metzner, A.P. 1970 Stress levels in rapid extensional flows of polymeric fluids. *rheol. Acta.* **9**, 174–181.

Min, T., Choi, H. & Yoo, J.Y. 2003 Maximum drag reduction in a turbulent channel flow by polymer additives. *J. Fluid Mech.* **492**, 91–100.

Min, T., Yoo, J.Y., Choi, H. & Joseph, D.D. 2004 Drag reduction by polymer additives in a turbulent channel flow. *J. Fluid Mech.* **486**, 213–38.

Moxey, D. & Barkley, D. 2010 Distinct large-scale turbulent-laminar states in transitional pipe flow. *Proc. Natl. Acad. Sci.* **107**, 8091–96.

Mysels, K.J. 1949 Flow of thickened fluids. *U.S. Patent 2,492,173, Dec. 27* .

Myska, J., Zakin, J.L. & Chara, Z. 1996 Viscoelasticity of a surfactant and its drag-reducing ability. *Appl. Sei. Res.* **55**, 297–310.

Nagata, M. 1990 Three-dimensional finite-amplitude solutions in plane couette flow: bifurcation from infinity. *J. Fluid Mech.* **217**, 519–27.

Nishi, M., Uensal, B., Durst, F. & Biswas, G. 2008 On transition in a pipe. part 2. *J. Fluid Mech.* **614**, 425–446.

Orr, W.M.F. 1907a Stability or instability of the steady motions of a perfect liquid. *Proc. Roy. Irish Acad. A* **27**, 9–69.

Orr, W.M.F. 1907b The stability or instability of the steady motions of a liquid. *Proc. Roy. Irish Acad. A* **27**, 69–138.

Park, J.T., Mannheimer, T.A. & Grimley, T.B. 1989 Pipe flow measurements of a transparent non-newtonain slurry. *ASME J. Fluids Eng.* **111**, 321.

Park, S. & Lauchle, G. C. 2009 Wall pressure fluctuation spectra due to boundary layer transition. *J. Sound Vibrat.* **319**, 1067–1082.

Paterson, R.W. & Abernathy, F.H. 1972 Transition to turbulence in pipe flow for water and dilute solution of polyethylene oxide. *Journal of fluid mechanics* **51**, 177–185.

Peixinho, J. & Mullin, T. 2006 Decay of turbulence in pipe flow. *Phys. Rev. Lett.* **96**, 094501.

Pereira, A. S & Pinho, F.T. 1994 Turbulent pipe flow characteristics of low molecular weight polymer solutions. *Journal of non Newtonian fluid mechanics* **55**, 321–344.

Pfenniger, W. 1961 *Transition in the inlet length of tubes at high Reynolds numbers: Boundary Layer and Flow Control*. Oxford: Pergamon ed. G Lachman.

Pomeau, Y. 1986 Front motion, metastability and subcritical bifurcations in hydrodynamics. *Physica D* **23**, 3–11.

Porteous, K.C. & Denn, M.M. 1972a Linear instability of plane poiseuille flow of viscoelastic liquids. *Trans. Soc. Rheology* **16(2)**, 295–308.

Porteous, K.C. & Denn, M.M. 1972b Nonlinear stability of plane poiseuille flow of viscoelastic liquids. *Trans. Soc. Rheology* **16(2)**, 309–319.

Povkh, I.L., Stupin, A.B. & Boyarkina, G.G 1979 hydrodynamic resistance of aqueous solutions of polymers and surface active substances in rough tubes. *Inzh. Fiz. Zh.* **36(1)**, 16–19.

Prigent, A., Gregoire, G., Chate, H. & Dauchot, O. 2003 Long-wavelength modulation of turbulent shear flows.,. *Physica D* **174**, 100–113.

Prigent, A., Gregoire, G., Chate, H., Dauchot, O. & van Saarloos, W. 2002*a* Large scale finite-wavelength modulation within turbulent shear flows,. *Phys. Rev. Lett.* **89**, 014501.

Prigent, A., Gregoire, G., Chate, H., Dauchot, O. & Sarloos, W. V. 2002*b* Large-scale finitewavelength modulation within turbulent shear flows. *Phys. Rev. Lett.* **89**, 014501.

Ptasinski, P.K., Nieuwstadt, F.T.M., van den Brule, B.H.A.A. & Hulsen, M.A. 2001 Experiments in turbulent pipe flow with polymer additives at maximum drag reduction. *Flow Turbul. Combust.* **66**, 159–82.

Ram, A. & Tamir, A. 1964 Structural turbulence in polymer solutions. *J. App. Poly. Sci.* **8**, 2751–2762.

Rayleigh, J.W.S. 1880*a* On the stability, or instability, of certain fluid motions. *Proc. Lond. math. soc.* **11**, 57–70.

Rayleigh, J.W.S. 1880*b* On the stability, or instability, of certain fluid motions,. *Proc. Lond. Math. Soc.* **7911**, 57–70.

Rayleigh, J.W.S. 1917 On the dynamics of revolving fluids. *Phil. Trans. Roy. Soc. Lond.* **93**, 148–154.

Reynolds, O. 1883 An experimental investigation of the circumstances which determine whether the motion of water shall be direct or sinuous, and of the law of resistance in parallel channels. *Proc.of Royal Society* **174**, 935–82.

Rodd, L.E., Scott, T., Boger, D.V., Cooper-White, J.J. & McKinley, G.H. 2005 Role of the elasticity number in entry flow of dilute polymer solutions in microfabricated contraction geometries. *J. Non-Newt. Fluid Mech.* **129**.

Ruelle, D. & Takens, F. 1971 On the nature of turbulence. *Commn. Math. Phys.* **20**, 167–192.

Ryskin, G. 1987 Turbulent drag reduction by polymers: a quantitative theory. *Phys. Rev. Lett.* **59**, 2059–62.

Salwen, H., Cotton, F.W. & Grosch, C.E. 1980 Linear stability of poiseuille flow in a circular pipe. *J. Fluid Mech.* **98**, 273–284.

Savas, O. 1985 On flow visualization using reflective flakes. *J. Fluid Mech.* **152**, 235–248.

Savins, J.G. 1967*a* A stress controlled drag reduction behavior. *Rheol. Acta* **6**, 323–330.

Savins, J.G. 1967*b* A stress controlled drag reduction phenomenon. *Rheol Acta* **6**, 323.

Schneider, T. M., Eckhardt, B. & Yorke, J.A. 2007 Turbulence transition and the edge of chaos in pipe flow. *Phys. Rev. Letters* **99**, 034502.

Schneider, T. M., Gibson, J. F. & Burke, J. 2010 Snakes and ladders: Localized solutions of plane couette flow. *Phys. Rev. Lett.* **104**, 104501.

Schoepe, W. 2004 Fluctuations and stability of superfluid turbulence at mk temperatures. *Phys. Rev. Lett.* **92 (9)**, 95301.

Shea-Brown, Moehlis, J., Kresimir, J. & Eric, T. 2006 Periodic orbit. *Scholarpedia* **1**, 1358.

Shimizu, M. & Kida, S. 2009 A driving mechanism of a turbulent puff in pipe flow.,. *Fluid Dyn. Res.* **41**, 1–27.

Smith, D.E. & Chu, S. 1998 Response of flexible polymers to a sudden elongational flow. *Science* **281**, 1335–1340.

Sommerfeld, A. 1908 Ein beitrag zur hydrodynamische erklaerung der turbulenten fluessigkeitsbewegungen. *Proc. 4th Intl Congr math. Rome* **III**, 116–124.

Sreenivasan, K.R. & White, C.M. 2000 The onset of drag reduction by dilute polymer additives, and the maximum drag reduction asymptote. *J. Fluid Mech.* **409**, 149–64.

Stone, H.A. 2010 Interfaces: in fluid mechanics and across disciplines. *J. Fluid Mech.* **645**, 1–25.

Tabor, M. & de Gennes, P.G. 1986 A cascade theory of drag reduction. *Europhys. Lett.* **2**, 519–22.

Tan, F. P. P., Borghi, A., Mohiaddin, R.H., Wood, N.B., Thom, S. & Xu, X.Y. 2009 Analysis of flow patterns in a patient-specific thoracic aortic aneurysm model. *Comput. Struc.* **87**, 680.

Taylor, G.I. 1923 Stability of a viscous liquid contained between two rotating cylinders. *Phil. Trans. Roy. Soc. Lond.* **223**, 289–343.

Tel, T. 1991 *Escape from strange repellers:Directions in Chaos vol 3*. Singapore: World Scientific.

Toms, B.A. 1948 Some observations on the flow of linear polymer solutions through straight tubes at large reynolds number. *Proc. 1st Intl. Congr. Rheol. N. Holland, Amsterdam* **2**, 135–41.

den Toondner, J.M.J., Hulsen, M.A., Kuiken, G.D.C. & Niewstadt, F. T. M. 1997 Drag reduction by polymer additives in a turbulent pipe flow : numerical and laboratory experiments. *J. fluid Mech.* **337**, 193.

Trefethen, L.N., Trefethen, A. E., Reddy, S. C. & Driscoll, T. A. 1993 Hydrodynamic stability without eigenvalues. *Science* **261**, 578–584.

Tritton, D.J. 1988 *Physical fluid dynamics*. Oxford Science Publications.

Unthank, J.L, Lalka, S.G., Nixon, J.C. & Sawchuk, A.P. 1992 Improvement of flow through arterial stenoses by drag reducing agents. *J. Surg. Res.* **53**, 625–630.

VanDyke, M. 1982 *Album of fluid motion*. Parabolic press.

Vanoni, V.A. 1946 Transportation of suspended sediment by water. *Trans. Am. Soc. Chem. Engg.* **35**, 111:67.

Virk, P.S. 1975 Drag reduction fundamentals. *AIChE J.* **21**, 625–56.

Virk, P.S., Mickley, H.S. & K.A., Smith 1970 The ultimate asymptote and mean flow structure in toms' phenomenon. *Journal of applied Mechanics* pp. 488–493.

Virk, P.S. & Wagger, D.L. 1990 Aspects of mechanism in type b drag reduction. *Iutam symposium on structure of turbulence and drag reduction, Zurich, Switzerland* pp. 201–213.

Waleffe, F. 2003 Homotopy of exact coherent structures in plane shear flows. *Phys. Fluids* **15**, 1517–34.

Ward-Smith, A.J. 1980 *Internal fluid flow. The fluid dynamics of flow in pipes and ducts.*. New York: Clarendon Press, Oxford University Press.

Warholic, M.D., Massah, H. & Hanratty, T.J. 1999 Influence of drag-reducing polymers on turbulence: effects of reynolds number, concentration and mixing. *Exp. Fluids* **27**, 461–72.

Webber, G.A., Handler, R.A. & Sirovich, L. 1997 The karhunenlove decomposition of minimal channel flow. *phys. Fluids* **9**, 1054.

Wedin, H. & Kerswell, R.R. 2004 Exact coherent structures in pipe flow: travelling wave solutions. *J. fluid Mech.* **508**, 333–371.

White, A. 1967 Flow characteristics of complex soap systems. *Nature* **214**, 585–86.

White, C.M., Dubief, Y. & Klewicki, J. 2012 Reexamining the logarithmic dependence of the mean velocity distribution in polymer drag reduced wall bounded flow. *Physics of fluid* **24**, 021701.

White, C.M. & Mungal, M. G. 2008 Mechanics and prediction of turbulent drag reduction with polymer additives. *Annual Rev. Of Fluid Mech.* **40**, 235–56.

White, W.D. & McEligot, D.M. 1970 Transiiton of mixtures of polymers in a dilute aqueous solution. *Journal of Basic engineering, trans. Of the A.S.M.E.* pp. 411–418.

Willis, A.P. & Kerswell, R.R. 2007 Critical behavior in the relaminarization of localized turbulence in pipe flow. *Phys. Rev. Lett.* **98**, 014501.

Willis, A. P. & Kerswell, R. R. 2009 Turbulent dynamics of pipe flow captured in a reduced model: puff relaminarization and localized edge states. *J. Fluid Mech.* **619**, 213–233.

Wygnanski, I.J. & Champagne, F.H. 1973 On transition in a pipe. part 1. the origin of puffs and slugs and the flow in a turbulent slug. *J. Fluid Mech* **59**, 281–335.

Wygnanski, I.J., Sokolov, M. & Friedman, D. 1975 On transition in a pipe. part 2. *J. Fluid Mech.* **69**, 283–304.

Xi, L. & Graham, M.D. 2010 Active and hibernating turbulence inminimal channel flow of newtonian and polymeric fluids. *Phys. Rev. Lett.* **104**, 218301–4.

Xi, L. & Graham, M.D. 2012 Dynamics on the laminar-turbulent boundary and the origin of the maximum drag reduction asymptote. *Phys. Rev. Lett.* **108**, 028301.

Zakin, J.L. & Bewersdorff, B.L.H. 1998 Surfactant drag reduction. *Reviews in chemical engineering* **14**.

Zakin, J.L., Myska, J. & Chara, Z. 1996 New limiting drag reduction and velocity profile asymptotes for nonpolymeric additives systems. *AIChE J* **42(12)**, 3544–46.

Zakin, J.L., Ni, C.C. & Hansen, R.J. 1977 Laser doppler velocimetry studies of early turbulence. *Physics of fluids* **20**, 85–88.

Zell, A., Gier, S., Rafai, S. & Wagner, C. 2010 Is there a relation between the relaxation time measured in caber experiments and the first normal stress coefficient? *J. Non-Newt. Fluid Mech* **165**, 1265.